PATHOLOGY AT THE NEUROMUSCULAR JUNCTION IN MOUSE MODELS OF SPINAL BULBAR MUSCULAR ATROPHY

By

Jessica Erin Poort

A DISSERTATION

Submitted to
Michigan State University
in partial fulfillment of the requirements
for the degree of

Neuroscience – Doctor of Philosophy

2014

ABSTRACT

PATHOLOGY AT THE NEUROMUSCULAR JUNCTION IN MOUSE MODELS OF SPINAL BULBAR MUSCULAR ATROPHY

By

Jessica Erin Poort

Spinal bulbar muscular atrophy (SBMA) is a progressive, late onset neuromuscular disease that results in muscle weakness and atrophy, as well as motoneuron death in men. While pathology at the neuromuscular junction (NMJ) is noted in numerous neurodegenerative diseases, disease-related changes at the NMJ in SBMA have not been explored. Characterizing such changes is not only important for determining whether the NMJ has any role in the functional changes underlying motor dysfunction, but also in determining how such potential pathology at the NMJ develops as disease progresses. If for example, pathology emerges first at the NMJ followed by motoneuron death, then the NMJ offers future promise as a therapeutic target for preventing or reversing symptoms of SBMA before motoneurons are lost. We evaluated three different mouse models of SBMA, one overexpressing a wildtype androgen receptor (AR) exclusively in muscle fibers (so called "myogenic" model), a second which expressed the endogenous AR gene with the first exon of the human mutant AR gene "knocked in" (the so called "knock-in" model), and a final model that broadly expresses a full length human AR transgene harboring the SBMA mutation (the so called "97Q" model). Using both confocal microscopy and electron microscopy, I found that all three mouse models show a pathological fragmentation of the NMJ suggestive of functionally weakened synapses. Other

changes at the neuromuscular synapse suggesting decreases in synaptic strength that were found in some but not all models include a decline in the number of docked vesicles ready for release in nerve terminals, a widening of synaptic clefts, simplified postsynaptic folds, and an abnormal accumulation of synaptic vesicle and neurofilament proteins. Retrograde axonal transport of endosomes was also characterized in the 97Q model using live imaging confocal microscopy. Despite previously published data, I found no evidence for a disease-related defect in retrograde transport in the 97Q model. The strikingly abnormal morphology of NMJs in all three models raises the possibility that synaptic function is impaired. Such synaptic dysfunction may contribute to or underlie the impairments in motor function associated with SBMA.

ACKNOWLEDGMENTS

I would like to express the deepest appreciation to Dr. Cindy Jordan, my graduate advisor. She has given direction to my research, invested substantial time into discussing its outcome, patiently directed my writing. Personally, it has been delightful building our relationship, from the early coffee walks across Grand River, to the recent California lunches. Thank you to Dr. Marc Breedlove, for your guidance in the lab and compassion outside of it. I recognize how fortunate I have been to be in an atmosphere encouraging of individual interests and one that recognizes and accepts an individual's circumstances. I know that Drs. Jordan and Breedlove are responsible for creating that culture and am grateful to have been included in it. Thank you to Dr. Kyle Miller for allowing the collaborative time spent in your lab, for your advice, and your role on my committee. Thank you to Dr. Cheryl Sisk and Dr. Hong Bing Wang, who comprise the rest of my committee and provided valuable input and guidance. Thank you to my collaborators, Dr. Mary Rheuben and Dawn Autio who provided valuable expertise on the electron microscopy portion of this undertaking. Thank you to Dr. Melinda Frame for her advice and company during the many hours on the confocal microscope. Thank you to Dr. Sue Hill who provided me the opportunity to teach, which helped me recognize how much I enjoy it, but also delivered the confidence that comes from having extended one's self and succeeded. Thank you to Sue Schiel, who first fostered my enjoyment of science

in the many late afternoon days in her classroom after school. The pleasure and satisfaction instilled then have carried me through many frustrations

Thank you to the other members of the Jordan Breedlove laboratory, both current and former. I am particularly grateful for the inclusive environment created in 216 Giltner and truly enjoyed the sociality surrounding it. I would specifically like to thank Diane Redenius for her technical assistance and advice. Thank you too, to Casey Henley, who made me feel like I had a friend at work again.

I am especially grateful to my family, and particularly my mother, for their encouragement, support and help moving on to the next step. It has been wonderful living so close and being able to spend time together so frequently. Finally, I have tremendous amounts of gratitude for my husband, Mulyanto. He has allowed me the freedom I needed, not only to cultivate personal growth during my time in East Lansing, but also to complete this project. His patience, perspective, and love have made me a better person and our life together a happy one.

This work was supported by NIH NS045195 (CLJ) and R01 NS045195 (CLJ).

TABLE OF CONTENTS

LIST OF TABLES

LIST OF FIGURES

KEY TO ABBREVIATIONS

97Q – 97Q mouse model

AChR – acetylcholine receptor

ALS – amyotrophic lateral sclerosis

AR – androgen receptor

BDNF – brain derived neurotrophic factor

BTX – bungarotoxin

Ca – calcium

EDL – extensor digitorum longus

GDNF – glial cell line-derived neurotrophic factor

HSA – human skeletal α-actin

IGF-1 – insulin-like growth factor

KI – knock-in mouse model

LA – levator ani skeletal muscle

NF – neurofilament

NT-4 – neurotrophin 4

SBMA – spinal bulbar muscular atrophy

SMA – spinal muscular atrophy

SMN – survival motoneuron gene

SOD1– superoxide dismutase 1

SOL – soleus muscle

SYN – synaptophysin

T – testosterone

TA – anterior tibialis muscle

TG – myogenic transgenic mouse model

tSC – terminal Schwann Cell

VEGF – vascular endothelial growth factor

WT – wildtype

YFP- yellow fluorescent protein

INTRODUCTION

The aim of my thesis research was to characterize the pathology present at the neuromuscular junction in the neuromuscular disease spinal bulbar muscular atrophy. Here, I offer an introduction to the disease and the models I have been studying, an overview of what the neuromuscular junction is, its component parts, and how each can be affected by disease based on animal model studies of other neuromuscular diseases. Finally, I discuss how axonal transport can be affected by pathological events occurring at the neuromuscular junction as a result of disease.

Spinal Bulbar Muscular Atrophy

An introduction to the disease

Spinal bulbar muscular atrophy (SBMA), or Kennedy's disease, is a slowly progressive, late onset neuromuscular disease that results in a reduced quality of life. Disease symptoms in affected men commonly present at mid-life (30-50 years) and initially begin with complaints of muscle cramping, fasciculations, and aching in the lower back (Takahashi, 2001). Symptoms progress with proximal muscle weakness in the shoulder and pelvic girdle muscles that will eventually affect distal musculature. As the disease progresses further, it extends to the bulbar muscles, resulting in difficulty swallowing and with speech. Some evidence points to mild sensory impairment in SBMA, which usually remains subclinical (Harding et al., 1982, Sobue et al., 1989, Li et al., 1995). In addition to motor symptoms, patients present with gynecomastia, impotence, decreased fertility and testicular atrophy, all thought to be due to the reduced sensitivity to androgens (Arbizu et al., 1983, Warner et al., 1992). Reduced sensitivity is a result of a combination of decreased androgen receptor (AR) expression levels (Choong et al.,

1996) and overall reduced transcriptional activation of AR protein per se (Mhatre et al., 1993, Dejager et al., 2002).

Clinical pathology

Neuromuscular diseases are typically thought to originate from pathology in peripheral motor axons that later affects the target muscles of motor axons. In SBMA in particular, the mutant AR is presumed to act in motoneurons, resulting in their death, and secondarily affecting the muscle, causing weakness and atrophy. This traditional view of SBMA as a neurogenic process emerges from clinical observations. The central pathology of SBMA is a loss of motor neurons in the anterior horn of the spinal cord and in the brainstem motor nuclei seen postmortem in patients affected by SBMA (Kennedy et al., 1968, Sobue et al., 1989). Ventral roots of the spinal cord containing only motor axons also show decreases in the numbers of large diameter myelinated axons, while reductions in the number of myelinated axons in sensory roots is relatively minor (Sobue et al., 1989). However, evidence for reduced or entirely absent sensory nerve action potentials demonstrate that sensory axons are not spared by disease (Harding et al., 1982, Li et al., 1995). Indeed, the loss of stretch reflexes in SBMA patients suggests that large myelinated axons innervating the intrafusal fibers in skeletal muscle may be selectively lost in this disease.

Skeletal muscles from SBMA patients also show prominent pathology. The muscles themselves are atrophic, with individual muscle fibers showing increased variability in size. Examples of hypertrophic fibers located within groupings of atrophic fibers have

even been noted (Kennedy et al., 1968). This fiber size inconsistency is thought to reflect the loss of innervation to some fibers, causing them to atrophy, while other fibers become hypertrophic as they assume the load of their denervated neighbors. Biopsies often contain evidence of myopathy, including internalized nuclei, angular fibers and evidence of split fibers. Frequently, myonuclei are so aggregated and condensed they are the only recognizable feature remaining in a cross section. ATPase staining of muscle biopsies shows large clusters of either slow oxidative or fast fatigue resistant fibers, as opposed to the normal intermixing of these two fiber types (Fig. 1). This suggests surviving motoneurons reinnervated nearby denervated fibers and converted them to the same fibers type as their original muscle fiber targets (Sobue et al., 1989). Histochemical staining has also revealed a shift towards enhanced oxidative metabolism, particularly in severely atrophic fibers. A surplus of Type 1a (slow oxidative) and Type 2a (fast fatigue resistant) fibers and a deficit of Type 2b (fast glycolytic) fibers is evident, also suggestive of a fiber type shift (Harding et al., 1982).

The molecular basis for the disease

SBMA is linked to a mutation in exon I of the *androgen receptor* (*AR)* gene (Lieberman and Fischbeck, 2000) which entails an expansion in the number of trinucleotide repeats from the normal range of 11-33 repeats to 36-64 repeats in the disease population (La Spada et al., 1991). The mutation codes for an increased number of glutamines (polyQ) in the AR protein, which is thought to confer new, toxic, and disease-causing functions to the protein (Fischbeck et al., 1991, La Spada et al., 1991). Because the *AR* is located on the X chromosome, SBMA has a recessive, X-linked pattern of heritability (Fischbeck

et al., 1986). Clinical studies have revealed an overall inverse correlation between the repeat length of the mutation and the onset and severity of the disease (Doyu et al., 1992, Igarashi et al., 1992, Suzuki et al., 2008). However, it important to note that reported examples of striking discordances between CAG repeat length and disease onset indicate that is not the only factor influencing the timing and severity of disease symptom expression (Hashizume et al., 2012).

SBMA is one of a family of polyQ neurodegenerative diseases, including Huntington's disease and multiple types of spinocerebellar ataxia, which may share similar mechanisms of pathogenicity. Examining molecular mechanisms in these diseases provides suggestions about how the mutant AR exerts its effect in SBMA. The molecular basis for the acquired toxicity of the mutant AR is thought to be from a number of sources, including aberrant protein interactions, alterations in degradation, transcriptional changes, and posttranslational modifications. One commonality of the polyQ diseases is the presence of nuclear accumulations (Ross, 2002, Orr and Zoghbi, 2007). Surviving spinal and brainstem motoneurons have nuclear inclusions containing the mutant AR protein and often co-localized with ubiquitin and the molecular chaperone heat shock proteins which promote refolding and/or degradation of misfolded proteins (Li et al., 1998a, Adachi et al., 2003). The role of inclusions in disease is not clear. On one side of the discussion, inclusions are a clear and consistent indicator of disease and have traditionally been viewed as the toxic agent causing neurons to degenerate (Li et al., 2007). Conversely, recent evidence from animal and cell models of disease suggest just the opposite—that inclusions may actually serve a protective

role, counteracting pathology by sequestering the mutant, misfolded proteins into aggregates (Klement et al., 1998, Saudou et al., 1998, Sisodia, 1998, Cummings et al., 1999, Taylor et al., 2003, Arrasate et al., 2004). Indeed, one recent report nicely demonstrates that cell survival is enhanced by the formation of inclusions using the mutant huntingtin protein (Arrasate et al., 2004). Moreover, in models of SBMA, numerous examples show that disease and the presence of inclusions need not correlate (Yu et al., 2006, Monks et al., 2007, Chevalier-Larsen and Merry, 2012). More recently, the field has focused on micro-aggregates or oligomers of mutant AR in cell nuclei as the toxic agent of disease (Katsuno et al., 2002, Adachi et al., 2003, Orr et al., 2010), believed to be the predecessors of nuclear inclusions. These diffuse mutant protein accumulations have been found to associate with neuronal dysfunction and the onset of symptoms, with the degree of protein accumulation in the spinal cord closely associated with CAG repeat length (Yamada et al., 2002, Adachi et al., 2005) (Ross, 1997). Animal models have shown that overexpressing heat shock proteins, which function to refold or degrade mutant AR, decreases aggregate formation and reduces cell death *in vitro* (Kobayashi et al., 2000, Bailey et al., 2002) and also rescues SBMA models from disease (Adachi et al., 2003, Wang et al., 2013). If the normal system for maintaining proper protein conformation is overwhelmed as a consequence of long-term exposure to the mutant protein, likely a source of chronic stress for the cell, it stands to reason that increasing the expression of molecular chaperones would be therapeutic.

In addition to altered protein conformation leading to problems in degradation and abnormal protein aggregates, altered posttranslational processes are another possible

source of toxicity. Proteolytic cleavage of the mutant protein is likely important for pathogenicity, as nuclear inclusions are detectable by the antibodies directed against the N-terminal epitope, but not by the C-terminal epitope (Li et al., 1998a, Li et al., 1998b). A cell model of SMBA also supports the idea that after cleavage mutant AR exerts a higher degree of pathogenicity than the full length protein (Merry et al., 1998). Testosterone also acts on the polyQ protein to induce a conformational change resulting in increased ease of cleavage. Posttranslational phosphorylation of AR is also modulated by testosterone, which likely contributes to pathogenicity (van Laar et al., 1991).

Testosterone as a requirement for disease

Although both males and females can pass on the disease allele, males are the sex primarily clinically affected (Kennedy et al., 1968, Schmidt et al., 2002), which we now know is because this disease is triggered by male levels of testosterone (T), the AR ligand. Affected males have normal to slightly elevated circulating T levels, while the much lower levels of circulating T in females is believed to be responsible for their lack of clinical symptoms, although female carriers do experience mild muscle cramping (Kennedy et al., 1968) (Harding et al., 1982). In the absence of T, ARs sit inactive in the cytoplasm, but upon binding to androgenic ligands, ARs form homodimers, enter the nucleus where they bind to androgen response elements on target genes to alter gene expression (Wong et al., 1993). Nuclear translocation of mutant AR is required for its toxic effects (Takeyama et al., 2002). Through Western blots, large, polymeric AR complexes associated with other molecules are shown to exert the toxicity, not

monomeric mutant AR, which supports T binding to the receptor as an essential step in the protein's toxicity (Katsuno et al., 2002) (Takeyama et al., 2002). However, not only does the mutant AR need to bind to its ligand and translocate to the nucleus, but a specific domain on the N-terminus of the receptor must be present for toxicity (Orr et al., 2010). Additionally, the half-life of AR is increased in the presence of T, which has a stabilizing effect on the mutant protein and results in the time course of toxic effects being extended (Kemppainen et al., 1992). Studies have also shown that mutant AR binds to nuclear proteins responsible for DNA repair, which results in accelerated muscle atrophy from decreased DNA damage in muscle cell nuclei (Xiao et al., 2012).

In addition to the recognizable sex difference in the human population, strong evidence from animal research clearly establishes the connection between SBMA and male levels of testosterone. For example, onset of disease symptoms is prevented or reversed by physical or chemical castration (Katsuno et al., 2002, Chevalier-Larsen et al., 2004, Yu et al., 2006, Johansen et al., 2009), while providing exogenous T to carrier females induces disease (Katsuno et al., 2002, Chevalier-Larsen et al., 2004, Monks et al., 2007). Not only is motor function improved when T levels are reduced, but histological markers of disease are also prevented or become less marked, including preventing the accumulation of diffuse AR positive aggregates in cell nuclei (Katsuno et al., 2002). While clinical studies are scant, the idea that SBMA is an androgen-dependent neuromuscular disease is supported by the finding that disease symptoms in SBMA patients are reduced when T treatment is terminated (Kinirons and Rouleau, 2008).

Models of Spinal Bulbar Muscular Atrophy

Several mouse models of SBMA have been developed that broadly express the mutant SBMA gene throughout all tissues in the mouse. Despite differences in the genetics of each model (e.g., knock-in versus transgenic, the use of different promoters which result in different patterns of mutant AR expression and different length CAG expansions), the disease phenotype remains quite similar, including a male biased disease phenotype which is androgen-dependent, reduced motor function, particularly in the hindlimbs, atrophic muscle fibers and reduced body weight (Jordan and Lieberman, 2008). One such example is a transgenic mouse model, referred to as the "97Q" model, which globally expresses a cDNA of full length human AR harboring 97 CAG repeats under the control of a CMV promoter/chicken β-actin enhancer (Katsuno et al., 2002). Another SBMA model that has been a focus for my thesis research is a knock-in (KI) model in which exon 1 of the endogenous *AR* gene in mice has been replaced with exon 1 of the human *AR* gene carrying 113 CAG repeats (Yu et al., 2006). Because expression of the *AR* gene is controlled by endogenous promoters, the level and expression pattern of AR mimics the normal murine pattern of expression, thus representing the closest approximation of SBMA in humans. Importantly, in this model, the only AR expressed is the mutant AR from the endogenous gene whereas in all transgenic models, a mutant AR allele is expressed against a background of normal wildtype AR from the endogenous *AR* gene.

Given the broad expression of the SBMA allele in such mouse models, they offer no information about the role of particular cell types in triggering disease and/or its progression. Our laboratory engineered a transgenic model (TG) that overexpresses normal, WT rat AR exclusively in skeletal muscle fibers using a human skeletal actin promoter (Monks et al., 2007). This model was developed to answer basic questions about the mechanisms of sexual differentiation but, unexpectedly, these TG males showed a disease phenotype that corresponds to the SBMA phenotype described in other mouse models. Thus, this so-called “myogenic” model is being used to shed light on the pathogenic mechanisms behind SBMA.

The myogenic model is unique, since expression of the disease-causing AR allele is limited to a particular cell type, the skeletal muscle fiber. This cell-specific pattern of expression allows us to characterize the role of skeletal muscle fibers in this disease. Despite exclusive expression in skeletal muscle fibers, our model displays the *same* androgen-dependent muscle weakness, atrophy and axonopathy that is seen in the other SBMA models (Katsuno et al., 2002, Chevalier-Larsen et al., 2004, Yu et al., 2006), telling us that signals from muscle are an essential component of the disease and challenging the long held view that SBMA is a motoneuron disease which originates in the motoneurons.

A neurogenic or myogenic disease?

Despite the conventional view that muscle pathology stems from motoneuron death, there is substantial support for the opposite, that diseased muscles may, in fact, cause

motoneurons to die. While some mouse models show reduction in the number and/or size of motoneurons (McManamny et al., 2002, Sopher et al., 2004), several SBMA models show that motor dysfunction can occur *without* motoneuronal cell death and that muscle pathology emerges first (Katsuno et al., 2002, Chevalier-Larsen et al., 2004, Yu et al., 2006, Monks et al., 2007). This observation suggests that motoneuronal death is a secondary response to a disease process that initially impairs cell function. Additionally, there are multiple features of the disease phenotype not explained by a neurogenic process. Levels of creatine kinase, an indicator of damaged muscle, are elevated well above what is typically seen in diseases involving denervation (Harding et al., 1982, Soraru et al., 2008, Chahin and Sorenson, 2009), a consistent feature of primary myopathies such as muscular dystrophy (Hoogerwaard et al., 2001). Moreover, the severity of muscle pathology corresponds to the degree of disability the patient experiences, rather than disease duration, indicating that this pathology might be a primary event rather than secondary to denervation. Finally, pathology seen in muscle biopsies from SBMA patients, such as centrally located myonuclei and split fibers, suggests a primary myopathy and that processes other than denervation contribute to the loss of muscle strength and atrophy, which are core features of SBMA (Soraru et al., 2008).

Our myogenic model provides direct support for muscle as a key site where AR action drives disease. In chronically symptomatic males, we see no evidence of motoneuron death, indicating the motor phenotype is independent of motoneuron cell death (Monks et al., 2007). However, such males do show some axonopathy. Furthermore, the

skeletal muscles of symptomatic males show substantial muscle pathology including reduced fiber size, number, and centralized nuclei. Additionally, females treated with T quickly become symptomatic, yet show no signs of axonopathy (Johansen et al., 2009). Finally, models using various neuron-specific promoters to overexpress the mutant AR exclusively in neurons failed to recapitulate the motor deficits or pathology associated with SBMA (Merry et al., 1996).

The possibility that skeletal muscle may be a primary player in motoneuron disease has also been suggested based on mouse models of amyotrophic lateral sclerosis (ALS). Although the cause behind the majority of ALS cases is unknown, ten percent have an inherited form of ALS, of which twenty percent are due to mutations in the gene producing superoxide dismutase (SOD1). In both ALS patients and traditional SOD1 models which globally express the human mutated form of SOD1 linked to ALS, the earliest sign of disease is denervation or dysfunction at the NMJ, closely followed by skeletal muscle atrophy, both occurring before evidence of motoneuron pathology or loss in the spinal cord (Chiu et al., 1995, Kennel et al., 1996, Frey et al., 2000, Fischer et al., 2004, Yoshikawa et al., 2009). Notably, expressing mutant SOD1 exclusively in skeletal muscle results in a full ALS phenotype (Wong and Martin, 2009), yet exclusive expression of the same disease allele in motoneurons produces no phenotype (Pramatarova et al., 2001, Lino et al., 2002). However, there is contradictory evidence suggesting that mutant protein in motoneurons is needed for disease symptoms. Selectively inactivating SOD1 in motoneurons using Cre/Lox gene inactivation demonstrates that the expression of SOD1 in motoneurons determines disease onset

(Boillee et al., 2006). Suppressing mutant SOD1 exclusively in muscle using siRNA is ineffective at delaying disease related muscle weakness, but when the mutant protein levels are reduced in both muscle and motoneurons, muscle strength is improved (Miller et al., 2006). Confounding the discussion of either a myogenic or neurogenic mode of disease is the suggestion that other cell types, such as glia and neurons other than motoneurons, have the ability to influence the disease state of motoneurons. Chimera mice expressing the SOD1 mutation in motoneurons combined with varying levels of either WT neurons or neurons expressing the SOD1 mutation show that the presence of WT neurons delays disease progression (Yamanaka et al., 2008). Additionally, in these chimeras, motoneuronal expression of the SOD1 mutation alone is not sufficient for disease, non-motoneuronal expression of SOD1 is required (Clement et al., 2003). Further evidence of non-cell-autonomous death of motoneurons is seen by the delay in late stage ALS disease progression when mutant SOD1 mutant protein levels are decreased in microglia (Boillee et al., 2006) and Schwann cells (Lobsiger et al., 2009).

The Neuromuscular Junction

An introduction to the tripartite synapse

In mammals, every skeletal muscle fiber is singly innervated by one motoneuron axon. Near the muscle, the axon loses its myelination and branches to form a junction with the muscle. The motoneuron terminal contains vesicles filled with acetylcholine, the neurotransmitter responsible for exciting muscle fibers, mitochondria, and filamentous proteins (Fig. 2). The neuromuscular junction (NMJ) is composed of three distinct cell types: motoneurons, terminal Schwann cells (tSCs), and muscle fibers, each

contributing to the maintenance and health of the junction. In healthy animals, these three cellular components of the junction are precisely aligned (Fig. 3). However, in neuromuscular disease, one of the earliest indicators of pathology is at the NMJ (Fischer et al., 2004, Yoshikawa et al., 2009). Under the influence of disease, the precise association seen in healthy junctions unravels and each of the three components can display pathology.

Correlates of disease in the nerve terminal

Retraction of the presynaptic motor nerve terminal away from the postsynaptic endplate is frequently observed in neuromuscular diseases (Fig. 4) (Sasaki and Maruyama, 1994, Balice-Gordon et al., 2000, Frey et al., 2000, Fischer et al., 2004, Gordon et al., 2009). When motoneurons retract their connections from the muscle, the signals normally exchanged between motoneurons and muscle are drastically affected. In this scenario, not just the structural relationship is weakened, but the functional properties of the muscle fiber are affected as well, with muscle fibers becoming progressively less active. Additionally, the capacity of the nerve terminal to take up substances from the muscle, such as life-sustaining neurotrophic factors, and retrogradely transport them back to the cell body is reduced. Dysfunction in retrograde transport is seen in multiple models of SBMA (Katsuno et al., 2006a, Kemp et al., 2009, Morfini et al., 2009) as well as in many models of other neurodegenerative disease. In short, once the process has begun, the neurodegenerative process seems to be caught in a positive feedback loop where positive signals are lost as the nerve terminal retracts, further driving withdrawal

of the presynaptic terminal, and resulting in eventual death of the motoneuron and progressive deterioration of the muscle fibers.

Typically, muscles do not become denervated all at once, but rather show what is referred to as “partial denervation,” meaning that some fibers are denervated whereas others remain innervated. In this scenario, the remaining nerve terminals are stimulated to grow sprouts, in an apparent attempt to re-innervate denervated endplate of nearby muscle fibers (Grimby et al., 1989, Cifuentes-Diaz et al., 2002, Monani et al., 2003). The formation of sprouts seems to be prompted by silent muscle fibers emitting signals (Love and Thompson, 1999) such as insulin-like growth factors, neurotrophic factors and many other signaling molecules (English, 2003). These molecules appear to signal nearby tSCs to sprout, forming bridges to guide nerve terminals sprouts and reinnervate nearby denervated endplates (Son and Thompson, 1995a). Because motoneurons determine whether fibers will be of a particular type (either fast or slow, glycolytic or aerobic), the growth of terminal sprouts to nearby muscle fibers is the presumed explanation for why fiber type grouping is seen in many neuromuscular diseases, including SBMA (Harding et al., 1982, Sobue et al., 1989).

Filamentous strands of neurofilament protein in terminal and preterminal axons form the structural framework for neurons and are involved in regulating axon caliber, axonal outgrowth and regeneration, and provide the scaffolding for microtubules on which cargo are trafficked up and down axons (Perrot et al., 2008). Disease-related changes in neurofilament distribution include alterations to either the structure of neurofilament

proteins or the function of transport proteins that move neurofilament proteins from the cell body where they are synthesized to the distal axon where they are essential for growth and guidance. In disease models where neurofilament accumulations (bulbous collections of the filaments) have been observed in axons, a distinct lack of sprouting was noticed, despite obvious signs of denervation, which suggests that such accumulations hinder regeneration (Cifuentes-Diaz et al., 2002). Functional blockade of motor proteins by these accumulations can also result in changes to axonal appearance and essential functions of the motor proteins (Uchida et al., 2009). In neuromuscular disease models, evidence of large, globular neurofilament accumulations in the presynaptic axon and nerve terminal is broadly observed pathology (Cifuentes-Diaz et al., 2002, Kariya et al., 2008, Murray et al., 2008, Kong et al., 2009). Not only are accumulations of neurofilament seen in the distal aspects of motoneurons of SBMA models, but their presence increases as symptoms worsen (Katsuno et al., 2006a). Neurofilament accumulations in the preterminal axon of SBMA models have also recently gained attention for their association with hindered transport in the axon (Piccioni et al., 2002, Katsuno et al., 2006b).

Nerve terminals also contain mitochondria. Besides their well-known function in energy metabolism, they are also heavily involved in cell signaling, differentiation and death. Healthy nerve terminals normally contain mitochondria, but with disease these mitochondria alter their size, appearance, and number. Multiple neurodegenerative diseases including Huntington's, ALS, Friedrich's Ataxia, muscular dystrophy, and SBMA have set a precedent for pathology in the mitochondria (Law et al., 1983, Panov

et al., 2002, Seong et al., 2005, Browne and Beal, 2006, Hervias et al., 2006, Slater et al., 2006, Trushina and McMurray, 2007).

While many genes necessary for mitochondrial function are independently located in mitochondrial DNA, the majority of genetic material encoding mitochondrial proteins is in the nuclear DNA. Transcriptional dysregulation of these proteins, like that occurring with mutant AR in SBMA, can alter mitochondrial turnover rate, metabolism, and oxidative phosphorylation (Puigserver, 2005, Spiegelman, 2007). Additionally, nuclear encoded mitochondrial proteins show up in the aggregates of mutant AR proteins (Beauchemin et al., 2001, Piccioni et al., 2002). This suggests they are associating with the mutant AR proteins, and that their conformation may be affected. There is further evidence suggesting mitochondria may be a direct site of action for mutant AR as mutant AR is found in mitochondria (Ranganathan et al., 2009). Mutant AR alters the expression of mitochondrial specific DNA, increases the amount of reactive oxygen species in an androgen-dependent fashion, and is associated with the depolarization of the mitochondrial membrane, an indicator of mitochondrial dysfunction (Ranganathan et al., 2009).

In models of SBMA, the mass, number and size of mitochondria are altered. In a neuronal cell model, both the mass and number of mitochondria are decreased (Ranganathan et al., 2009). In contrast, *in situ* observations show mitochondria are larger and more numerous in skeletal muscles near the NMJ (Musa et al., 2011). In both of these models, structural abnormalities such as vesiculated inner cristae are noted

(Ranganathan et al., 2009, Musa et al., 2011). These morphological changes result in functional consequences like decreased mitochondrial membrane potential and increased levels of reactive oxygen species (Ranganathan et al., 2009). There are also indications of increased electron transport chain activity in the form of increased oxidative metabolism, which suggests metabolic rate increases (Musa et al., 2011). This pathology is reliably associated with other disease symptoms and suggests that mitochondrial dysfunction is another pathological feature of SBMA that underlies losses in motor function.

Neurotransmitter vesicles are another prominent feature of the nerve terminal commonly affected by disease. There are three different pools of vesicles in the terminal; the reserve, the recycling and the readily releasable. The majority of synaptic vesicles falls within the reserve pool and do not get released unless those in the recycling pool have been depleted (Kuromi and Kidokoro, 1998, Richards et al., 2000, Richards et al., 2003). While there is nothing discernibly different between the vesicle pools, those from the reserve pool must undergo processing before they are considered part of the recycling pool. The vesicles associated with the recycling pool are defined by their ability to maintain release with moderate stimulation and are about 5-20% of all vesicles in the terminal (Rizzoli and Betz, 2005). This pool is continually refilled with newly recycled vesicles (Harata et al., 2001, Kuromi and Kidokoro, 2003). Actin and synapsin, localized to the terminal, are involved in the mobility of the vesicles during the stages of vesicle clustering, endocytosis, and exocytosis (Doussau and Augustine, 2000, Bloom et al., 2003). The proximity to the synapse does not influence if the vesicle

is associated with the reserve or recycling pool, rather there is evidence suggesting the two pools may intermingle (Rizzoli and Betz, 2005). The final vesicle category is the rapidly releasable pool and includes vesicles that have been primed, docked and are directly associated with the active zones and membrane. These vesicles are depleted very quickly with high frequency stimulation (Birks and Macintosh, 1957, Kamenskaya et al., 1975), and they take a relatively long time to replenish (Hubbard et al., 1969). While vesicles in the readily releasable pool are capable of exocytosis, not all docked vesicles are necessarily immediately releasable (Rettig and Neher, 2002).

With neuromuscular disease, the distribution of vesicles in the nerve terminal is commonly affected, and their density in each pool altered. How the vesicles are transported to each pool can all also be impaired, which in turn impedes synaptic function and the efficiency of muscle contraction activation. Whether the distribution of synaptic vesicles is affected by disease is usually explored using labels that bind to synaptophysin. Synaptophysin is a synaptic vesicle protein that associates with synaptobrevin, one of the integral membrane proteins of secretory vesicles that play a role in exocytosis. Synaptophysin accumulations have been seen in the distal aspects of motor axons in muscle of an SBMA mouse model, with their presence related to the severity of disease symptoms (Katsuno et al., 2006a). Changes to the distribution of synaptic vesicles has also been observed in models of other neurodegenerative diseases including spinal muscular atrophy (SMA) and ALS (Boon et al., 2009, Kong et al., 2009, Wang et al., 2009)

Relevant to synaptic vesicles is the active zone, an area of electron dense membrane where synaptic vesicles merge with the nerve terminal membrane to release neurotransmitter into the synaptic cleft (Couteaux and Pecot-Dechavassine, 1970). It is closely and precisely aligned with the synaptic cleft and is in direct apposition to the mouths of postsynaptic folds (Engel, 1994). Juxtaposed on the presynaptic membrane is a matrix of thin fibrins that forms a web connecting dense, pyramidal-shaped particles composed of synaptic vesicle binding proteins, such as synapsin (Bloom and Aghajanian, 1968, Hilfiker et al., 1999, Phillips et al., 2001, Zhai and Bellen, 2004). This web creates a matrix of 10-15 possible vesicle release sites (Zhai and Bellen, 2004). The increased electron density of the active zone suggests it is a protein rich area important for vesicle docking. Vesicles docked at these sites are ready to be exocytosed upon depolarization and calcium influx (Heuser et al., 1979). However, for the number of active sites, there are relatively few (around 10%) docked vesicles at those sites (Wood and Slater, 2001). Along with the dense particles and vesicles, voltage gated Ca^{++} channels are the third component of the active zone. These channels are integrated into the intramembranous rafts along with Ca^{++} activated potassium channels (Robitaille et al., 1993). When opened by the cell's depolarization, the calcium influx combined with high potassium concentrations triggers the fusion of vesicles with the membrane and the release of acetylcholine at the NMJ (Lang et al., 1987, Nagel et al., 1988).

Even without differences in the density or distribution of synaptic vesicles, they can exhibit other signs of pathology such as alterations in their shape from the typical

spherical morphology to a flattened more ovoid appearance (Deiraldi et al., 1963, Walberg, 1963). Whether the nerve terminal has been recently active can also affect the circularity of the vesicles, with recent activity being associated with more flattened or elongated vesicles (Jones and Kwanbunbumpen, 1970, Korneliussen, 1972, Heuser and Reese, 1973, Birks, 1974, Pysh and Wiley, 1974, Rastad et al., 1977). Responses of the postsynaptic cell to recently released neurotransmitter can also change the shape of synaptic vesicles (Eccles, 1957, Kandel and Kupfermann, 1970).

Altered osmolarity in either the cytoplasm or the interior of the vesicle could also be responsible for changes to vesicle shape (Valdivia, 1971, Thureson-Klein et al., 1975). Changes to vesicle contents would affect the osmolarity of the solution surrounding the vesicle. The amount of acetylcholine contained within a vesicle is also dependent upon the size of the terminal. Smaller terminals release comparable number of quanta per unit area, but the amount of transmitter is decreased (Kuno et al., 1971). This is of particular note, as many neuromuscular disorders list muscle atrophy and smaller terminals as pathology.

Correlates of disease in the synaptic cleft and terminal Schwann cells

The synaptic cleft is a 20 – 100 nm wide space separating the nerve terminal from the postsynaptic specialization, called an “endplate” on a muscle fiber. In the basal lamina, which surrounds the muscle fiber, are numerous synapse-specific glycoproteins and proteins. For example, the enzyme that degrades acetylcholine, acetylcholinesterase, is localized in the basal lamina at the synapse (Sanes and Lichtman, 1999). Before

proteolytic cleavage, acetylcholine diffuses across the synaptic cleft to bind with acetylcholine receptors (AChRs) located on the tops of postsynaptic folds. Changes to the cleft, such as the widening seen in myasthenia gravis (Engel and Santa, 1971) and muscular dystrophy models (Law et al., 1983), reduces the probability acetylcholine will reach its receptors to have a postsynaptic effect (Law et al., 1983) and increases the likelihood released neurotransmitter will be degraded, diffuse away from the cleft or be taken back up by the nerve terminal for recycling.

Each NMJ is capped by tSCs, which play essential roles in the development and maintenance of the junction. Two to four tSC bodies are in contact with the nerve terminal and their processes extend along the axon branches forming the nerve terminal (Kang et al., 2003). TSCs are crucial for stabilization and long-term maintenance of nerve terminals; without them nerve terminals begin to withdraw (Reddy et al., 2003). It is important that tSCs only blanket the terminal, and not invade the synaptic cleft, as the close apposition of the nerve terminal the muscle fiber basal lamina is essential for proper synaptic transduction. S-laminin, which is concentrated in the synaptic cleft, helps ensure tSCs do not encroach into the cleft (Patton et al., 1998). After damage to the axon, the tSCs act as phagocytes to scavenge debris released from the terminal, presumably in preparation for reinnervation (Miledi and Slater, 1970). Invasion of tSCs into the synaptic cleft is one of the indicators of pathology in diseased junctions (Miledi and Slater, 1970, Jirmanova, 1975).

Another key role the tSC fill is to supply trophic factors to the nerve terminal (Friedman et al., 1992, Sendtner et al., 1992). One of the consequences of muscle fiber denervation is that remaining tSCs undergo a change in gene expression, upregulating the synthesis of neurotrophic factors (Heumann et al., 1987, Meyer et al., 1992, Georgiou et al., 1994, Son and Thompson, 1995a, O'Malley et al., 1999). Some of these trophic factors play a role in motoneuron growth or survival while others influence the formation of tSC sprouting (Anton et al., 1994, Henderson et al., 1994). When axon terminals begin to withdraw or degenerate, tSCs from denervated endplates form a dense network of fine projections that extend beyond the junctional area (Reynolds and Woolf, 1992, Woolf et al., 1992, Astrow et al., 1994, Love and Thompson, 1999). Eventually these fine tSC projections originating at denervated endplates form bridges to neighboring innervated endplates, inducing the intact nerve terminal to extend sprouts which eventually innervate the nearby denervated endplate (Son and Thompson, 1995a, b, Love and Thompson, 1999, Tam et al., 2001). While short-term denervation induces a proliferation of tSCs, tSCs migrate away from the NMJ if chronically denervated (Lubischer and Bebinger, 1999, O'Malley et al., 1999). Chronic muscle inactivity also causes tSC projections to form, suggesting cues that induce tSCs sprouting are not strictly dependent on the presence or absence of nerve terminals (Duchen and Strich, 1968, Brown and Ironton, 1977, Reynolds and Woolf, 1992, Son and Thompson, 1995b).

In addition to providing neurotrophic support and responding to denervation, tSCs have a variety of neurotransmitter receptors which allow them to respond to synaptic activity,

especially through calcium mediated mechanisms (Chiu, 1991, Robitaille, 1995, Robitaille et al., 1996). Importantly, the ability of tSCs to sense synaptic activity also means tSCs directly regulate synaptic function by either potentiating or depressing synaptic function depending on the intracellular signaling molecules involved (Robitaille, 1998, Castonguay and Robitaille, 2001).

Correlates of disease at the postsynaptic endplate

The endplate is a morphologically distinct structure characterized by a folded membrane containing AChR densely inserted into the membrane forming a paracrystaline array and an accumulation of specialized myonuclei called the “sole plate” just under the endplate. Receptors on healthy muscle fibers are situated directly opposite the terminal profile in a continuous, pretzel like configuration. The receptors themselves are very stable and are slow to reflect other changes occurring at the junction (Avila et al., 1989). However, with disease-related denervation, the concentration of AChRs at the junction decreases. Simultaneously, AChR is expressed outside the junction as the fiber itself atrophies (Guzzini et al., 2008). Nonetheless, this residual AChR footprint of the junction remains well after the junction is denervated, making it possible to detect denervated junctions that were once innervated. Disease can also change the overall distribution of AChR from the continuous pretzel-like pattern to one that has a clustered, fragmented appearance. This phenotype has been noted in multiple neuromuscular diseases, including myasthenia gravis (Slater et al., 2006), in *Drosophila* models of SMA (Chan et al., 2003, Chang et al., 2008), mouse models of muscular dystrophy (Grady et al., 1997), and in models with mutations to dynactin, a motor associated protein involved in

retrograde axonal transport (Chevalier-Larsen et al., 2008). Although this may not reflect denervation, the fragmented morphology of junctions in disease may nonetheless lead to drastic changes in synaptic function.

The most conspicuous postsynaptic feature of the junction is the pattern of deep infoldings of the sarcolemma. The crests of the folds have a high density of AChR in their membrane, which continues around the fold crest into the secondary synaptic cleft (Salpeter and Loring, 1985). Progressing deeper into the secondary synaptic cleft, the density of AChR decreases and the density of sodium channels increases (Flucher and Daniels, 1989). Density of the secondary synaptic cleft and their depth is correlated with different fiber types. For example, the junctions of red muscle fibers (fast twitch, oxidative) typically have fewer, shallower and simpler folds than those of white fibers (slow twitch, oxidative). The combination of more complex folds with sodium channels located in the depths of secondary clefts is thought to amplify membrane depolarization and enhance neuromuscular transmission (Flucher and Daniels, 1989). Another contributing factor in the ease of depolarization is the width of the secondary synaptic cleft; narrower clefts increase the resistance for current flow, also enhancing the magnitude of depolarization for a given quanta of acetylcholine (Vautrin and Mambrini, 1989, Slater, 2003).

Disease often affects postsynaptic folds with decreases in their complexity (Engel and Santa, 1971, Deconinck et al., 1997, Grady et al., 1997, Kariya et al., 2008, Kong et al., 2009) which is associated with shallower fold depths (Slater et al., 2006). There are two

different hypotheses for the resultant phenotype. The first is that junctions remained immature in their morphology, never developing the narrower, more complex folds characteristic of adult junctions. Alternatively, the postsynaptic folds become simpler and shallower as disease progresses. Regardless of how it occurred, simpler postsynaptic folds in diseased muscle suggest that 1) membrane depolarization will be more difficult and 2) that diseased muscles may have shifted to a more uniform slow-twitch muscle, which evidence suggests occurs in the face of neuromuscular disease.

Axonal Transport

An introduction to molecular trafficking in neurons

Materials produced in the cell body necessary for axonal and synaptic function must be anterogradely transported from the cell body to the synapse. The molecular motor kinesin is responsible for transport in the anterograde direction (Wagner et al., 1989). In contrast, retrograde transport from the axon to the cell body is imperative for neuronal maintenance and survival (Delcroix et al., 2004). Dynein, the multi-subunit molecular motor, is the main motor moving cargo from axon terminals to the cell bodies. The function of dynein is helped by dynactin, a protein complex associated with dynein that binds the cargo and increases the efficiency of cargo transport by decreasing the frequency of stalls made by dynein (Fig. 5) (Susalka and Pfister, 2000). Specifically, the dynactin subunit p150 binds to both the dynein intermediate chain and microtubules while the Arp1 subunit of the dynactin complex binds cargo. The presence and

proportion of each component of the dynactin complex has proven essential to the dynein function. For example, overexpression of the subunit dynamintin (p50) results in dissociation of the dynactin complex, inhibiting dynein-mediated transport (Burkhardt et al., 1997). Altering the levels of either dynein or dynactin also results in recapitulation of neurodegenerative disease (LaMonte et al., 2002, Chevalier-Larsen et al., 2008, Laird et al., 2008, Teuling et al., 2008).

Together, kinesin and dynein are responsible for transport of all cargo being trafficked along axons. An array of membrane-bound organelles are transported in this fashion, including mitochondria, synaptic vesicles, and constitutive building blocks of the axon (Leopold et al., 1992, Elluru et al., 1995). Targeted phosphorylation of cargo proteins by specific kinases ensures the correct cargo arrives at the intended location (Brill and Pfister, 2000).

How disease affects axonal transport

Multiple adult-onset, progressive neurodegenerative diseases exhibit age-dependent decline in function and survival of a select population of neurons. Projection neurons are particularly vulnerable to disease and tend to be the populations that die. Nonetheless, even within the class of projection neurons, only some projections neurons die in a given disease. It is a particular conundrum to understand why some neurons are more susceptible to disease, given that mutant protein linked to particular diseases are rather ubiquitously expressed, including in both neuronal and non-neuronal cells. Nonetheless, one idea is that early defects in axonal transport may explain why projection neurons fall

victim to disease since once transport becomes defective, neurons and their axons may quickly lack essential constituents.

Among the neurodegenerative disease associated with transport defects are ALS, Parkinson's, Huntington's, SMA, and most recently, SBMA. In each, transport deficits are seen well before any signs of motoneuronal death, suggesting that such defects trigger other pathology and eventually leads to neuronal death (Collard et al., 1995, Warita et al., 1999, Williamson and Cleveland, 1999, Murakami et al., 2001, LaMonte et al., 2002, Katsuno et al., 2006a, Kemp et al., 2009, Perlson et al., 2009). In short, impairments in axonal transport may be a common pathway that leads to degeneration in each of these diseases. Importantly, evidence suggests that disease-related defects in axonal transport can be reversed, offering hope that treatment can be found to rescue patients from neurodegenerative disease.

Dysfunction of molecular motors in disease

Some cases of ALS or SMA have been linked to mutations in the motor protein dynein or in subunits of the dynactin complex which bind to dynein (Hafezparast et al., 2003, Puls et al., 2003, Jiang et al., 2005, Munch et al., 2005, Puls et al., 2005). Often when such mutated proteins are expressed in mice, transport deficits are detected before disease symptoms emerge (Laird et al., 2008). In addition to dynactin having a clear involvement in transport, expression of mutant Arp1 or p150 subunits of the dynactin complex seems to cause presynaptic retraction (Eaton et al., 2002), neurofilament accumulations in the preterminal axon, and nerve terminal sprouting (Laird et al., 2008).

These results suggest that particular subunits within the dynactin complex also critically mediate synapse stability at the NMJ. However, most neurodegenerative diseases exhibiting transport dysfunction are not linked to mutations in molecular motor proteins (Hafezparast et al., 2003, Puls et al., 2003), indicating the cause of transport dysfunction lies elsewhere. Indeed, in some cases disease is associated with changes in the expression of kinases that alter phosphorylation status of critical proteins and influence axonal transport (Wagey and Krieger, 1998). ALS, for example, has been repeatedly associated with hyperphosphorylation of neurofilaments (Ackerley et al., 2004) whereas inhibition of transport via the JNK kinase pathway has been implicated in SBMA (Morfini et al., 2006).

Transport deficits in SBMA

Despite the majority of evidence for transport deficits in motoneuron disease coming from ALS models, recent evidence suggests that SBMA should be included among the neuromuscular diseases that have transport dysfunction. Transport deficits were first reported in the AR-97Q model. Using Fluoro-gold as a retrograde tract tracer, Katsuno et al. (2006) observed a reduction in the number of labeled motoneurons, suggestive of retrograde transport deficits. Further analyses using a nerve ligation approach revealed the sciatic nerve from diseased mice has decreased accumulation of synaptophysin in the distal segment, indicative of a retrograde transport defect. This deficit emerged early, before AR-97Q mice were symptomatic (Katsuno et al., 2006a), supporting the hypothesis that a deficit in retrograde transport may trigger disease. Interestingly, both dynactin-1 and dynein levels were decreased in AR-97Q mice, which could dramatically

affect transport and may underlie the deficit in synaptophysin transport. The appearance of nuclear accumulations, dynactin 1 expression levels and Fluoro-gold labeled motoneurons were also shown to return to WT levels with castration, demonstrating the androgen dependence of these effects.

We find comparable retrograde labeling deficits in both our myogenic TG and KI models of SBMA. For example, injecting cholera toxin conjugated to horseradish peroxidase (CT-HRP) into muscle to retrogradely label motoneurons, we find that diseased myogenic TG males show a deficit in the number of motoneurons labeled 12 hours after injection (Kemp et al., 2011). Interestingly, this deficit disappears 24 hours after injection, suggesting that motoneurons accumulate retrogradely transported cargo more slowly. We find a similar deficit in the number of retrogradely labeled motoneurons in affected KI mice. Directly examining retrograde trafficking of cargo in living axons of diseased myogenic mice reveals that endosomal flux is impaired, indicating that there are fewer endosomes moving along the axon over some unit of time. Deficits in endosomal flux may mean that uptake of label by the nerve terminal is compromised. While both models show deficits in endosomal flux, only the KI model shows a deficit in endosomal velocity, which suggests dynein-based processivity problems. Because the disease-causing AR allele is expressed in different cells in these two models, these data suggest that the mechanisms controlling axonal trafficking are regulated by both cell autonomous and non-cell autonomous signals.

Overview

While pathology at the NMJ had been implicated in numerous neurodegenerative diseases, disease related changes at the NMJ due to SBMA have not been explored. Characterizing such changes is not only important for determining the role of the NMJ in functional changes occurring at the synapse, but in determining how pathology at the NMJ develops as the disease progresses. In chapter one, evaluation of two mouse models, one overexpressing a wildtype AR exclusively in muscle fibers and the other having a knock-in of a humanized AR gene containing the CAG repeat mutation, demonstrates pathology at the junction is indicative of weakened synapses. Both models show a fragmented pattern of AChRs forming the endplate, widened synaptic cleft width and simplification of the postsynaptic folds. Additionally, in chapter three, the junctions of a third model of SBMA are evaluated. The 97Q model broadly expresses the full length AR transgene. Again, we find evidence of AChR fragmentation, as well as neurofilament accumulations in the preterminal axon suggestive of trafficking deficits. Finally, we evaluated the 97Q model for trafficking deficits by imaging the live transport of endosomes in the axons of the sciatic nerve. Despite evidence of trafficking deficits in the other two models, we found no deficit in the 97Q model.

CHAPTER 1: Morphology Changes at the Neuromuscular Junction in Mouse Models of Spinal Bulbar Atrophy

Abstract

Spinal bulbar muscular atrophy (SBMA) is a progressive, late onset neuromuscular disease that results in muscle weakness and atrophy, as well as motoneuron death in men. While pathology at the neuromuscular junction (NMJ) is noted in numerous neurodegenerative diseases, disease-related changes at the NMJ in SBMA have not been explored. Characterizing such changes is not only important for determining whether the NMJ has any role in the functional changes underlying motor dysfunction, but also in determining how such potential pathology at the NMJ develops as disease progresses. If for example, pathology emerges first at the NMJ followed by motoneuron death, then the NMJ offers future promise as a therapeutic target for preventing or reversing symptoms of SBMA *before* motoneurons are lost. I evaluated how disease affects the morphology of NMJs in two different mouse models of SBMA, one that overexpress a wildtype androgen receptor (AR) exclusively in muscle fibers (so called "myogenic" model) and another that expresses the endogenous AR gene with the first exon of the human mutant AR gene "knocked in" (the so called "knock-in" model). Both models show an androgen-dependent loss of motor function characteristic of SBMA and an androgen-dependent defect in retrograde axonal transport suggesting pathology originating in the axon terminal (Kemp et al., 2011). To determine whether NMJs show signs of pathology in these models of SBMA, muscles were harvested from diseased and healthy mice and stained to visualize the three different cellular components of the NMJ. Motor nerve terminals were visualized using antibodies for neurofilament (NF),

synaptophysin combined with expression of a transgene for yellow fluorescent protein in motor axons and terminals, terminal Schwann cells (tSCs) were visualized using an antibody for S100 and the postsynaptic specialization of muscle fibers was visualized using tagged alpha bungarotoxin that binds to acetylcholine receptors in the postsynaptic junction. A confocal microscope was used to systematically analyze twenty junctions per animal. We report that while neither mouse model show any indication of denervation, both have pathological fragmentation of the NMJ and abnormal synaptophysin distribution, suggestive of functionally weakened synapses. Preterminal motor axons and nerve terminals of the myogenic TG model also contained neurofilament accumulations, pathology often associated with axonal transport deficits. Confirming the presence of pathology in the NMJ prompted a more in depth examination of the ultrastructure of these diseased NMJs. Pre- and postsynaptic features were systematically measured in electron micrographs of NMJs from affected myogenic TG and KI males and their respective WT brothers. I find several indicators of pathology in the ultrastructure of diseased NMJs, including a widening of the primary synaptic cleft indicating that acetylcholine and other signaling molecules released from the nerve terminal may have a delayed or weaker postsynaptic effect. In the myogenic TG model we observe a decline in the number of docked vesicles ready for release in nerve terminals corresponding to recent functional data suggesting decreased quantal content in this model. In the KI model, secondary postsynaptic folds are also simplified, with wider, yet deeper, folds. The strikingly abnormal morphology of NMJs in these models raises the possibility that synaptic function is impaired and that diseased mice

may be less effective in triggering muscle fiber contraction. Such synaptic dysfunction may contribute to or underlie the impairments in motor function associated with SBMA.

Introduction

Neuromuscular diseases are typically thought to originate in the motoneuron, progressing distally to affect their target muscles. However, in many models of neuromuscular disease, pathological changes in muscle and at the neuromuscular junction (NMJ) are among the first indications of disease, seen well before pathology in the motoneurons (Balice-Gordon et al., 2000, Frey et al., 2000, Fischer et al., 2004, Katsuno et al., 2006a, Yu et al., 2006, Kariya et al., 2008, Yoshikawa et al., 2009). This observation raises the possibility that disease may originate in muscle first, later affecting motoneurons. Despite substantial evidence suggesting that the NMJ may be an early site of pathology for many motoneuron diseases, whether NMJs are affected by disease in spinal bulbar muscular atrophy (SBMA) is largely unexplored.

SBMA is a progressive, late onset neuromuscular disease that results in motoneuron loss, muscle weakness, and atrophy. Its known cause is an expansion of a CAG/glutamine repeat (polyQ) in the first exon of the *androgen receptor (AR*) gene (Fischbeck et al., 1991). Recent evidence suggests that expression of the disease depends not only on having the known disease allele of *AR*, but also on male levels of testosterone (T), possibly explaining why only males are clinically affected (Katsuno et al., 2002, Kinirons and Rouleau, 2008, Johansen et al., 2009). The hallmark pathology of SBMA is motor neuron loss in the anterior horn of the spinal cord and in the brainstem motor nuclei, but skeletal muscles are also affected (Kennedy et al., 1968,

Sobue et al., 1989). Indeed, examining muscle biopsies reveals that affected muscles contain both atrophic and hypertrophic fibers suggestive of neurogenic causes, but also angular and/or split fibers and fibers with internalized nuclei suggestive of primary myogenic causes (Kennedy et al., 1968).

While denervation of NMJs is perhaps the most easily detected change during disease, *any* alteration to the motor nerve terminal, the associated terminal Schwann cell (tSCs) or the muscle endplate has the potential of affecting synaptic function and thus motor function. Models of another neuromuscular disease, spinal muscular atrophy (SMA), exhibit no signs of anatomical denervation but nonetheless show both morphological and functional changes consistent with the idea that such changes may underlie the loss of motor function in this disease (Kariya et al., 2008). Notably, these pathological changes at the NMJ were found to precede overt deficits in motor function.

We are using two different SBMA mouse models to evaluate whether this disease is associated with pathological changes at the NMJ. One model is a transgenic (TG) model in which wildtype rat AR is expressed exclusively in skeletal muscle fibers and will be referred to as the myogenic model of SBMA. The second model is a knock-in (KI) model in which the first exon in the endogenous *AR* gene is replaced by the first exon of the human *AR* gene harboring 113 CAG repeats. Remarkably, despite their genetic difference, both models display common features characteristic of human SBMA, suggesting that both are valid models of this disease. For example, like SBMA in humans, only TG and KI males, and not females, show the expected symptoms of

disease. Likewise, the disease phenotype is androgen-dependent, with symptoms being reversed or prevented when gonads are removed from male SBMA mice. Moreover, diseased males of both models show the expected histopathology in skeletal muscle, including evidence of atrophic fibers and internalized nuclei (Yu et al., 2006, Monks et al., 2007, Johansen et al., 2009, Johansen et al., 2011). Of note, neither model shows evidence of motoneuron cell death at a time when motor function is visibly compromised; raising the question of what might underlie the loss of motor function. Because affected males do show pathological changes in the motor axons as well as changes in muscle gene expression suggestive of denervation (Yu et al., 2006, Monks et al., 2007), we speculate the SBMA may progress as a distal to proximal “dying back” process which begins at the NMJ, as has been suggested for amyotrophic lateral sclerosis (ALS) (Fischer et al., 2004).

In this study, we directly examined the morphology of junctions in myogenic and KI males and compared their junctions to those of age-matched WT controls. Using both confocal and electron microscopy, we conducted an extensive analysis and report striking pathology at the junction including evidence of pre- and postsynaptic morphologic changes. Core features of pathology shared by both models include abnormal endplate morphology and postsynaptic simplification of the NMJ. Not only are these data consistent with the idea that pathology at the NMJ may contribute to impairment of motor function at the behavioral level but also AR acting in muscle fibers as an important source of toxicity for triggering pathology at the NMJ.

Methods

Spinal Bulbar Muscular Atrophy mouse models

KI SBMA model KI mice express a humanized AR from the endogenous *AR* mouse gene containing the first exon of the human *AR* gene with an expanded number of CAG repeats, as previously described (Yu et al., 2006). Because expression of the *AR* gene is controlled by endogenous promoters and enhancers, levels and patterns of mutant protein expression mimic those in wildtype mice. KI males and age-matched Wt controls on a C57/B6J background were obtained from our own breeding colony. Animals with a mean age of 183 days (± 15.92 SEM) were used for the light level analysis and a mean age of 144 days (± 11.9 SEM) when sacrificed for electron microscope imaging.

Myogenic SBMA model Tg mice express a transgene encoding for the full length rat wildtype AR exclusively in skeletal muscle fibers and have been described previously (Monks et al 2007). Tg males and age-matched Wt controls on a C57/B6J background were obtained from our own breeding colony. Given that many Tg males die at birth without intervention, subcutaneous flutamide injections (5mg/0.1ml propylene glycol) were given to pregnant dams on gestational days 15-20 to increase survival. These flutamide rescued Tg males demonstrate the same androgen-dependent disease phenotype as those who did not receive prenatal flutamide (Johansen et al., 2011). Tg and Wt males used for EM analysis were 93 days old (± 0.21 SEM).

Introduction of YFP in Tg mice. Female mice carrying the myogenic SBMA transgene were crossed with transgenic mice expressing YFP in motoneurons (Jackson

Laboratories, stock number 003709). For confocal analysis, we studied the male progeny of this cross—mice carrying a disease-causing *AR* allele or not (control) and the YFP allele. Adult (mean age = 265 days (± 6.49 SEM)) myogenic Tg and age matched control males (both carrying the YFP gene) were used to study NMJs at the light microscopic level.

Animals were group housed on a 12:12 light dark cycle with food and water provided *ad libitum*. Animals were weaned at 21 days and screened for either the expanded repeat region in exon I of the androgen receptor or the HSA transgene promoter using PCR as previously described (Yu et al., 2006, Monks et al., 2007). All animal procedures were approved and performed in compliance with the Michigan State University Institutional Animal Care and Use Committee, in accordance with the standards in the NIH Guide for the Care and Use of Laboratory Animals.

Motor function measurements

Due to the predictable development of the motor phenotype in the myogenic model, animals were tested each of three days prior to muscle harvest to confirm a deficit. Displayed values are the mean of the three test days. On the other hand, KI males show a large degree of variability in the onset of motor deficits and were tested weekly until they demonstrated a 70% deficit compared to WT controls in forepaw, hindpaw, and triangle bar grip strength tests. Displayed behavior for KI animals is the mean of the final testing week.

Motor function was assessed based on measures of grip strength, capacity to hang and activity in the open field test as previously described (Johansen et al., 2009). Male mice were held by the tail and lowered to a grid attached to a force gauge (Chatillon Force Measurement Systems, Largo FL), allowing either forepaws or all paws to grasp the grid. They were pulled perpendicular to the grid with grip force recorded at the moment of release. This test was repeated six times in a single session, with the average of the four median values recorded as the grip strength score for that session and mouse. To assess grip strength of KI mice, the triangle attachment was used as previously described (Yu et al., 2006, Kemp et al., 2009), pulling the tail in the horizontal plane to assess grip strength at the moment of release. The grip strength score for that session was the mean of five scores. For assessing muscle strength based on the hang test in both SBMA models, mice were placed upright on a metal grid 40 cm above the bench top, which was subsequently rotated 180 degrees. Latency to fall was measured up to a maximum of 120 seconds. For the open field test, mice from both models were placed in an open field (VersaMax400, Accuscan Instruments, Columbus, OH) where movement was tracked for five minutes. The system measured movement in the horizontal and vertical planes in addition to the number of movement initiations and time spent moving and resting. The chamber was cleaned with 70% ethanol between animals.

Light microscopy analysis of the NMJ

Immunocytochemistry In KI males, NMJs were stained in the perineal levator ani (LA) muscle which is ideally suited for studying NMJs, given that it is a relatively flat muscle

with a highly defined endplate band. However, we could not study the LA in the myogenic model. The LA requires perinatal androgen to survive and one result of prenatally exposing males to the androgen receptor antagonist flutamide, is that the LA is absent in perinatally rescued males (both Tg and Wt) of the myogenic model (Breedlove and Arnold, 1983, Sengelaub et al., 1989). Consequently, we selected a hindlimb muscle, the anterior tibialis (TA), another fast twitch muscle which does not require androgen exposure for its survival perinatally.

Muscles were harvested from male mice that were deeply anesthetized with isoflurane and pinned flat as whole mounts in Sylgard-coated petri dishes, rinsed thoroughly with cold phosphate-buffered-saline (PBS, 0.14 M NaCl, 2.7 mM KCl, 1.5 mM KH_2PO_4 and 8 mM dibasic Na_2HPO_4 $7H_20$, pH 7.4), fixed for 30 minutes with phosphate-buffered (0.1M, pH 7.4) 4% paraformaldehyde and cryoprotected in phosphate-buffered 20% sucrose for a minimum of three hours. Muscles were longitudinally sectioned on a sliding, freezing microtome at 60 um, generating three series of sections that were subjected to different staining protocols to visualize different elements of the junction (synaptic vesicles, neurofilament or terminal Schwann cells (tSCs)). Postsynaptic acetylcholine receptors (AChRs) were also visualized in all three series. Sections were collected and rinsed as free floating sections in a PBS vehicle containing triton X-100 (0.3%), bovine serum albumin (0.2%) and sodium azide (0.1%) and incubated overnight at room temperature in PBS vehicle containing primary antibody directed against one of the three elements of the junction. The following day, sections were rinsed in vehicle and incubated for two hours in vehicle containing fluorescently tagged secondary and α-

bungarotoxin. In the first series, synaptic vesicles were labeled using a rabbit anti-synaptophysin polyclonal primary (Zymed, 18-0130, diluted 1:50) and visualized with a sheep anti-rabbit Cy-3 labeled secondary (Sigma, C2306, diluted 1:100). In the second series, tSCs were labeled using rabbit anti-S100 polyclonal primary, a Schwann cell specific antigen (Dako, Z0311, diluted 1:400), and visualized with the same Cy-3 labeled secondary. The final series of sections was labeled using a mouse anti-neurofilament monoclonal antiserum (Developmental Studies Hybridoma Bank, 2H3 diluted 1:200) and visualized with a rabbit anti-mouse TRITC labeled secondary (Sigma, T2402, diluted 1:100). Acetylcholine receptors were labeled in all three series using AlexaFluor 647 conjugated alpha-bungarotoxin (Invitrogen, B35450, diluted 1:100). Moreover, motor axons and their nerve terminals were visible in all series by virtue of YFP transgene expression. After several final rinses in PBS vehicle, muscle sections were mounted onto gel-subbed slides and allowed to dry in the dark for at least 24 hours. Slides were then dehydrated in graded ethanols, cleared in Hemo-De, and coverslipped using DPX, a non-fluorescing coverslipping medium. All fluorescently labeled material was stored at -20°C after the DPX had set.

Confocal Imaging Sequential confocal images of the general structure and overlay of the presynaptic and postsynaptic junctions were taken on a Zeiss LSM 510 Meta Confocal Microscope (Carl Zeiss, Oberkochen Germany) at the Center for Advanced Microscopy at Michigan State University (www.ceo.msu.edu). Areas of interest were located using epifluorescent illumination beginning at one margin of a muscle section and systematically working along the endplate band. Only junctions that presented in an

en face orientation were imaged. Images were scanned using an Olympus 63x 1.4 NA oil objective, without digital zoom. The confocal pinhole aperture was set to 1.11 Airy disk, the image size was set at 1024x1024 pixels and the Z-step size was set at 0.9um. For each junction, a stack of images was collected through the entire depth containing visible signal. Lasers at 488, 543 and 633 nm were used in sequential mode to visualize different components of the same junction and ensured no crossover from other channels. Each of the channels was visualized independently to determine there was no channel crossover. For each of the series and labels, channel settings were optimized and then held constant for the following parameters: laser power, detector gain, amplifier gain, pinhole and offset. Image processing was completed using Zeiss LSM Image Browser.

Confocal Image Analysis For each animal, twenty *en face* junctions were imaged and analyzed for each stained series. Images of NMJs were constructed by making projections of the most intense pixel from each plane through the Z-axis for each of the three laser channels to create a composite image of a junction.

Using the YFP/synaptophysin-labeled series, we quantified 1) the extent of partial or full denervation (defined by exposed acetylcholine receptor footprints lacking overlying nerve terminal), 2) area of endplates, based on area occupied by AChR staining, 3) the degree of junctional fragmentation (fully connected pretzel-like pattern of receptor labeling (none), a pattern of partially disconnected AChR-rich domains (partial) or completely punctate domains (complete)) and 4) area of synaptophysin staining (Table

1). Using the YFP/neurofilament labeled series, we counted 1) the number of neurofilament accumulations in the terminal and the preterminal axon and 2) the number of terminal and collateral sprouts (Table 2). Finally, using the YFP/tSC labeled series, we counted the number of tSCs and assessed their morphology by counting the number of tSCs sprouts, defined as fine processes extending beyond the outer perimeter of the endplate as marked by AChR staining (Table 3). To assess area occupied by either synaptophysin or AChR staining, images were exported from Zeiss LSM Image Browser, cropped in Adobe Photoshop CS5, subjected to unsharp mask filter (parameters set to amount:500, radius:50, and threshold:1) and thresholded. When thresholding, the grey values of the unsharp mask image were adjusted to the best fit of the original image. Thresholded images were re-opened in ImageJ and the number of pixels occupied by synaptophysin or AChR staining were quantified using the Analyze Particles function. Corresponding thresholded images of presynaptic and postsynaptic staining of individual junctions were used to determine the percent of synaptophysin staining covering the endplate. ImageJ was also used to measure the width of muscle fibers at the middle of the junctions in the max projection images from the synaptophysin-labeled series.

EM analysis of NMJ morphology

Fixation The LA in the KI model and the EDL in the myogenic model were harvested from male mice deeply anesthetized with isofluorane. The TA muscle was not satisfactory for EM because its large size, as well as the need to do the initial fixation *in situ*, led to uneven fixation. Muscles were pinned under tension in Sylgard dishes,

cleaned, and allowed to recover at room temperature for 5 - 30 minutes in oxygenated Normal Mouse Saline (135 mM NaCl, 5 mM KCl, 2 mM $CaCl_2$, 1 mM $MgCl_2$, 14 mM Hepes buffer, 11 mM dextrose, pH 7.4). Muscles were then incubated in cold 0 Ca++ Normal Mouse Saline (same recipe as above with $CaCl_2$ omitted and replaced by equimolar amounts of $MgCl_2$) for 2 - 7 minutes. Muscles were then fixed using a cold aldehyde fixative (4% paraformaldehyde, 1% glutaraldehyde, in 0.1 M Millonig's phosphate buffer, pH 7.2) for two to two and a half hours at 4°C. During this time, small pieces of the muscle were dissected and placed in vials of fresh fixative. After aldehyde fixation, the muscle pieces were rinsed six times in 0.1M Millonig's phosphate buffer, pH 7.2 and left overnight at 4°C. Samples were postfixed in 1% OsO_4 in 0.1M Millonig's phosphate buffer for two hours, rinsed in buffer, and then dehydrated in a graded series of ethanols and propylene oxide. They were then infiltrated in a graded series of proplylene oxide/Araldite 502 resin mixtures to 100% resin over a period of 24 hours. The pieces of muscle were flat embedded in aluminum dishes and the resin was cured at 60°C under vacuum for three days.

Sectioning and Imaging Blocks were thick sectioned perpendicular to the long axis of the muscle fibers until junctions could be identified at which point ultrathin sections were taken. Thin sections were stained with 10% uranyl acetate in 50% methanol and Reynold's lead citrate. The last thick section cut prior to taking thin sections was photographed with a light microscope, and individual junctions were identified and numbered. Every junction identified in the block face was photographed using the

electron microscope (JEOL 100CX, Michigan State University Center for Advanced Microscopy) at 80kV at three magnifications. Each junction was first imaged using a lower magnification to provide contextual information about the profile, an intermediate magnification, and all measurements were taken using high magnification (approximately 20,000X) to provide adequate detail for extensive quantitative analysis. Exact magnifications were determined by photographing a calibration grating of 2160 lines/mm.

Plastic negatives (3.25” x 4”) were developed and scanned with an Epson Perfection V750 Pro scanner at 600 dpi and the resulting files saved for analysis without further enhancement.

Presynaptic EM measures Measured presynaptic features include the entire membrane bound terminal profile and, alternatively, the profile area not including mitochondria or large vacuoles. Mitochondrial cross sectional area and density were also measured. In addition to the determination of a straightforward profile vesicle density measure, a second vesicle density from the area 480 nm from the synaptic cleft was measured with the aim of targeting the density of the pool of readily releasable vesicles. Vesicle diameter was measured from this subset of vesicles by taking the horizontal and vertical diameter from the center of each vesicle that fell with in the 480 nm range from the synaptic cleft. The aspect ratio of the horizontal and vertical diameter of these vesicles was used as a measure of vesicle roundness to determine vesicle shape differences. Details on these measures are further defined in Table 4.

Postsynaptic EM measures We also extensively measured features of the primary and secondary synaptic clefts. Measures such as the secondary cleft number (defined as the indentation area between two postsynaptic folds that is deeper than 104.5 nm), the entire perimeter of the postsynaptic folds and secondary clefts, and the number of active zone regions (an electron dense regions directly across from a secondary cleft) were taken. These features were divided by terminal apposition length, defined as the distance beginning at one end of the presynaptic terminal directly across the cleft from the center of the first visible postsynaptic fold and finishing directly opposite the center of the final postsynaptic fold, to maintain consistency between terminal profiles when the terminal contact length was variable. While we were evaluating the number of active zone densities, we also measured the number of active zones occupied by vesicles (those actually touching the presynaptic membrane across from a secondary cleft), presumably that were docked and prepared for release. The area and depth of the synaptic cleft and the area, width and depth of the secondary cleft were also measured. When there were multiple measures per terminal profile, the values were averaged together so that N=terminal profile. Details on these measures are further defined in Table 5.

In addition to the numerous quantitative measures, profiles were qualitatively evaluated, noting evidence of anomalous features in the appearance of tSCs, structures in the terminal, or abnormalities in the profile structure that might indicate pathology associated with disease.

EM Image Analysis Each election micrograph was digitally scanned at 600 dpi. From the entire selection of available images, one full profile at the highest magnification that showed clear postsynaptic folds, presynaptic densities representing active zones, and tSCs was randomly chosen for quantitative analysis from each junction. Ten different junctions per animal were sampled. Digitized images were opened in Adobe Photoshop and precisely aligned to reconstruct a junction if the profile filled more than one view frame. Using the Photoshop Layers feature, numerous layers were superimposed upon the original image, and each layer was used to trace, count, or measure various features of the terminal profile and exported from Photoshop as individual files. Layers that required area, length or number measurements were reopened in FIJI (Schindelin et al., 2012), a mask was created, and then measurements were taken, with Particle Count applied for estimating number of objects. Layers featuring non-straight lines were opened in Adobe Illustrator and Live Trace was used with a threshold of 184 to produce a continuous stroke from which the continuous path length could be read.

Statistical analysis

Single measures were compared using independent t-tests comparing each experimental group to its age matched WT control. Results are presented as group means (N= number of animals/group for the light microscope analysis and junction/group for the EM analysis) ± standard error of the mean (SEM).

Results

SBMA models show the expected deficit in motor function.

As expected, myogenic TG males demonstrate profound motor deficits in all measures (Monks et al., 2007, Johansen et al., 2011). Both fore- and hindpaw grip strength and hang tests reveal significant deficits when compared to WT controls (Fig. 6A - C; p-values < 0.001 for all measures). In contrast to the severe deficits seen in the myogenic model, effects on motor function in KI males is much more subtle. Nonetheless, significant deficits were apparent in both fore- and hindpaw grip strength (Fig. 6D and 1E, ps < 0.05). Since grip strength in this model was originally characterized based on a triangle bar rather than the grid (Yu et al., 2006), we also assessed grip strength using the triangle bar and confirmed the deficit previously reported based on this method (84.4 g ± 18.4 g for WT and 41.1 g ± 1.6 g for KI, $p < 0.02$). However, we saw no deficit based on the hang test in KI males (Fig. 6F).

Diseased NMJs are morphologically intact with no evidence of denervation.

We initially began by looking for morphological evidence of denervated endplates in TA muscles of affected TG and the LA of KI males, given that terminal retraction from junctions is commonly observed in mouse models of neuromuscular disease (Frey et al., 2000, Pun et al., 2006). Additionally, muscles of diseased males from both models show upregulated expression of molecular markers suggestive of denervation (Yu et al., 2006, Monks et al., 2007). Our approach was to label the axon and nerve terminal using antibodies directed against synatophysin and neurofilament proteins (in combination with YFP expressing motoneurons for the TG animals) and label the postsynaptic

endplate using fluorescently-tagged α-bungarotoxin. NMJs were evaluated for evidence of denervation based on whether the endplate marked by AChR either fully or partially lacked an overlying nerve terminal. Despite the molecular evidence suggesting otherwise, we find that no evidence of synaptic retraction of the junction from muscles in either the myogenic TG or KI models. Indeed, we find precise alignment of pre- and postsynaptic features at virtually every endplate (merged images in Fig. 7A and 7B) indicative of complete innervation (Fig. 7C and 7E). Given that physical denervation did not appear to contribute to the decrease in motor strength nor underlie the increased expression of genes associated with denervation, we next examined the NMJ for other signs of pathology that might account for these dysfunctions.

Disease is associated with fragmented NMJs.

In both models, we find a pronounced change in the configuration of the NMJ in muscles from diseased SBMA males. While normal mammalian junctions typically have a continuous pretzel-like appearance, diseased junctions in the two SBMA models have a distinct fragmented appearance, comprised of many small punctuate domains (Fig. 7A and 6B). In the myogenic model, quantitative analysis of TA endplates show that few (1.25% ± 1.25) WT junctions are fragmented whereas most (96.25% ± 3.75%, Fig. 7D, $p < 0.05$) are fragmented in TGs. Furthermore, over 60% of TG endplates display an extreme degree of fragmentation with only about 28% showing partial fragmentation (Fig. 7G). NMJs in affected KI animals also look fragmented (Fig. 7B), but as expected, this phenotype is not as severe as in TG males. Of the ~60% of junctions in the LA muscle of KI males that are fragmented (Fig. 7F), nearly 40% are partially fragmented

where as complete fragmentation is the predominant phenotype in TG (Fig. 7G versus 7H), with nearly 80% showing this phenotype as opposed to 20% in KIs. Nonetheless, LA muscle from KIs contains significantly more fragmented junctions compared to WT LA (Fig. 7F, $p < 0.05$), indicating its pathological nature. However, it is notable that the LA from WT males contains an appreciable number (~25%) of fragmented junctions. Obviously, junctions in the LA are inherently more fragmented than junctions in the TA, the muscle examined in the myogenic model. This difference may be related to their different functions. Nonetheless, it is important that disease in *both* models is associated with fragmentation of the NMJ, despite expressing quite different disease alleles. These data beg the question of whether fragmentation of junctions might also occur in men affected by SBMA and be causally linked to neuromuscular dysfunction in men with SMBA experience.

Disease is associated with smaller muscle fibers in both models but smaller endplates only in the myogenic model.

We find that the size of endplates and muscle fibers in the TA of myogenic males is decreased significantly compared to their sizes in WTs (Fig. 8A and 8B, ps < 0.035). In contrast to the myogenic model, the size of endplates in the KI LA is unchanged (Fig. 8C), but as previously shown (Yu et al., 2006) the size of LA muscle fibers is reduced in this model (Fig. 8D, $p = 0.003$).

Disease is associated with abnormal synaptophysin staining only in the myogenic model.

We have previously shown that both models have a defect in the retrograde transport of endosomes, which likely originates in the motor nerve terminal (Kemp et al., 2011). This prompted us to examine synaptophysin staining as an indirect measure of the distribution of synaptic vesicles in nerve terminals. Additionally, synaptophysin accumulations in perijunctional, preterminal axons has been reported in SBMA mice (Katsuno et al., 2006a). Thus, we assessed the distribution of synaptophysin in the nerve terminal and its preterminal axon. We find an increase in the amount of nerve terminal containing synaptophysin (i.e., "synaptophysin coverage") in TGs compared to WTs (0.748 ± 0.155 versus 0.451 ± 0.067, respectively; Fig. 9A and 9B), though this difference fell short of significance ($p = 0.125$). We also find that 35% of junctions in diseased TG males had abnormally located synaptophysin in the preterminal axon (just proximal to the terminal) compared to only ~1% of junctions in WT males (Fig. 9A and 9C $p = 0.004$). The unusual pattern of synaptophysin labeling is consistent with transport dysfunction in motoneurons of diseased SBMA mice reported previously (Table 6). Although none of the abnormal synaptophysin distribution was found in LA junctions of KI males (Table 7), we did find comparable synaptophysin pathology in the TA of KI males (Table 8), consistent with the transport dysfunction seen in motor axons which innervate this muscle (Kemp et al., 2011).

NF accumulations are present in the myogenic model.

One factor potentially affecting endosomal movement is the condition of the neurofilament proteins in the cytoskeleton. Indeed, we find substantial evidence for neurofilament accumulations in both nerve terminals and preterminal axons in muscle of diseased myogenic males (Fig. 9D and 9E). Large, bulbous enlargements comprised of neurofilament proteins were rare in WT control axons, but over 50% of motor axons showed evidence of neurofilament accumulations in diseased myogenic muscle (Fig. 9F, $p < 0.05$). Similarly, over 40% of nerve terminals in diseased muscle contain neurofilament accumulations whereas ~8% of WT nerve terminals contained comparable accumulations (Fig. 9G, $p = 0.005$). There was no evidence of presynaptic neurofilament accumulations or in the terminal of the KI model, neither in the LA (Table 7) nor TA muscle (Table 8).

Pathology in the ultrastructure of nerve terminals.

Results from the light level analysis prompted a more in depth evaluation of potential pathology at the NMJ at the ultrastructural level. In particular, the abnormal distribution of synaptophysin prompted questions about the distribution of synaptic vesicles, which could only be assessed at the electron microscopic level. Qualitatively, terminal profiles in both models look quite normal. Nerve terminals in neither model showed evidence of neurofilament accumulations, altered distribution of vesicles, or abnormal features of internal structures, such as unusual mitochondrial cristae. Moreover, quantitative measurements indicated no differences between WT and diseased nerve terminals in terminal profile size, vesicle size, overall vesicle density, or the density of vesicles in the

readily releasable pool (Table 11 for TG data, Table 12 for KI data). As expected, the vesicle density in the readily releasable pool (measured in a 480 nm band across from the secondary clefts) was about twice as dense as the overall vesicle pool. Despite the general normal appearance of the junctions, several features of pathology stood out. For example, in the myogenic model, the size of mitochondria was increased in diseased nerve terminals compared to WT controls (Fig. 10A and 10B, $p = 0.004$). While the number of mitochondria was increased in the myogenic model compared to WT controls, this apparent difference was not significant (Table 11). Neither the size nor number of mitochondria was affected in diseased KI males (Table 12).

While we find no difference in overall vesicular distribution, we refined our analysis by quantifying the number of active zones and assessing whether or not they contained docked vesicles (Fig. 10C, arrows indicate active zones with docked vesicles in WT and active zones without docked vesicles in TG). In the myogenic model, we find no disease-related difference in the number of active zones (Table 11), but we did find a striking decrease in density of vesicles docked at active zones in myogenic males compared to the WT controls (Fig. 10D, $p = 0.032$). Consequently, the proportion of active zones without docked vesicles was also increased by disease (Fig. 10E, $p = 0.037$). However, we find no effect of disease in the KI model on active zones, either on their overall number or those containing docked vesicles (Table 12).

We also find disease-related changes in the shape of vesicles in both SBMA models. To evaluate the shape of vesicles, we measured the length of each vesicular axis in the

readily releasable pool to create an aspect ratio, which provides information on the roundness of each vesicle. We find that vesicles in both the TG and KI models are less round than those in matched WT controls (Fig. 10F, H, $p < 0.01$ and $p = 0.024$, respectively). While there was no difference in mean vesicular diameter in either model (Table 11 for TG data and Table 12 for KI data), the distribution of vesicle sizes appeared somewhat narrower, centering more around the mean in diseased versus controls in both models, although this difference was not significant (Fig. 10G and 10I).

Pathology at the primary cleft.

A factor that could impair synaptic signaling to the muscle is the width of the primary cleft. This represents the distance acetylcholine must travel before reaching the muscle (distance demarcated by thick lines in Fig 11A). Measuring distance from the top of each postsynaptic fold to the outer plasma membrane of the nerve terminal revealed that disease in both models is associated with an increased width in the primary cleft (Fig. 11A – D; $p = 0.040$ and 0.001 for TG and KI models, respectively).

Pathology in the ultrastructure of the postsynaptic specialization.

Models of neuromuscular disease often show a simplification of the postsynaptic folds that constitute the secondary clefts, manifesting as shallower clefts, and wider cleft mouths (Deconinck et al., 1997, Slater et al., 2006, Kariya et al., 2008). We find that diseased muscle from KI males showed a striking simplification in postsynaptic features. Whereas the WT secondary folds have closely spaced, long, thin structure of typical junction profile, the KI secondary clefts are spaced further apart, are wider, and larger in

area (Fig. 11E). However, KI males showed an increase in the postsynaptic perimeter compared to WT controls (Fig. 11F, $p = 0.01$). As an added measure of secondary fold complexity, the number of secondary cleft terminations was counted and averaged for each junction profile. We found an increase in the number of terminal branches in KI males compared to WT controls (1.44 terminations per cleft ± 0.05 and 1.19 terminations ± 0.03, respectively, $p < 0.000$). While the number of secondary clefts did not differ between KIs and WTs (Table 14), both the width at the mouth of the fold (indicated by the horizontal lines in Fig. 11E) and the depth of the cleft (indicated by dotted lines in Fig. 10E) were significantly increased in KI males (Fig. 11H and I, $ps < 0.001$). While measures of secondary folds in diseased myogenic males indicated that secondary clefts were wider and shallower, creating a shorter postsynaptic perimeter and fewer terminal branches, these changes were not significant (Table 13).

Discussion

The effects of SBMA on NMJs has not been previously explored, despite considerable precedence in models of other motoneuron diseases showing junctions are vulnerable to disease (Balice-Gordon et al., 2000, Frey et al., 2000, Fischer et al., 2004, Katsuno et al., 2006a, Yu et al., 2006, Kariya et al., 2008, Yoshikawa et al., 2009). Thus, we examined NMJs in chronically diseased males of two different SBMA mouse models, a muscle-specific TG model in which a wildtype allele of the AR is overexpressed exclusively in muscle fibers (referred to as the myogenic TG model) and a KI model expressing the endogenous mouse AR gene containing the first exon from the human *AR* gene harboring a disease-causing CAG expansion (Monks et al. 2007; Yu et al. 2006). We used both confocal and electron microscopy to characterize the effects of

disease on NMJs. We find that both models exhibit some of the same pathology at the NMJ, most notably, junctional fragmentation, commonly observed in models of other motoneuron diseases. While widely assumed to arise via action of the disease allele directly in motoneurons (Kennedy et al., 1968), it is noteworthy that the same sort of junctional pathology is evident in models of muscular dystrophy (Grady et al., 1997), strictly a myogenic disease. Given that the disease allele acts solely in muscle in the myogenic model, it is likely that fragmentation and postsynaptic simplification of the junction, which are seen in both the myogenic and KI models, are triggered by action of the disease allele directly, and perhaps exclusively, in skeletal muscle. This argues for a role of muscle in determining the fate of motoneurons in disease. Additionally, obvious pathology was seen in the myogenic model in the form of neurofilament accumulations and abnormal synaptophysin distribution. These findings support the ideology that SBMA is neither a motoneuron nor muscle based disease, but rather expression in one cellular system can result in expression of pathology in the other.

Males in both models showed marked androgen-dependent impairments in motor function (Fig. 6). The associated muscle atrophy and changes in muscle gene expression seen in both models suggest this loss of motor function may be mediated by a loss of muscle innervation (Yu et al., 2006, Monks et al., 2007). However, we found no evidence supporting the idea that muscle fibers were denervated. For every endplate examined in diseased muscle of both models, we found an overlying nerve terminal, precisely aligned with the underlying postsynaptic endplate as is typical of normal endplates, with no part of the endplate exposed due to retraction of the nerve terminal.

Neither did we see evidence of denervation at the ultrastructural level. In short, disease is not associated with morphological denervation of the endplate in these two models of SBMA, not even partial denervation. However, these results do not rule out the possibility muscles are becoming *functionally* denervated, meaning that nerve terminals lose their ability to reliably elicit fiber contractions, which could explain why diseased muscles exhibit characteristics typical of denervation, such as angular atrophic fibers, elevated levels of AChR mRNA, and enhanced spontaneous activity, despite the apparent lack of morphological evidence for denervated endplates.

The morphology of the NMJs in both models were strikingly abnormal, with marked fragmentation comparable to what has been reported previously for other mouse models of neuromuscular disease, including one of distal SBMA (Grady et al., 1997, Shiao et al., 2004, Slater et al., 2006, Chevalier-Larsen et al., 2008, Pratt et al., 2013). It is important to note that while separate clusters of AChRs comprise the postsynaptic endplate, the overlying clusters of nerve terminal are interconnected via fine processes that appear to lack the synaptic machinery necessary to be functional (data not shown).

The cause behind this pathology which shifts junctions from the normal pretzel-like appearance to distinct and apparently separate punctate domains is still unknown, but mechanisms of aging may be involved (Butikofer et al., 2011). When agrin, a motoneuron-derived proteoglycan that stabilizes the junction, undergoes enhanced cleavage, endplates become notably fragmented in mouse models of aging. Of note, even though agrin and the protease neurotrypsin, which cleaves agrin, are both

expressed in motoneurons, the effect of this enhanced cleavage is realized at the level of the muscle fiber basal lamina, where fully intact agrin normally acts to inhibit the AChRs dispersal. The distribution of agrin and neurotrypsin underscores the importance of birectional communication between motoneurons and muscle fibers at the synaptic interface. Fragmented junctions in other models of neuromuscular disease have been attributed to terminal Schwann Cells (tSCs), which are thought to extend their processes into the primary cleft to wrap around and eventually engulf nerve terminals for their removal from the junction (Miledi and Slater, 1970, Jirmanova, 1975). While our EM analysis did not reveal any signs of tSC invasions into the primary cleft, we did note that the small interconnectives between bulbous contacts appeared fully ensheathed by tSCs. Such ensheathing did not align with postsynaptic densities or folds that would suggest this area of the junction is or was once functional. However, given the chronic nature of the disease in both models, it is still possible that this region of synaptic contact was once functional. On the other hand, both models express their respective disease alleles from very early in development, so it is possible that some aspect of the normal maturation of NMJs was affected by the disease allele. Androgen during postnatal development can arrest the normal maturation of NMJs, by arresting synapse elimination but also inducing a persistent and stably maintained fragmented morphology (Jordan et al., 1989a, b). It is clear, however, that NMJs in diseased muscle have developed normally in many ways, since postsynaptic folds are well developed and fibers are singly, and not multiply, innervated. Given that we find no evidence of junctional fragmentation in acutely diseased female myogenic mice (Kemp et al., 2011),

it is likely that junctional fragmentation does not mediate the loss of motor function and rather is a secondary effect of chronic disease.

It is noteworthy that such fragmentation of the junction is present in both models, albeit less severe in the KI model, indeed correlating with the less severe motor phenotype seen in KI males. Because the disease allele is exclusively expressed in muscle fibers in the myogenic model, these data suggest the pathological change at the junction is induced by AR toxicity originating from the muscle. The idea that pathological signals from the muscle can induce such changes is supported by evidence of comparable fragmentation of NMJs in muscles from muscular dystrophy models, where either utrophin or dystrophin is knocked out of muscle (Lyons and Slater, 1991, Grady et al., 1997). Interestingly, the phenotype of fragmented junctions was seen entirely in regenerated connections with the muscle and no direct effect on the function of the junction was noted (Lyons and Slater, 1991). The importance of postsynaptically-located dystrophin suggests that synaptic maintenance occurs through association with the muscle cytoskeleton (Banks et al., 2009). A *Drosophila* model of SMA also displays similar alterations to junction morphology when SMN (survival motor neuron, an ortholog of the *Survival Motor Neuron* gene) expression is eliminated in muscle, although a similar but less severe effect occurs when expression is eliminated from the motoneuron (Chan et al., 2003, Chang et al., 2008). Like agrin, SMN is localized in the postsynaptic junction, and *not* presynaptically in the nerve terminal, continuing to underscore the muscle's importance in controlling this aspect of NMJ morphology.

Other junctional pathology shared by both models includes a wider primary cleft, meaning that released neurotransmitter must travel further before binding to postsynaptic AChRs. Increases in the distance that neurotransmitter must diffuse results in a slower rise to peak concentration of neurotransmitter at the postsynaptic receptors and a reduced peak (Renger et al., 2001). This aspect of the disease phenotype could lead to weaker synapses. Similar widening of the synaptic cleft in myasthenia gravis and muscular dystrophy models (Engel and Santa, 1971, Law et al., 1983) are associated with decreases in synaptic strength (Conti-Fine et al., 2006, Wairkar et al., 2008). Other evidence suggests that a wider cleft also decreases the electrical resistance within the cleft, which also adds to the reduction in local receptor currents (Savtchenko and Rusakov, 2007). Interestingly, both modeling and altering physiological parameters indicate the motoneuron and muscles appear to have the capacity to actively regulate the width of the synaptic cleft to maximize synaptic strength, an ability that may be impaired in diseased junctions (Savtchenko and Rusakov, 2007).

Compounding the effect of less acetylcholine reaching the postsynaptic membrane due to the widened primary cleft width is the increased proportion of active zones without docked vesicles in the myogenic model. Defects in retrograde transport have largely been attributed to deficits in endosomal flux. This suggests that vesicular trafficking within the nerve terminal is impaired and may be behind the reduction in docked vesicles (Kemp et al., 2011). If mobilization of vesicles is impaired, or there are issues with targeting them for their intended destination, it could cause the apparent reduction

in docked vesicles. Other studies show decreases in the number of docked vesicles when endocytotic functions are impaired, suggesting that the diseased junctions may specifically have problems with vesicular turnover (Renger et al., 2001). Although we saw more empty active zones at diseased junctions than normal, this may not be an accurate indicator of vesicles in the readily releasable pool, since evidence suggests some of the docked vesicles are not immediately releasable and there is no discernable morphological difference between those that are and those that are not (Rettig and Neher, 2002). Although considerably more work is needed, preliminary results from intracellular recording of muscle synaptic potential indicate significant deficits in quantal content in both the myogenic and KI models of SBMA (Xu and Jordan, unpublished observation), indicating that fewer quanta are released from the nerve terminal upon activation.

The flux deficit in TA axons (Kemp et al., 2011) may also be behind the aberrant accumulation of synaptophysin in both nerve terminals of TA junctions in the myogenic and KI models, and in the preterminal segment of axons in the myogenic model. Although the KI males did not have any change in synaptophysin distribution in the LA muscle, they did show increases in synaptophysin coverage in the TA, which suggests different muscle types are differentially affected by disease. However, we did not observe an alteration in vesicular distribution at the ultrastructural level as expected, with the exception of the deficit in docked vesicles. There are a variety of reasons for why we may not have detected a change in vesicular distribution that actually exists. First, synaptophysin-containing vesicles may represent only a subset of the total

vesicles examined, washing out our ability to detect specific effects that may be limited to only a specific subpopulation at the EM level. Previous evidence suggests that vesicles containing synaptophysin are sorted into distinct subtypes (Leube et al., 1994) and localized to small vesicles, specifically colocalizing with early endosomal markers (Feany et al., 1993). It is also possible that disease only affects synaptophysin-containing vesicles in the preterminal segment, which we did not analyze at the ultrastructural level. Third, we simply may not have had sufficient power to detect what may be subtle differences in the overall distribution of vesicles in the nerve terminal. While we saw no alterations in overall vesicle density or size in either model, we did find that the shape of vesicles in both models was more ovoid then in WT controls. Changes to the shape of vesicles has previously been shown to be affected by the osmolarity or the content within vesicles (Thureson-Klein et al., 1975, Langmeier et al., 1986) and recent activation of the nerve terminal has been associated with less round vesicles (Jones and Kwanbunbumpen, 1970, Korneliussen, 1972, Heuser and Reese, 1973, Pysh and Wiley, 1974). Regardless of why vesicles might be less round than those in WT terminals, the fact that both models show this same change in vesicular shape suggest it is a core feature of disease at the neuromuscular synapse and may shed light mechanisms that effect synaptic function in disease.

In the myogenic model, it possible that the reduced size of endplates leads to less acetylcholine release, causing synapses to fall below threshold. However, we also find that the size of muscle fibers is similarly decreased, so a net reduction in the amount of acetylcholine released by the nerve terminal may not result in failure to trigger an action

potential in the muscle fiber. On the other hand, the amplitude of endplate potentials are indeed smaller in diseased muscle from myogenic males due to a significant drop in quantal content (Xu and Jordan, unpublished data), suggesting that a loss of synaptic function may indeed underlie the denervation-like profile seen in diseased muscle. In contrast, there was no change in endplate size in KI males despite a significant decrease in fiber size. This might actually lead to a net strengthening of the synapse, if all else stayed the same, but recordings of synaptic potentials suggest otherwise (Xu and Jordan, unpublished data), consistent with the denveration-like profile also seen in muscles of KI males (Yu et al., 2006). That disease is associated with smaller endplates in the myogenic model but not in the KI model, despite evidence of muscle atrophy in both, may be related to differences in the time course of disease. Myogenic males show impaired motor function from birth, whereas KI males develop a mild motor phenotype over months, emerging sometime in adulthood. Thus, it is possible the slow progression and later onset of disease in KI males allowed junctions to develop normally, and perhaps better maintain junctional morphology in the face of ensuing disease. Junctions in myogenic males are very likely abnormal from early on. Regardless, it seems improbable that atrophic endplates or muscle fibers can account for the loss of motor function as myogenic TG mice can show profound impairments in motor function without decreases in either muscle fiber or endplate size (Kemp et al., 2011, Oki et al., 2013).

Disease was also associated with wider and deeper secondary clefts, but only in the KI model, though trends of wider secondary clefts were also seen in the myogenic model.

Such changes provide more membrane for AChRs at the crests of the fold and for sodium channels in the depths of the clefts. These alterations enhance the effect of released neurotransmitter and lower the threshold for depolarization of the muscle fiber, potentially an appropriate modification in a diseased system that may be struggling with weakened synapses (Flucher and Daniels, 1989). Of note, dystrophin promotes the development of complex folds (Banks et al., 2009) (Torres and Duchen, 1987, Lyons and Slater, 1991, Deconinck et al., 1997, Grady et al., 1997) raising the possibility that SBMA may involve some of the same mechanisms of disease as muscular dystrophy. Thus far, evidence suggests that critical mechanisms mediating myotonic dystrophy are also relevant to the disease state in muscles of KI males (Yu et al., 2006, Yu et al., 2009).

Mitochondrial size was increased but only in myogenic TG males and density of mitochondria area in the terminal was also increased for KI males, but not significantly so. This result was expected given previous results in a cell culture model of SBMA indicating an increase in mitochondrial mass, number, and size (Ranganathan et al., 2009). Additionally, enlarged mitochondria have been previously noted in the muscle of the myogenic TG males (Musa et al., 2011). Upregulation of mitochondria size and number in disease states is a fairly common phenomenon and is reliably associated with other disease pathology (Lin and Beal, 2006, Keating, 2008, Di Carlo et al., 2012), specifically in myotonic dystrophy (Oude Ophuis et al., 2009, Rusconi et al., 2010). These changes in mitochondria result in functional changes such as decreased

mitochondrial membrane potential, increased reactive oxygen species, and increased oxidative metabolism (Musa et al., 2011).

It is interesting that neurofilament accumulations were found in the axons and presynaptic terminals of muscle in the myogenic model, but not in the KI model given that the disease allele is expressed in both motoneurons and muscle in the KI model but only in muscle of the myogenic model. It is possible the lack of neurofilament accumulations in the KI model is related to the mild disease phenotype, raising the possibility that only some perturbations would be expected in this model. While clear evidence of neurofilament accumulations was found in the myogenic model based on confocal microscopy, we saw no evidence of neurofilament accumulations at the ultrastructural level. Given that the TA was used in the light level analysis whereas the much smaller EDL muscle had to be used for the ultrastructural analysis, it is possible that only axons to the TA and not the EDL contain NF accumulations and/or the analysis was restricted to the nerve terminal and did not include the preterminal segment. Neurofilament accumulations in motor axons and their terminals have been previously reported not only in a model of spinal muscular atrophy (SMA) (Cifuentes-Diaz et al., 2002), another lower motor neuron disease, but also in a third model of SBMA (Katsuno et al., 2006a). However, despite the association between neurofilament accumulations and neurodegenerative disease, motor function has been shown to be *unaffected* by their presence (Teuling et al., 2008) questioning the functional significance of neurofilament accumulations. Regardless, it remains unclear whether

neurofilament accumulations are a cause or simply an effect of disease, despite the fact that they are a common correlate of many neurodegenerative diseases.

We have utilized two models that show comparable androgen-dependent motor dysfunction but have distinct differences in the underlying genetics triggering the disease. Disease in the myogenic model is induced by expression of a WT AR allele exclusively in muscle whereas disease in the KI model is induced by expression of a polyglutamine-expanded AR allele under the control of the endogenous AR promoters. Finding common correlates of disease across SBMA models that differ in the specifics of the AR allele and where AR is expressed offers an opportunity for finding essential pathologic mechanisms underlying the loss of motor function in human affected by SBMA. When our results are considered in whole, both of these SBMA models show pathological fragmentation of the NMJ, despite their differences in genetics. This change in NMJ morphology suggests these models may have functionally weakened synapses. In addition to this shared pathological feature, these models independently have pathology supporting the idea of synapses with reduced capacity to elicit a postsynaptic response from the muscle. Evidence of a decline in the number of docked vesicles ready for release in nerve terminals, widened of synaptic clefts, simplified postsynaptic folds, and an abnormal accumulation of synaptic vesicle proteins all suggest reduced synaptic strength. Synaptic dysfunction may contribute to or underlie the impairments in motor function associated with SBMA.

CHAPTER 2: Neuromuscular Junction Pathology but No Trafficking Deficit in 97Q Mouse Model of Spinal Bulbar Muscular Atrophy

Abstract

Spinal bulbar muscular atrophy (SBMA) is a late-onset, slowly progressing motoneuron disease characterized by androgen-dependent motor dysfunction and motoneuron death in men. The disease is caused by a CAG repeat expansion in the first exon of the androgen receptor (AR) gene. I recently showed that the neuromuscular junction (NMJ) in two different mouse models of SBMA contains pathology indicative of weakened synaptic function, and I now report of the same analysis in a third model that broadly expresses a full length human AR transgene harboring the SBMA mutation (referred to as the 97Q model). Characterizing the pathology at the NMJ in a third model begins to shed light on possible core pathology characteristic of SBMA in humans. The three cellular components of the NMJ were visualized in the same way as described for chapter one, but without expression of the transgene for yellow fluorescent protein, and systematically examined for pathology using confocal microscopy. I report that, while NMJs in affected 97Q males show *no* indications of denervation, they do show pathological fragmentation, also seen in the other two models, and preterminal sprouts, suggestive of functionally weakened synapses. Motor axons and terminals in affected 97Q males also contain neurofilament accumulations, pathology often associated with axonal transport deficits. Because previous evidence indicates an androgen-dependent defect in retrograde axonal transport in this same model (Katsuno et al., 2006a), I also used a novel live imaging approach that I helped develop to further characterize this reported retrograde transport deficit. Despite previously published data, I found no

evidence for disease-related deficits in retrograde transport in the 97Q model, suggesting that impairments in motor function may not depend on defective retrograde transport. However, the pathology observed at the NMJ in this model, as well as two other models of SBMA, suggests that disease weakens synaptic strength, which may underlie the loss of motor function characteristic of SBMA in humans.

Introduction

Pathology associated with motoneuron diseases has historically been viewed as resulting from processes beginning in the motoneurons and progressing to the muscle. Moreover, motoneuron death has long been assumed to be a pivotal event leading to the loss of motor function in motoneuron disease. Recent evidence, however, challenges both of these assumptions. The earliest signs of disease occur in skeletal muscle, often involving defects at the neuromuscular junction (NMJ) and in retrograde transport of cargo in motor axons. Both tend to emerge well before any evidence of motoneuron death, and before a behavioral phenotype (Balice-Gordon et al., 2000, Frey et al., 2000, Fischer et al., Katsuno et al., 2006a, Kariya et al., 2008). This evidence raises the question of whether motoneurons are the initial site of disease, and whether target muscles play an important role in disease progression. This updated picture of motoneuron disease has come from models of several different motoneurons diseases including amyotrophic lateral sclerosis (ALS), spinal muscular atrophy (SMA) and spinal bulbar muscular atrophy (SBMA), a motoneuron disease distinct from SMA.

SBMA is a hereditary neuromuscular disease in which patients present with muscle atrophy and weakness of the proximal limbs. The molecular basis for the disease is a mutation to the first exon of the androgen receptor (*AR)* gene, consisting of an expansion to the trinucleotide CAG repeat region (Fischbeck et al., 1991). Because of the androgen dependence of the disease, only men are affected, due to their higher levels of testosterone (Katsuno et al., 2002, Johansen et al., 2009). Core pathology of the disease includes loss of motoneurons in the anterior horn of the spinal cord and brainstem motor nuclei and pathology in the skeletal muscle fibers (Kennedy et al., 1968, Sobue et al., 1989). Patients with SBMA have elevated levels of creatine kinase, and the muscle fibers of affected individuals are typically irregularly sized, have split fibers, and internalized nuclei, all of which are indicative of disease originating in the muscle (Kennedy et al., 1968).

Many changes associated with the NMJ have been connected with neuromuscular diseases and may underlie the motor deficit in SBMA. We previously examined the NMJs of two SBMA models (Poort, Chapter 2), a muscle-specific transgenic model (TG) in which a wildtype allele of the AR is overexpressed exclusively in muscle fibers and a knock-in model (KI) expressing the endogenous mouse AR gene containing the first exon from the human *AR* gene harboring a disease-causing CAG expansion (Monks et al. 2007; Yu et al. 2006). Based on confocal and electron microscopy of their NMJs, we observed numerous indications that neuromuscular synapses were weakened in diseased animals. While we saw no evidence of denervation, the junctions were abnormally punctate and fragmented, showed impaired docking of vesicles, and

widened primary clefts. Junctions also displayed wider postsynaptic folds that suggest functional changes in the muscle fiber response to acetylcholine binding. These same two models also exhibit deficits in the retrograde transport of endosomes (Kemp et al., 2011).

We now examine the NMJ in a third model, the AR 97Q transgenic (97Q) model, to determine whether pathology at the junction is evident in this model, and if so, identify which pathological characteristics are common to all three models. The 97Q model globally expresses a cDNA of full length human AR with 97 CAG repeats under the control of a CMV promoter/chicken β-actin enhancer (Katsuno et al., 2002). Like other SBMA models, the 97Q transgenic males demonstrate core features of SBMA. As in humans affected with SBMA, the disease is androgen dependent, with only males exhibiting the motor phenotype (Katsuno et al., 2006a). TG males expressing the 97Q AR also show the expected nuclear inclusions of AR in affected tissues (Adachi et al., 2003), and muscle pathology (Katsuno et al., 2003). While previous studies have done cursory examinations of the NMJ in the 97Q model, finding qualitative evidence of abnormal synaptophysin distribution and neurofilament accumulations, the effect of disease on the NMJ is not well characterized (Katsuno et al., 2006a). Previous examinations of transport components suggest aspects of retrograde transport are affected by disease (Katsuno et al., 2006a).

This strategy of identifying common pathological features across SBMA mouse models helps to pinpoint potentially primary causes of the androgen-dependent motor

dysfunction that all three SBMA models share and are core attributes of SBMA in humans. In this study, we used live imaging to characterize the retrograde transport defect previously reported in the 97Q model, a method that has also been used to characterize retrograde transport defects in the both the myogenic TG and KI models of SBMA (Kemp et al., 2011).

We examined the NMJ in affected 97Q males and their WT brothers using confocal microscopy to characterize features of the nerve terminal, the underlying endplate and the overlying terminal Schwann cells (tSCs), which closely adhere to the nerve terminal, showing pathology. We now report that pathology at the NMJ in the 97Q model includes fragmentation of the endplate and neurofilament accumulations in the preterminal axon and terminal. Additionally, we see increases in the number of tSCs and preterminal branches. Details of analysis of retrograde transport based on live imaging of trafficking endosomes in axons of the sciatic nerve of affected males revealed no effects of disease on transport. Abnormal morphology of NMJs in all three models raises the possibility that synaptic function is impaired which may contribute to or underlie the impairments in motor function associated with SBMA.

Methods

AR 97Q mouse model and hormone manipulations

97Q animals globally express cDNA encoding a full length human AR with 97 CAG repeats under the control of a CMV promoter/chicken β-actin enhancer (Katsuno et al., 2002). 97Q mice and their WT brothers maintained on a C57 BL/6J background were

obtained from our breeding colony. Even though all progeny come from the same founding line, disease progression is highly variable across individual 97Q males. To achieve a more predictable time course of disease, we castrated 97Q males and their WT brothers at a mean of 34 days (± 1.0 SEM) (the start of puberty) and implanted them with a Silastic capsule containing crystalline testosterone (1.57 mm inner diameter and 3.18 mm outer diameter, effective release length of 6mm). Such Silastic T implants result in T serum levels comparable to those in adult male mice (Johansen et al., 2009). While this strategy led to a more predictable timing of disease symptoms, there was still variability in disease onset and progression that is not well understood. Animals developed the motor deficit and were sacrificed at a mean age of 64 days (± 1.9 SEM).

Animals were group housed on a 12:12 light dark cycle with food and water provided *ad libitum*. Animals were weaned at 21 days and screened for transgene presence using PCR. All procedures involving mice were approved by Michigan State University Institutional Animal Care and Use Committee, and are in accord with NIH guidelines for care and use of experimental animals.

Motor function measurements

Tests of motor function were conducted on age-matched 97Q and WT males beginning with baseline measurements an hour prior to castration and T implantation. Motor function was assessed weekly after that point, beginning one week after the surgeries. Open field, hang test, and grip strength were conducted as previously described (Yu et al., 2006, Johansen et al., 2009, Kemp et al., 2011). Briefly, for open field, animals were

placed in a VersaMax400 activity monitor (Accuscan Instruments, Columbus, OH) and motor activity was recorded for five minutes. The system measures movement in the horizontal and vertical planes in addition to the number of movement initiations and time spent moving and resting. The chamber was cleaned with 70% ethanol between animals. To assess grip strength, animals were held by the tail and lowered to a grid attached to a force gauge (Chatillon Force Measurement Systems, Largo FL), allowing either forepaws or all paws to grasp the grid. After the animals grasped the grid, they were pulled perpendicular to the grid and force readout was recorded. Grip strength was measured six times in a single session and the average of the four median values was recorded. In the hang test, animals were placed upright on a metal grid 40 cm above the bench top that was subsequently rotated 180 degrees and latency to fall was measured for a maximum of 120 seconds. Of these three motor tests, the hang test best predicts disease onset. 97Q and WT brothers were sacrificed when the 97Q male's latency to fall on hang test was zero for two consecutive weeks. Reported values are means from both animals used for junction analysis and trafficking studies and are the means from the final day of testing just prior to euthanasia. After meeting the established criteria for motor deficits, 97Q mice and their WT brothers were randomly assigned for assessing the morphology of neuromuscular junctions (NMJs) or evaluation of endosomal trafficking deficits.

Light microscopy analysis of the NMJ

Immunocytochemistry The anterior tibials (TA), a fast twitch hindlimb muscle was harvested from isoflurane-anesthetized male mice and pinned flat in a Sylgard-coated

petri dish, rinsed thoroughly with phosphate-buffered-saline (PBS, 0.14 M NaCl, 2.7 mM KCl, 1.5 mM KH2PO4 and 8 mM dibasic Na2HPO4 7H20, pH 7.4), fixed for 30 minutes with phosphate-buffered (0.1M, pH 7.4) 4% paraformaldehyde and cryoprotected in phosphate-buffered 20% sucrose for a minimum of three hours. Muscles were longitudinally sectioned on a sliding, freezing microtome at 60 um, distributed across three different series of sections used to visualize different elements of the junction (synaptic vesicles, neurofilament or terminal Schwann cells (tSCs)). Postsynaptic acetylcholine receptors (AChRs) were also visualized in all three series. Sections were collected and rinsed as free floating sections in a PBS vehicle containing triton X-100 (0.3%), bovine serum albumin (0.2%) and sodium azide (0.1%) and incubated overnight at room temperature in PBS vehicle containing primary antibody directed against one of the three elements of the junction. The following day, sections were rinsed in vehicle and incubated for two hours in vehicle containing fluorescently tagged secondary and α-bungarotoxin. In one series, synaptic vesicles were labeled using a rabbit anti-synaptophysin polyclonal primary (Zymed, 18-0130, diluted 1:50) and visualized with a donkey anti-rabbit Alexa Fluor 488 labeled secondary (Jackson Immunoresearch, 711-545-152, diluted 1:100). In a second series, terminal Schwann cells were labeled using rabbit anti-S100 polyclonal primary, a Schwann cell specific antigen (Dako, Z0311, diluted 1:400), and visualized with the same Alexa Fluor 488 labeled secondary. In the third series, neurofilament in motor axons and nerve terminal branches were labeled using a mouse anti-neurofilament monoclonal antiserum (Developmental Studies Hybridoma Bank, 2H3 diluted 1:100) and visualized with a rabbit anti-mouse Alexa Fluor 488 labeled secondary (Jackson Immunoresearch, 315-545-003, diluted 1:100).

Acetylcholine receptors were labeled using Alexa Fluor 555 conjugated alpha-bungarotoxin (Invitrogen, B35451, diluted 1:100). After several rinses in PBS vehicle, muscle sections were mounted on to gel-subbed slides and allowed to dry in the dark for at least 24 hours. Slides were then dehydrated in graded ethanols, cleared in CitriSolv (Fisher Scientific) and coverslipped with DPX, a non-fluorescing coverslipping medium. All fluorescently labeled material was stored at -20°C once the DPX was set.

NMJ imaging Simultaneous confocal images of the general structure and overlay of the presynaptic and postsynaptic junctions were imaged using a Zeiss LSM 510 Meta Confocal Microscope (Carl Zeiss, Oberkochen Germany) at the Center for Advanced Microscopy at Michigan State University (www.ceo.msu.edu). Areas of interest were located using epifluorescent illumination beginning at one margin of a muscle section and systematically working along the endplate band. Only junctions that presented in an *en face* orientation were imaged. Images were scanned using an Olympus 63x 1.4 NA oil objective without digital zoom. The confocal pinhole aperture was set to 1.11 Airy disk, the image size was set at 1024x1024 pixels and the Z-step size was set at 0.9 um. For each junction, a stack of images was collected through the entire depth containing visible signal. Lasers at 488 and 543 nm were used to visualize different components of the same junction, such as synaptic vesicles and postsynaptic AChRs. Prior to the analysis, we confirmed that each label used in the study fluoresced when excited with the laser at the correct wavelength and did not fluoresce when excited by other lasers, In short, there was no crossover from other channels. For each of the series and labels, settings were optimized and then held constant throughout the scanning for the

following parameters: laser power, detector gain, amplifier gain, pinhole and offset. Image processing was completed using Zeiss LSM Image Browser.

NMJ analysis For each animal, twenty *en face* junctions were analyzed for each series. Images of NMJs were constructed by making projections of the most intense pixel from each plane through the Z-axis for each laser channel to create a composite image of a junction.

The series in which synaptophysin and AChRs were labeled was used to quantify 1) the extent of partial or full denervation (indicated by exposed AChR footprints lacking overlying nerve terminal), 2) the degree of junctional fragmentation (indicated by either a fully connected pretzel-like pattern of receptor labeling (no fragmentation), a pattern of partially disconnected AChR-rich domains (partial fragmentation) or completely punctate domains (complete fragmentation) 3) the area of endplates based on AChR staining, 4) endplate coverage based on synaptophysin labeling, and 5) the presence of synaptophysin outside of the terminal and in the axon (terminal area was defined using the postsynaptic overlay of AChR). The series in which junctions were stained for neurofilament and AChR was used to measure 1) the number of neurofilament accumulations in both the terminal and preterminal axon (defined as bulbous swellings of neurofilament, often flanked by regions of a much smaller diameter proximally and distal to the accumulation) and 2) the number of terminal sprouts (fine, neurofilament labeled processes extending away from the terminal whose distal ends were not associated with the main terminal). Finally, the morphology of tSCs (specifically,

evidence of tSC sprouting) and their number at each junction was assessed in the series in which tSC and AChRs were labeled. Terminal Schwann cell sprouts were defined as fine processes extending beyond the outer perimeter of the NMJ as marked by AChR staining. These measures are listed and defined in more detail in Tables 1 - 3.

To quantitatively measure area of either synaptophysin or AChR labeling at NMJs, we evaluated the number of pixels occupied by the label using a thresholding protocol. Images were exported from Zeiss LSM Image Browser, cropped to the relevant region in Adobe Photoshop CS5, subjected to unsharp mask filter (parameters set to amount:500, radius:50, and threshold:1) and thresholded. When thresholding, the grey values of the unsharp mask image were manually adjusted to best fit the contours of the original image. Thresholded images were re-opened in ImageJ and the number of pixels occupied by synaptophysin or AChR staining were quantified using the Analyze Particles function. Corresponding thresholded images of presynaptic and postsynaptic staining of individual junctions were used to determine the ratio of synaptophysin staining covering the endplate. ImageJ was also used to measure muscle fiber diameter through the center of the junctions in the max projection images from the synaptophysin-labeled series.

Live trafficking experiments

Endosome labeling and nerve explant Endosomal trafficking was visualized in a second cohort of T-treated castrated 97Q males and their WT brothers. Once 97Q males reached criteria in the hang test, males were anesthetized with isoflurane and the

anterior tibialis and gastrocnemius muscles were injected with 3 uL cholera toxin B conjugated to Alex Fluor 488 (CT-AF_{488}, Molecular Probes, C22841; 5 ug/uL CT-AF_{488} in 0.9% saline containing 1% DMSO). Each muscle received two injections, 1.5 uL distally and 1.5 uL proximally, as previously described (Kemp et al., 2011). Mice were re-anesthetized four hours later for harvesting the sciatic nerves. A 10 mm section of sciatic nerve distal to the greater trochanter and proximal to the knee was removed and mounted on a coverslip using VetBond 3M adhesive. The preparation was covered in warm oxygenated Ringer's solution (0.135M NaCl, 0.005M KCl, 0.001M MgCl2, 0.015M NaHCO3, 0.001M Na2PO4, 0.002M CaCl2 and 0.011M glucose, pH 7.2) for imaging transporting endosomes in living axons. The temperature of the sciatic nerve explant during confocal imaging was maintained at 37°C using a ring incubator. The initial side imaged (left versus right) was randomly alternated across mice and the contralateral side remained *in situ* in the anesthetized mouse until the imaging in the initial nerve was completed.

Endosome visualization Transporting endosomes were visualized using an inverted LiveScan swept field confocal microscope (Nikon Eclipse TE2000-E, Japan) with a 60X oil immersion objective (1.4 na) and the 488 nm line of a 150 mW argon laser (Melles Griot). Time-lapse recordings were made using a Photometrics CoolSNAP HQ2 camera (USA) and NES Elements software. Laser power and aperture settings were identical for all imaging. Noting distal to proximal ends of the nerve with respect to their orientation *in vivo*, the nerve was scanned for moving endosomes starting at the center of the sciatic nerve segment and moving distally along the nerve to reduce variability

introduced by systematic differences in endosomal movement along the nerve (Miller and Sheetz, 2006). When the first moving endosomes were brought into focus, the first of two seven minute movies was recorded from each explant. Images were captured every two seconds using a one second exposure for a total of 211 images. For the subsequent movie, a different axon, distal to the first was used to limit effects of photobleaching.

Quantification Kymographs are two-dimensional representations of trafficking endosomes along the axon as a function of time and space. From these kymographs, we measured flux, net velocity, instantaneous velocity, and processivity events (number and length of stalls, velocity changes, reversals, and run length) of transporting endosomes.

Kymographs were made by opening a movie in FIJI as a 16-bit stack, straightening a single axon, rotating it 90 degrees, cropping the axon to a 60 pixel length, reslicing into one pixel width sections and creating a Z-projection using the Max Intensity option, converting it to a 16-bit image and saving as a tiff file. These images were reopened in Adobe Photoshop 7.0 (USA), inverted and resampled to increase size by 500%. Brightness and contrast settings were manually optimized for each image before analysis.

Endosomal net velocity was defined as the total retrograde distance travelled by an endosome in a given amount of time, including stalls, reversals and velocity changes. It

was determined based on the height and width (in pixels) of a box around single endosomal traces according to the following formula: [Time (pixels) X 0.10526 (microns/pixel)/ Length (pixels) X seconds per frame]. In contrast to net velocity, measures of instantaneous velocity are based on endosomes moving at a constant speed, absent of stalls or reversals, and was determined by drawing a one pixel wide line parallel to the time axis, bisecting the kymograph with respect to distance. For each endosomal trace crossing this line, a 20 pixel box was drawn centered on the line, with width and height of the box representing distance and time. Occasionally, perturbations in endosomal velocity, including changes in speed, stalls, and/or reversals appeared within the box. In such cases, the box was moved immediately distal to the perturbation until the box included a segment of the trace without perturbations. The same formula was used to calculate instantaneous velocity as net velocity.

In addition to the speed of endosomes, we evaluated the number of labeled endosomes transported within the axon. Flux is the number of endosomes that pass through a point in a given time period. It was determined by counting the number of endosomal traces passing through a line in the center of the kymograph running parallel to the time axis. The number of traces was then divided by the seven recorded minutes represented by the kymograph to give flux in units of endosomes/minute.

Processivity events reflecting the efficiency and fidelity of endsomal transport machinery were also assessed, including stalls, reversals and estimates of run length of individual endosomes. Stalls were defined as an endosome that was stationary for > 2 seconds.

Stalling prevalence was assessed by determining the number of stalls per endosomal trace, the proportion of traces that have stalls, and the amount of time an endosome was stationary. Average run length per animal was estimated by adding the total distance of endosomal transport observed in a kymograph (endosome number X axon length) divided by the number of stalls.

For each of animal, two to four different axons were used to produce two to four different kymographs. For each of these measures, values were averaged within a single kymograph and means from each kymograph were averaged to obtain overall estimates for each animal (N= animals/group).

Statistical analysis

When the number of experimental groups exceeded two, significant differences between groups were determined based on a two way ANOVA design with genotype and age as independent variables (SPSS Inc., Chicago, IL). $P < 0.05$ taken as significant. Paired t-tests were used to determine significant group differences in which AR 97Q males were compared to their wildtype brothers. Results are presented as group means (N= number of animals/group) ± standard error of the mean (SEM).

Results

Male 97Q mice show the expected deficit in motor function.

As previously demonstrated (Katsuno et al., 2002), transgenic 97Q males had equivalent motor function as their WT brothers at four weeks of age but during the subsequent weeks (5 – 10), motor function of 97Q males dropped significantly and progressively. Statistical analyses revealed significant main effects of both genotype and age with significant interactions of these two factors for all measures of motor function (Table 15). Hang time was the best predictor of approaching end-stage as significant decreases in hang times were the first to occur (Fig. 12A, p values < 0.05). Unlike their WT brothers, 97Q males did not gain body weight during the second month of postnatal life (Table 16), consequently weighing an average of 28% less than their WT brothers at the end of the study (Fig. 12B). Fore- and hindpaw grip strength (Fig. 12D – E) as well as horizontal and vertical activity in an open field (Fig. 12F – G) were also comparably impaired relative to WT controls (p values < 0.001) at end stage. In the aggregate, these data indicate that 97Q mice are much weaker than WT controls, a phenotype that emerges around five weeks in mice which ubiquitously express transgenic AR containing a tract of 97 glutamine repeats in the N-terminal domain.

Diseased NMJs are not denervated but show other signs of pathology.

NMJs were evaluated for denervation by determining whether the postsynaptic endplate (visualized by labeling AChRs) either partially or fully lacked an overlying nerve terminal (visualized using synaptophysin labeling). While previous published evidence led us to expect denervated junctions, we found no evidence of denervation; i.e., for every

endplate examined, we found an overlying nerve terminal that precisely and fully covered the underlying endplate. These data suggest that motor nerve terminals in diseased muscle are as structurally stable as in WT muscle and not undergoing retraction that is commonly associated with motoneuron disease (merged image in Fig. 13A, B, Table 17). We did note, however, striking qualitative changes in the morphology of NMJs in diseased muscle. While junctions in WT muscle displayed the typical continuous pattern of AChRs, some junctions in 97Q muscle appeared punctate and fragmented. This fragmented phenotype, while striking, affected only 28% of the junctions in diseased 97Q muscle and fell short of significance when compared to the frequency (4%) of fragmented junctions in WT muscle (Fig. 13C; $p = 0.085$). Of those fragmented junctions, diseased muscle shows a greater degree of fragmentation compared to fragmented junctions in WT muscle (Fig. 13D). Decreases in muscle fiber diameter and endplate area are frequently associated with disease, and although we saw only modest decreases in both measures, and neither were significant (Table 17, Fig. 13E). Notably, we saw a significant increase in the ratio of synaptic area occupied by synaptophysin in the nerve terminal relative to the size of the endplate (referred to as “synaptophysin coverage”) in affected 97Q males compared to WTs (Fig. 13F; $p < 0.05$) suggesting that the distribution of synaptic vesicles may be perturbed. On the other hand, we find no evidence of aberrantly located synaptophysin in the preterminal axon (Table 17) as expected based on previous findings (Katsuno et al., 2006a)

Prominent NF accumulations are present in the 97Q model.

We find substantial evidence for neurofilament accumulations in both nerve terminals and preterminal axons of diseased 97Q males (Fig. 14A and 9B, indicated with arrows) as previously suggested based on qualitative observation (Katsuno et al., 2006a). Large, bulbous enlargements comprised of neurofilament proteins were rare in preterminal axons of WT controls, but over 50% of motor axons in diseased 97Q muscle contained neurofilament accumulations (Table 18, Fig. 14C; $p < 0.001$). Similarly, 58% of junctions examined in diseased muscle contain neurofilament accumulations in their nerve terminals compared to only 14% for WT junctions (Fig. 14D; $p < 0.001$).

Diseases increases terminal sprouting and preterminal branching in muscles of affected 97Q males.

Nerve terminals are commonly observed to sprout in diseased, dysfunctional, or inactive muscle (after partial denervation or silencing by toxins). When we examined NMJs for evidence of sprouting, either preterminally (emanating from axonal nodes proximal to the junction) or terminally (emanating from the nerve terminal itself), we found evidence of terminal sprouts in 14% of 97Q junctions, compared to only 3% of junctions in WT controls (Table 18, Fig. 14F; $p = 0.02$). Because preterminal branching is sensitive to androgens and other factors such as photoperiod (Jordan et al., 1992, Hegstrom et al., 2002), we evaluated the number of branches from single axons that contact the fiber to form the nerve terminal. We found an increase in the number of preterminal branches innervating each junction in diseased 97Q males compared to WT controls (Fig. 14G; $p = 0.02$). We did not, however, find any evidence that junctions were innervated by axons

from more than one motoneuron in muscle from 97Q males, suggesting that developmental synapse elimination had preceded normally and has not been perturbed in this model of motoneuron disease. Finally, the number of tSCs, though slightly elevated in the 97Q males compared to WT controls, was not significant (Fig. 14H, $p = 0.08$). There was also no evidence of tSC sprouting (Table 19).

Disease does not impair transport of endosomes in live axons of 97Q males.

Earlier findings indicate that retrograde transport in motor axons of 97Q males is impaired (Katsuno et al., 2006a). The goal of the present study was to characterize in detail the nature of this defect by determining whether the apparent slower rate of transport was due to deficits in flux, speed, and/or the fidelity by which endosomes are transported retrogradely along motor axons based on time-lapse video microscopy of endosomal transport in living axons *ex vivo*. Contrary to expectations, we find no effect of disease on any of the parameters measured (Table 20). We saw no change in net velocity (Fig. 15B), instantaneous velocity or endosomal flux (Fig. 15C, D) that might explain the deficit in retrograde transport previously reported. We did find a small increase in the percentage of stalled endosomes (Fig. 15E) along with a small decrease in run length (Fig. 15F), consistent with the reported deficit in dynactin expression, but neither the frequency or stalls nor run length were significantly affected by disease.

Discussion

Despite significant precedence for the vulnerability of NMJs in neuromuscular disease (Balice-Gordon et al., 2000, Frey et al., 2000, Fischer et al., 2004, Kariya et al., 2008,

Yoshikawa et al., 2009), little attention has been given to the question of whether NMJs are pathological in SBMA. Like other neuromuscular diseases, SBMA involves marked muscle atrophy and weakness and changes in gene expression that suggest ongoing denervation of skeletal muscles (Yu et al., 2006, Monks et al., 2007) but no direct evidence exists to support or reject this possibility. Nonetheless, one hint that NMJs may be affected by disease in SBMA is the presence of abnormal synaptophysin accumulations in the motor axons just proximal to muscle endplates in diseased 97Q male mice, a transgenic model of SBMA (Katsuno et al., 2006a). To further explore whether NMJs are affected by disease in models of SBMA, we used confocal microscopy to examine the morphology of the three different cellular components of the neuromuscular synapse: the nerve terminal, the underlying postsynaptic endplate, and the tSCs that cover and closely adhere to the nerve terminal in muscles from diseased 97Q males and their WT brothers. Transgenic mice in this model of SBMA globally express a cDNA encoding a full length human AR with 97 CAG repeats in the first exon (Katsuno et al., 2002). Given that defects in retrograde transport are associated with disease in this model (Katsuno et al., 2006a), we also used time lapse video confocal microscopy to image retrogradely transported endosomes in living axons of sciatic nerve *ex vivo* of healthy and diseased 97Q mice with the goal of more fully characterizing the reported transport defect (Katsuno et al., 2006a). We find that diseased 97Q males show no signs of denervation, but do exhibit a characteristic fragmented appearance that is seen in two other SBMA mouse models (Poort, Chapter 2). We also find abnormal neurofilament accumulations in the preterminal axon and nerve terminal, as well as terminal sprouting and increased preterminal branching.

Despite previous evidence indicating the retrograde transport is perturbed in this model, we find no evidence for a defect in retrograde transport based on live imaging of transporting endosomal.

Affected 97Q males exhibit overt motor deficits (Fig. 11), showing profound deficits in hang test, grip strength, and vertical and horizontal movements. This loss of muscle strength and mass has been assumed to reflect ongoing denervation of target muscle fibers (Katsuno et al., 2002, Yu et al., 2006, Monks et al., 2007, Mo et al., 2010). However, we find no evidence to support this idea. Nerve terminals and endplates colabeled with antibodies for synaptophysin and tagged alpha bungarotoxin, respectively, revealed that the branches of the nerve terminal precisely aligned with the underlying postsynaptic specialization of the endplate, as is normally the case in healthy muscle. Moreover, we found no indication of even partial exposure of the endplate indicative of a denervation process in its initial stages. Despite the apparent muscle wasting and weakness, NMJs in diseased 97Q males appear fully innervated with no evidence of structural instability. This result agrees well with our findings from two other mouse models of SBMA where NMJs also appear uniformly innervated with no evidence of denervation (Chapter 2). Notably, while each model expresses a different disease allele controlled by different promoters, all three models show the same androgen-dependent loss of motor function. That we find no evidence of denervation in muscles in any of the three mouse models strongly argues that a mechanism other than overt muscle denervation accounts for the loss of motor function and muscle mass in SBMA. Our data does not, however, rule out the possibility that muscle fibers are

functionally denervated; that is, while junctions appear morphologically intact, such junctions may no longer reliably trigger a muscle contraction. Future studies of the safety factor of neuromuscular synapses in diseased and healthy muscle will shed light on this possibility.

Although NMJs were not denervated in diseased 97Q males, their morphology was not normal. While the presence of fragmented junctions was not increased in the muscle of affected 97Q males, a large proportion of their junctions show a fragmented appearance, a pathological feature also found in the two other models of SBMA (Chapter 1). Such fragmentation of the junction is also commonly observed in other neuromuscular diseases (Grady et al., 1997, Chan et al., 2003, Shiao et al., 2004, Slater et al., 2006 {Chang, 2008 #577, Chevalier-Larsen et al., 2008, Pratt et al., 2013). Despite its common occurrence, the cause behind endplate fragmentation is not clear. One possibility is that tSCs invade the primary cleft to wrap around terminals to eventually engulf them (Miledi and Slater, 1970, Jirmanova, 1975). However, even if this was the explanation, it is unclear whether tSCs are responding to disease or mediating it. Models of muscular dystrophy, created by removing either the *utrophin* or *dystrophin* gene, lead to a very similar fragmented phenotype as that seen in SBMA mouse models (Deconinck et al., 1997). Introducing a functional *dystrophin* gene into these models also has the capacity to reverse the junctional fragmentation (Banks et al., 2009). These data raise the possibility that some aspect of dystrophin function may be disrupted in SBMA. Fragmented junctions are also seen in aging muscles. Agrin, a proteoglycan, acts to stabilize the junction by preventing the dispersal of AChRs away from the

postsynaptic specialization. In a model of aging, where agrin function is disabled by cleavage, NMJs are also characterized by a fragmented phenotype (Butikofer et al., 2011), raising the question that SBMA may involve defects in agrin function. Another possibility is that when junctions were formed, they started out as fragmented. While 97Q males start to show a motor phenotype around five or six weeks of age, expression of the mutant AR allele begins prenatally. This early expression of the disease gene may have influenced the normal development of NMJs. While such a scenario argues against the idea that junctional fragmentation alone causes disease, it is possible that such pathology, in combination with other pathological features, predisposes individuals carrying the SBMA AR allele to eventually develop disease symptoms. Given the marked discordance in disease onset and severity among individuals with comparable CAG repeat lengths (Hashizume et al., 2012), it is likely that many factors, yet to be identified, regulate the toxic impact of the CAG-expanded AR on motor function.

One of the common pathological signs of neuromuscular disease is the presence of fine extensions of nerve terminal projecting beyond the boundaries of the endplate, or so-called terminal sprouts (Grimby et al., 1989, Cifuentes-Diaz et al., 2002, Monani et al., 2003). Such terminal sprouts typically occur when muscles are inactive, perhaps as an adaptive response to strengthen the functional connection so that muscle activity can be restored. While we found no signs of denervation, we did find that disease circumstances stimulated the growth of terminal sprouts. This observation suggests that synapses may indeed be functionally weak, possibly falling below threshold for activating fibers. While considerably more work is needed, preliminary evidence based

on intracellular recording of endplate potentials confirms that neuromuscular synapses are significantly weaker in motor-impaired 97Q males compared to healthy WT males. (Xu and Jordan, unpublished data) Terminal sprouting has also been associated with aging, when oxidative stress and mitochondrial dysfunction has occurred (Jang and Van Remmen, 2011). Thus, diseased mice may also be facing similar challenges. Indeed, increased proliferation of hypertrophic mitochondria and enhanced activity of the respiratory chain enzymes in muscle of one SBMA model supports this idea (Musa et al., 2011), and suggests that increased oxidative stress is also a feature of diseased muscle fibers in SBMA.

Another pathological trait of NMJs in 97Q males is prominent neurofilament accumulations in both the preterminal axon and the nerve terminal. Neurofilament accumulations were also found in diseased muscle of the myogenic model of SBMA in which the wild-type AR is overexpressed exclusively in muscle fibers (Chapter 2). Accumulations have previously been noted in several different models of neurodegenerative diseases, including models of both amyotrophic lateral sclerosis and spinal muscular atrophy (Cifuentes-Diaz et al., 2002, Kariya et al., 2008, Murray et al., 2008, Kong et al., 2009). Qualitative evidence of such accumulations has also been previously noted in the 97Q model, but not quantified (Katsuno et al., 2006a). While the presence of neurofilament accumulations in motor axons is common to many neuromuscular diseases, it is again not clear whether they are a cause or effect of disease. While there are numerous examples of accumulations in models exhibiting motor dysfunction (Piccioni et al., 2002, Katsuno et al., 2006b, Kemp et al., 2011), there

is also evidence for the presence of accumulations without motor weakness (Teuling et al., 2008). This suggests that while neurofilament accumulations may be an indicator of disease, they do not play a role in mediating disease.

The most unexpected result from this study was the lack of trafficking deficits. Previous studies on this same model demonstrated decreases in dynactin 1 mRNA levels, low accumulation of transporting synaptophysin and neurofilament in the distal segment of ligated axons, and deficits in the accumulation of retrogradely transported Fluoro-gold in motoneuronal cell bodies (Katsuno et al., 2006a). All of these defects were evident before neuronal degeneration and were dependent on circulating adult levels of androgen, making a compelling case that transport dysfunction exists in this model and may play a central role in the disease. That we find no evidence for defects in retrograde transport based on live imaging of transporting endosomes in this same model calls this conclusion into question. However, in this previous study (Katsuno et al., 2006a), Fluoro-gold was used as the a retrograde tracer and not fluorescently labeled CTX, and little is known about Fluor-Gold enters neurons and the vesicle population that it labels. While more is known about the transport of synaptophysin, it is possible the 488-conjugated CTX used to label endosomes in our live trafficking experiments entered a different subset of vesicles that are unaffected by disease. Indeed, there is precedence that only select populations of cargo can be affected by disease (Perlson et al., 2009). However, reduced expression of dynactin 1 is in the 97Q model predicts that retrograde transport *per se* would be impaired, since the same molecular machinery involving dynein, the molecular motor, and dynactin, a motor-

associated protein complex that increases the efficiency of the motor (Susalka and Pfister, 2000), seems to be the only mechanism available for retrograde transport along axons. Another possibility is that only subtle deficits in both flux and velocity when combined add up to a significant deficits in the accumulation of synaptophysin in distal ligated segment of axon and Fluoro-Gold in motoneuronal cell bodes. While not significant, we did see a reduction in run length in affected 97Q males, which is consistent with decreases in dynactin 1 expression and the deficit in accumulated cargo reported previously for diseased 97Q males (Katsuno et al., 2006a). Finally, because muscles in diseased 97Q males have a much smaller mass than in healthy WT males, it is possible that this difference in muscle mass effectively increased the concentration of tracer, since the same amount of tracer was injected in both healthy and diseased muscles. This difference in muscle mass might have artificially increased the number of labeled endosomes being retrogradely transported in sciatic nerves of diseased mice, washing out any real deficit in endosomal flux. Arguing against this possibility is that the same differences in muscle mass nonetheless revealed transport deficits based on the same live imaging approach in two other SBMA models (Kemp et al., 2011). Despite all of these possibilities, it may be that such transport deficits do not underlie the robust deficits in motor function. In another mouse model of distal SBMA, resulting from a mutation to the p150 dynactin subunit, fragmentation similar to that seen in this model is evident and there is a strong behavioral phenotype of motor dysfunction, yet there are no trafficking deficits (Chevalier-Larsen et al., 2008). Evidence from this model suggests there can be dysfunction in the trafficking machinery without outright deficits in

retrograde transport. Clearly, there is considerable more work to be done to understand if and how axonal transport dysfunction affects the course of disease.

In sum, these studies, which focus on the 97Q model of SBMA that globally expresses a cDNA encoding full length human AR with 97 CAG repeats reveal that the NMJ contains pathology but endosomal transport appears intact. In view of results from two other SBMA models (Chapter 2), an essential component of disease may be a progressive decline in the strength of neuromuscular synapses, suggested by the fragmented phenotype of NMJs in the three SBMA models. Despite the presence of neurofilament accumulations in axons of diseased 97Q males, suggestive of trafficking deficits, we saw no impairment of endosomal trafficking, indicating that motor dysfunction in this model may be independent of impairments in retrograde transport.

GENERAL DISCUSSION

General Findings

My analysis of neuromuscular junctions (NMJs) using morphological approaches in three different mouse models of SBMA shows for the first time that NMJs in diseased muscle of SBMA mice exhibit striking pathology. I analyzed NMJs in the myogenic model which overexpresses the WT AR transgene exclusively in muscle fibers, the KI model which expresses the endogenous AR gene with the first exon replaced with the first exon of the human mutant AR gene and the 97Q model that broadly expresses full-length human AR transgene with a 97 CAG repeat expansion mutation. The one consistent pathology shared by all three models was fragmentation of the NMJ. Specifically, the morphology of the postsynaptic endplate in diseased muscle was transformed from the normal, continuous, pretzel-like pattern of AChRs to one of separate, punctate domains of AChRs. Other morphological changes present in some, but not all models, included decreased number of active zones with docked vesicles, wider primary synaptic clefts, simplified postsynaptic folds and abnormal distribution of synaptophysin and neurofilament proteins. I also examined live endosomal trafficking in the 97Q model, and despite previous evidence of transport dysfunction, I find no evidence of a transport deficit based on live imaging of transporting endosomes. That the NMJ of SBMA models is affected by disease is entirely novel. That junctional fragmentation is a core pathological feature of disease also predicts deficits in synaptic strength in all three models. Such deficits in synaptic strength may contribute to, if not underlie, the loss of motor function characteristic of all three models. Identifying core features of disease by conducting cross model comparisons for phenotypes also

occurring in humans affected by SBMA highlights the NMJ as a new therapeutic target for treatment of SBMA symptoms.

Commonalities Between the Models

Using confocal microscopy to evaluate the distribution of AChR at the endplate, synaptophysin and neurofilament in motor axons and nerve terminals, and S100 in tSC numbers in the myogenic, KI and 97Q models, I found a cohesive list of pathology within the models. Despite previous indications that muscles of diseased SBMA mice are denervated {Monks, 2007 #252;Yu, 2006 #256}, I found no morphological evidence of fully or even partially exposed endplates in any model. This strongly suggests that muscle atrophy and the changes in gene expression normally associated with deliberate denervation are caused by mechanisms other than denervation. Although there was no evidence of denervation occurring in these models, it does not exclude the possibility that disease results in functional changes at the synapse that might decrease the ability of the motoneurons to reliably cause a muscle contraction. Indeed, all three models show striking alterations to the morphology of the postsynaptic distribution of AChRs in the endplate. Typical of wildtype junctions is a continuous, pretzel-like distribution of AChRs, but affected males in all three models show a fragmented morphology of more clustered, punctate domains of AChRs. Interestingly, nerve terminals precisely align with this altered configuration of the endplate, with fine intervaricosities connecting each of the punctate terminal domains. While at face value, lack of denervation may suggest that synaptic connections between the motoneuron and muscle are unaffected by disease, the extensive alterations seen in the morphology of the NMJ raises the

possibility that synaptic function has been drastically compromised. While finding this fragmented phenotype of NMJs in models of SMBA is entirely novel, such pathology has been frequently noted in models of other motoneuron diseases (Grady et al., 1997, Shiao et al., 2004, Slater et al., 2006, Chevalier-Larsen et al., 2008, Pratt et al., 2013).

While not consistently seen across the models, other pathological changes in the NMJ were seen that might also be indicative of a weakening synapse. For example, in the anterior tibialis (TA) muscle of myogenic and KI males, I found increases in the intensity of synaptophysin labeling in the nerve terminal suggesting a disease-induced accumulation of synaptophysin in the nerve terminal. In addition, synaptophysin was found in the preterminal axon just proximal to the nerve terminal where it is usually not detectable. Recent research indicates that there are two vesicle pools associated with synaptophysin; one in the terminal and one in the preterminal axon (Turko, 2013). My results suggest that both pools have been affected by disease. Terminal sprouts were also part of the junctional pathology in diseased 97Q males. Since terminal sprouts develop when muscles are inactive, this could mean that one disease associated event is that synapses fall below threshold, effectively becoming silent (Love and Thompson, 1999) (Son and Thompson, 1995a). While in this case, the motoneuron and muscle are clearly connected, since animals are still capable of ambulating, though with great difficulty, it is likely that only some synapses are ineffective and perhaps only at certain times. It is noteworthy that only 14% of the junctions had terminals sprouts.

Characterizing these changes at the light microscopic level inspired a deeper exploration of changes occurring at the NMJ using electron microscopy to evaluate the ultrastructure of NMJs in myogenic and KI models. In particular, the changes in synaptophysin staining seen at the light level prompted the question of whether the distribution of synaptic vesicles in the nerve terminal was also altered. To answer this question required that I use electron microscopy. A host of quantitative measurements of presynaptic, synaptic, and postsynaptic ultrastructure were taken including vesicle number, size, shape, and distribution, terminal size and presynaptic to postsynaptic apposition length, primary synaptic cleft width and area, secondary postsynaptic cleft number, width, depth, and area, and postsynaptic perimeter length. Junctions in both the myogenic and KI model were characterized by having a wider primary synaptic cleft. This increase further supports the idea that synapses in diseased muscle are very likely weaker than normal, as released neurotransmitter must diffuse a longer distance before binding to postsynaptic receptors. This increased distance can result in a slower rise to peak concentration of bound neurotransmitter and a reduced peak due to transmitter leakage out of the cleft (Renger et al., 2001). Both effects would result in a decreased response from the postsynaptic muscle.

Each model also exhibited pathological features unique to that model but nonetheless consistent with the idea that synaptic strength is compromised. For example, the KI model displayed extensive changes postsynaptically, having wider and deeper secondary postsynaptic clefts than normal. Similar changes were also seen in the myogenic model, but were not significant. Such simplification of the postsynaptic

membrane has been noted in muscular and myotonic dystrophy (Banks et al., 2009) (Torres and Duchen, 1987, Lyons and Slater, 1991, Deconinck et al., 1997, Grady et al., 1997). Because the distribution of AChRs and sodium channels is dependent upon the membrane in which they are inserted, these changes to the postsynaptic membrane are likely to alter the strength of the synapse. Nerve terminals in the myogenic model also contain fewer docked vesicles at their active zones suggesting that fewer vesicles are released when the nerve terminal is activated. The widened synaptic cleft is then likely to further exacerbate the declining strength of synapses, since less released acetylcholine has to travel further before binding to its receptor

Because all three mouse models share the fragmented phenotype, it is likely that this pathology also occurs in humans with SBMA and thus, may underlie the loss of motor function in the human disease. However, other pathology at the junction, though not shared by all three models, should not be discounted as those pathological changes may also occur in the human disease. The most significant aspect of these findings is that they are all correlates of a functionally weaker synapse and likely to lead to compromised motor function.

Causes of Fragmentation

The strongest collective feature of pathology in these three models of SBMA is the fragmented phenotype of the postsynaptic endplate. However, even though a similar phenotype is observed in multiple other disease models, the mechanism behind the fragmentation is still unknown. Looking outside of the field of neuromuscular disease, a

couple of mouse models that selectively alter the expression of proteins with a putative role in synaptic stability also result in endplates with the fragmented phenotype. The first of these is a model resulting in enhanced cleavage of agrin, a motoneuron-derived proteoglycan. Intact agrin, although expressed in motoneurons, acts on the postsynaptic AChRs to limit their dispersal, resulting in the fragmentation of the endplate (Butikofer et al., 2011). A second group of models knocks out either utrophin or dystrophin, two proteins located in the basal lamina involved in postsynaptic organization (Lyons and Slater, 1991, Grady et al., 1997). The resulting fragmented phenotype in these models further emphasizes the importance of the muscle in controlling the confirmation of the NMJ. A final example involves the implicated role of tSCs with the presynaptic terminal. When synaptic connections are removed, as during developmental synapse elimination or during axonal regeneration, tSCs invade the synaptic cleft and wrap around the terminal to eventually engulf it (Miledi and Slater, 1970, Jirmanova, 1975). Interestingly, I found that the fine intervaricosities between punctate endplate domains were fully wrapped by tSC processes but were not associated with postsynaptic specializations, suggesting that this was a stable arrangement and did not reflect a dynamic process of ongoing synaptic retraction.

Androgen Receptors in Skeletal Muscle can Induce Disease in Motoneurons

Traditionally, SBMA has been viewed as one of many neurodegenerative diseases where the disease allele is assumed to work directly in the motoneurons, in a cell autonomous fashion, to cause their death, secondarily impairing muscles. However, several mouse models of SBMA, most notably our myogenic TG model, demonstrate

that motor deficits occur without motoneuron loss and that muscle pathology precedes deficits in behavior (Katsuno et al., 2002, Chevalier-Larsen et al., 2004, Yu et al., 2006, Monks et al., 2007). Because of primary pathology originating in muscle can indeed induce pathology in the motoneuron, NMJs are a worthy area of focus since presumably critical disease signals pass from muscles to the motoneurons via the NMJ.

As discussed above, both utrophin and dystrophin are important players in regulating the morphology of the postsynaptic junction as well as synaptic function (Lyons and Slater, 1991, Grady et al., 1997). The resultant phenotype of their removal recapitulates myotonic dystrophy (Grady et al., 1997). Interestingly, muscles of KI SBMA males also show several characteristic features of myotonic dystrophy (Yu et al., 2006), reinforcing the idea that ARs may act directly in muscles to drive the disease process in SBMA. That the fragmented phenotype also occurs when the disease allele of SMA is expressed exclusively in muscle (Chan et al., 2003, Chang et al., 2008) reinforces the robust influence muscle can have on the fate of the NMJ and in turn, the motoneuron.

One of the roles of skeletal muscles is the expression of trophic factors, such as brain-derived neurotrophic factor (BDNF), glial cell line-derived neurotrophic factor (GDNF), neurotrophin 4 (NT-4), and insulin-like growth factor (IGF-1). The skeletal muscles supply these neurotrophic factors to the motoneurons which innervate them and facilitates the survival of those motoneurons and their synapses (Caroni and Becker, 1992, Kwon and Gurney, 1996, Nguyen et al., 1998, Dobrowolny et al., 2005, Pitts et al., 2006). Such trophic factors are also known to enhance the efficacy of

neuromuscular transmission synapses (Lohof et al., 1993, Lu and Figurov, 1997, Fitzsimonds and Poo, 1998). The motoneurons, in turn, are prepared to respond to these muscle-derived neurotrophic factors since they express their respective receptors (Henderson et al., 1993, Koliatsos et al., 1993, Funakoshi et al., 1995).

There is substantial evidence that increasing the level of muscle-derived neurotrophic factors delays the onset and progression of neuromuscular disease (Musaro et al., 2001, Azzouz et al., 2004, Dobrowolny et al., 2005, Li et al., 2007, Bosch-Marce et al., 2011), suggesting that depletion of muscle-derived neurotrophic factors could be a key factor mediating the disease phenotype in our models. Indeed, muscles from affected males of the KI model shows decreased levels of GDNF and NT-4 expression (Yu et al., 2006) and all three models show decreases in the expression of vascular endothelial growth factor (VEGF) (Monks et al., 2007, Mo et al., 2010). Recent evidence also indicates that the expression of BDNF is significantly decreased in an androgen-dependent fashion in diseased muscles of both the 97Q and myogenic models. Not only is the expression of several muscle-derived neurotrophic factors perturbed, but restoring their levels have been shown to rescue SBMA mice from disease. For example, overexpression of IGF-1 exclusively in muscle fibers by virtue of transgene expression is able to rescue both the behavioral phenotype and associated histopathology in the 97Q model (Palazzolo et al., 2009, Rinaldi et al., 2012). VEGF given to myogenic males reverses the effects of disease in an axonal transport model (Kemp et al., 2011). The clear importance the supply of muscle-sourced trophic factors is for the health of the

motoneuron and the function of the animal strongly suggests trophic factor expression may be key to the pathology seen at the NMJ and to functional deficits in SBMA.

Future Directions

Now that it has been established that the NMJ is also a site of SBMA-related pathology, it would be informative to know the time course for development of this pathology since it would provide hints on whether such changes contribute to the emergence of disease symptoms. The fact that the disease can be acutely induced in adult, asymptomatic myogenic females by simply exposing her to male levels of testosterone offers one strategy for relating pathology at the NMJ to the loss of motor function (Johansen et al., 2009). Another strategy is castrating symptomatic myogenic males who recover much of their motor function (Johansen et al., 2011). One important question to ask is whether the fragmented morphology of the junction persists in recovered TG males. If so, it is unlikely that the fragmented phenotype underlies the loss of motor function. In fact, it seems much more likely that junctional features such as nerve terminal sprouting or the distribution of synaptophysin, which are inherently more dynamic in nature, are the attributes of disease that may well be acute induced or reversed as symptoms of disease are turned on or off with changes in androgens.

Given that the expression of neurotrophic factors in muscle correlates with disease and at least one can rescue mice from disease, it would also be useful to know where in the muscle neurotrophic factors are expressed and whether their distribution is altered by disease. For example, if neurotrophic factors are normally concentrated at the NMJ,

where their availability would be enhanced for nerve terminals, then a loss of neurotrophic factor at the junction might be particularly devastating to the motoneurons. Considering the data as a whole, it seems clear that the next step is to characterize the function of synapses in diseased muscle of the three different SBMA models and begin to relate changes in their morphology to changes in their function and to relate all these changes with changes in motor function at the organismal level. Because neurotrophic factors may mediate many of the associated changes in neuromuscular function and structure in disease, it will also be important to relate changes in neurotrophic factors expression to the other correlates of disease.

Conclusions

While motoneurons have traditionally been the focus in understanding pathogenic mechanisms in mouse models of SBMA, recently attention has shifted more toward skeletal muscle and their potential influence in triggering disease. This shift in focus has been prompted by an unexpected outcome, the emergence of a disease phenotype recapitulating SBMA, when normal ARs are overexpressed in muscle fibers. Despite the general realization that both motoneurons and muscles are affected in motoneuron disease, and that often motoneuron disease involves a distal axonopathy culminating in the loss of motoneurons, whether disease affected NMJs in SBMA was entirely unknown. I now show that, not only is the NMJ affected by disease, but that such changes in morphology suggest synaptic efficacy is compromised by disease and may play an important role in development of the motor deficit. While I observed pre- and postsynaptic pathology, I saw no evidence of partial or complete denervation. This

raises the possibility that the effects of disease may be realized first at the NMJ followed by progression of the disease process to the motoneuronal cell bodies in the spinal cord, which has important implications for preventing or rescuing male individuals from the toxic effects of SBMA on motor function.

APPENDIX

Table 1. Definition of Measures- Synaptophysin Series

Denervation	Junctions were judged as innervated or denervated (partial or full) based on the amount of exposed AChR footprint (Fig. 3). Fully innervated junctions had the entire AChR footprint covered by synaptophysin label. Partially or fully denervated junctions were judged as such if the AChR footprint was partially or fully exposed.
Fragmentation	Postsynaptic endplates (marked by the presence of AChR) were judged as intact, partially fragmented, or completely fragmented based on the degree of separation between AChR domains. Intact endplates exhibited a fully connected pretzel-like pattern of receptor labeling. Partially fragmented endplates contained some areas of separate AChR stained domains while the remaining parts were fully connected as in normal endplates. Endplates judged as completely fragmented were comprised entirely of punctate domains without any apparent continuity.
Synaptophysin Intensity	Nerve terminals stained for synaptophysin were judged as having intense, intermediate or faint label. Intense synaptophysin label was characterized by continuous, bright staining of the entire terminal while intermediate intensity were terminals that exhibited moderately intense labeling with some areas lacking synaptophysin label. Faint synaptophysin was characterized by a few bright punctate areas of synaptophysin label with the remaining showing either faint labeling or lacking label all together.
Synaptophysin Area	Images of synaptophysin-stained nerve terminals were thresholded to quantitatively determine the number of pixels occupied by synaptophysin.
Endplate Area	Images of endplates labeled for AChR were thresholded to quantitatively determine the number of pixels occupied by the endplate.
Synaptophysin to Endplate Area Ratio	Quantitative values of synaptophysin area, based on the number of pixels of synaptophysin labeling above threshold, were divided by endplate area, based on the number of pixels above threshold of AChR staining.
Preterminal Synaptophysin	The presence of synaptophysin labeling in the preterminal axon, just proximal to the nerve terminal. The nerve terminal was defined as the axon in contact with the underlying muscle fiber endplate (as marked by AChR staining).
Muscle Fiber Diameter	The diameter of the muscle fiber was measured perpendicular to the longitudinal axis of the fiber, through the center of the NMJ.

Table 2. Definition of Measures- Neurofilament Series

Preterminal Branch
Neurofilament-positive bifurcations of the axon occurring proximal to the endplate and distal to the last segment of myelin.
Terminal Branch
The distal tip of each neurofilament-positive branch of the nerve terminal.
Nerve Terminal Accumulations
Neurofilament-positive bulbous swellings were judged as such when they were at least twice the diameter of the rest of neurofilament-stained branches of the nerve terminal and colocalized within the AChR labeled endplate.
Axonal Accumulations
Neurofilament-positive bulbous swellings located in the myelinated axon, proximal to the preterminal branching.
Terminal Sprouts
Fine, neurofilament-labeled processes extending beyond the perimeter of the junction (based on AChR labeling of the endplate) of no less than 15 microns and having blunt, bulbous endings in contrast to the thin tapered ends of terminal branches. Such processes were not associated with AChR labeling.

Table 3. Definition of Measures- S100 Series

Number of Terminal Schwann Cells
Terminal Schwann cells were defined as S100 positively stained cells that were located distal to the preterminal segment of the axon and within the margin of the AChR labeling. Each cell contained a round, slightly transparent cell body with contained a distinct nucleus.
Terminal Schwann Cell Sprouts
Fine S100-positve processes extending from a terminal Schwann cell, away from the junction and beyond the boundary of the AChR-stained endplate of no less than 15 microns.

Table 4. Electron Microscopy Definition of Measures- Presynaptic

Area of Nerve Terminal Profile
Total area of the terminal profile, measured along the perimeter of the inner plasma membrane of the terminal and including all internal cellular structures.
Terminal Apposition Length
Length of the presynaptic membrane starting across from the left most postsynaptic fold not obstructed by a terminal Schwann cell process and continuing across to the right most fold not obstructed by a terminal Schwann cell process.
Mitochondrial Number
Intercellular structures in the nerve terminal proper with a double membrane and containing cristae were counted.
Mitochondrial Area
Composite area occupied by all mitochondria in a single nerve terminal.
Vesicle Density
Number of vesicles contained in single nerve terminal, divided by the area of the nerve terminal profile.
Vesicle Density in the Synaptic Zone
Number of vesicles within a 480nm strip of nerve terminal proximate to the synaptic cleft (“synaptic zone”) marked by postsynaptic folds, divided by the area of that strip.
Vesicle Diameter
Average of the sum of the horizontal and vertical diameters (relative to the image) of each vesicle within the synaptic zone.
Vesicle Shape
Aspect ratio of the shortest and longest diameter for each vesicle in the synaptic zone.
Active Zone
A presynaptic, electron dense region directly across from a secondary cleft.
Active Zones with Docked Vesicles
A presynaptic, electron dense region directly across from a secondary cleft that contains at least one synaptic vesicle in direct contact with the presynaptic membrane.
Active Zones without Docked Vesicles
A presynaptic, electron dense region directly across from a secondary cleft without a synaptic vesicle in direct contact with the presynaptic membrane.

Table 5. Electron Microscopy Definition of Measures- Postsynaptic

Postsynaptic Fold
Postsynaptic membrane across from the terminal and between two secondary clefts. The crests of the folds have electron dense regions indicating AChR distribution.
Synaptic Cleft Width
Measurement of the shortest distance from the outer presynaptic membrane to the outer surface of the postsynaptic membrane taken from the center of every postsynaptic fold, starting on the left most postsynaptic fold and working toward the right. Only folds not obstructed by a terminal Schwann cell process were included. Estimated synaptic cleft width was based on the mean distance of several values per terminal profile.
Synaptic Cleft Area
The area between the left most postsynaptic fold not obstructed by a terminal Schwann cell and continuing to the center of the right most fold not obstructed by a terminal Schwann cell and everything between the presynaptic and postsynaptic membrane, not including the area of the secondary clefts.
Secondary Cleft Number
Average number of invaginations between two postsynaptic folds deeper than 104.5 nm per synaptic cleft. Only folds not obstructed by a terminal Schwann cell process in the cleft were included. and the right most fold not obstructed by a terminal Schwann cell were counted.
Number of Secondary Cleft Branches
Average of the number of secondary cleft branches per terminal profile.
Secondary Cleft Depth
The shortest distance from the primary synaptic cleft (marked by the top of the fold) to the bottom center of the secondary cleft, averaged to calculate a mean secondary cleft width per terminal profile.
Secondary Cleft Width
Width of the secondary cleft taken 104.5 nm into the cleft, averaged to calculate a mean secondary cleft width per terminal profile.
Secondary Cleft Area
Area of secondary clefts that were counted, measured from the top of each fold and divided by the secondary cleft number to obtain an overall mean estimate of secondary cleft area per terminal profile.

Table 5 (cont'd)

Length of Postsynaptic Perimeter
The postsynaptic membrane was traced, starting from the center of the left-most fold and continuing to the center of the right most fold, including only folds not obstructed by a terminal Schwann cell process. This value was divided by the length of the terminal apposition to ascertain an overall estimate of postsynaptic membrane available per unit length of nerve terminal contact.

Table 6. Possible Indices of Histopathology for NMJs in the Myogenic Model based on Synaptophysin and AChR Co-Staining of Junctions

Measure (% of Junctions)	WT	TG	p
No Denervation	100.00±0.00	100.00±0.00	N/A
Fragmentation: None	98.75±1.25	3.75±3.75	**0.000**
Fragmentation: Partial	1.25±1.25	27.50±7.77	**0.041**
Fragmentation: Complete	0.00±0.00	68.75±9.66	**0.006**
Synaptophysin Intensity: Faint	0.00±0.00	0.00±0.00	N/A
Synaptophysin Intensity: Intermediate	72.50±10.9	47.50±16.52	0.253
Synaptophysin Intensity: Intense	27.50±10.9	52.50±16.52	0.253
Presence of Preterminal Synaptophysin	1.25±1.25	35.00±4.56	**0.004**

Measure	WT	TG	p
Synaptophysin Area	325.07±53.74	176.12±31.88	**0.031**
Endplate Area	129.33±14.84	87.33±10	**0.035**
Synaptophysin to Endplate Area Ratio	0.45±0.07	0.75±0.15	0.125
Muscle Fiber Diameter	39.53±2.34	26.86±1.23	**0.003**

Table 7. Possible Indices of Histopathology for NMJs in the LA of the KI Model based on Synaptophysin and AChR Co-Staining of Junctions

Measure (% of Junctions)	WT	KI	p
Denervation: None	98.00±2.00	97.00±2.00	0.733
Denervation: Partial	2.00±2.00	2.00±1.22	1.000
Denervation: Complete	0.00±0.00	0.00±0.00	N/A
Fragmentation: None	75.00±8.37	42.00±7.18	**0.017**
Fragmentation: Partial	19.00±4.58	38.00±3.39	**0.010**
Fragmentation: Complete	6.00±4.00	20.00±8.37	0.170
Synaptophysin Intensity: Faint	13.00±5.61	0.00±0.00	**0.049**
Synaptophysin Intensity: Intermediate	67.00±6.24	83.00±6.24	0.108
Synaptophysin Intensity: Intense	19.00±5.34	15.00±7.07	0.664
Presence of Preterminal Synaptophysin	43.00±1.22	40.00±5.24	0.593

Measure	WT	KI	p
Synaptophysin Area	309.93±18.22	314.47±21.35	0.876
Endplate Area	323.91±35.90	307.74±36.94	0.762
Synaptophysin to Endplate Area Ratio	1.01±0.09	1.08±0.08	0.574
Muscle Fiber Diameter	29.15±1.21	23.02±0.81	**0.003**

Table 8. Possible Indices of Histopathology for NMJs in the TA of the KI Model based on Synaptophysin and AChR Co-Staining of Junctions

Measure (% of Junctions)	WT	KI	p
Denervation: None	98.00±1.22	93.33±4.01	0.334
Denervation: Partial	2.00±1.22	6.67±4.01	0.334
Denervation: Complete	0.00±0.00	0.00±0.00	N/A
Fragmentation: None	81.00±6.40	81.67±6.15	0.942
Fragmentation: Partial	20.00±5.70	17.50±6.16	0.776
Fragmentation: Complete	0.00±0.00	0.83±0.83	0.389
Synaptophysin Intensity: Faint	0.00±0.00	0.00±0.00	N/A
Synaptophysin Intensity: Intermediate	60.00±7.25	35.00±5.16	**0.018**
Synaptophysin Intensity: Intense	40.00±7.25	65.00±5.16	**0.018**

Measure	WT	KI	p
Synaptophysin Area	158.08±23.45	215.75±11.64	**0.045**
Endplate Area	333.62±16.10	297.88±19.07	0.196
Synaptophysin to Endplate Area Ratio	0.50±0.07	0.77±0.04	**0.005**
Muscle Fiber Diameter	44.28±2.85	42.37±2.85	0.649

Table 9. Possible Indices of Histopathology for NMJs in the Myogenic Model based on Neurofilament and AChR Co-Staining of Junctions

Measure	WT	TG	p
Preterminal Branches (Per Junction)	1.34±0.08	1.40±0.040	0.567
Terminal Neurofilament Accumulations (% of Junctions)	7.86±2.92	42.5±10.10	**0.008**
Number of Terminal Accumulations	0.08±0.03	0.91±0.23	**0.005**
Presence of Axonal Accumulations	7.90±3.02	58.42±15.88	**0.048**
Number of Axonal Accumulations	0.10±0.04	1.04±0.31	**0.011**

Table 10. Possible Indices of Histopathology for NMJs in the Myogenic Model based on S-100 and AChR Co-Staining of Junctions

Measure	WT	TG	p
Number of tSCs	2.75±0.03	0.03±0.11	**0.005**
Presence of tSC Sprouts (% of Junctions)	0.10±0.03	0.22±0.06	0.144

Table 11. Myogenic Model EM Presynaptic Analysis Results

Measure	WT	TG	p
Terminal Profile Cross Section (μm^2)	3.05±0.34	3.91±0.53	0.174
Mitochondrial Number	7.97±1.22	10.33±1.27	0.180
Mitochondrial Area	0.48±0.08	1.01±0.16	**0.004**
Vesicle Density (Vesicles/μm^2)	58.19±4.16	48.97±3.6	0.100
Readily Releasable Vesicle Density (Vesicles/μm2)	101.33±5.66	97.9±6.64	0.696
Vesicle Diameter (nm)	24.39±0.51	23.92±0.23	0.416
Vesicle Shape (Aspect Ratio)	1.17±0.01	1.22±0.01	**0.001**
Active Zones (Per μm of apposition length)	0.62±0.07	0.59±0.06	0.791
Active Zones with Docked Vesicles (Per μm of apposition length)	0.42±0.07	0.23±0.04	**0.032**
Active Zones Without Docked Vesicles (Empty AZ/Total)	0.32±0.07	0.53±0.07	**0.037**

Table 12. KI Model EM Presynaptic Analysis Results

Measure	WT	KI	p
Terminal Profile Cross Section (μm^2)	3.2±0.38	2.89±0.33	.541
Mitochondrial Number	9.07±1.38	7.1±1.03	.259
Mitochondrial Area	0.58±0.10	0.35±0.05	.054
Vesicle Density (Vesicles/μm^2)	63.26±8.26	60.04±3.92	.726
Readily Releasable Vesicle Density (Vesicles/μm2)	93.98±6.73	94.21±5.17	.978
Vesicle Diameter (nm)	24.25±0.4	24.07±0.19	.684
Vesicle Shape (Aspect Ratio)	1.2±0.01	1.23±0.01	**.024**
Active Zones (Per μm of apposition length)	0.33±0.06	0.33±0.07	.786
Active Zones with Docked Vesicles (Per μm of apposition length)	0.31±0.05	0.32±0.06	.925
Active Zones Without Docked Vesicles (Empty AZ/Total)	0.29±0.07	0.26±0.07	.789

Table 13. Myogenic Model EM Postsynaptic Analysis Results

Measure	WT	TG	p
Synaptic Cleft Width	52.23±1.40	65.8±4.27	**0.004**
Synaptic Cleft Area (Per µm of apposition length)	51.66±1.54	71.28±9.61	**0.049**
Secondary Cleft Number (Per µm of apposition length)	2.62±0.14	2.23±0.25	0.169
Secondary Cleft Termination Number (Per Cleft)	1.29±0.04	1.27±0.05	0.690
Synaptic Cleft Depth	485.59±18.78	468.88±30.59	0.644
Secondary Cleft Width	94.23±4.56	104.73±5.76	0.158
Secondary Cleft Area (Per secondary cleft number, nm^2)	67655.89±4360.05	79372.9±7899.94	0.199
Postsynaptic Perimeter Length (Per µm of apposition length)	4.74±0.26	4.00±0.32	0.080

Table 14. KI Model EM Postsynaptic Analysis Results

Measure	WT	KI	p
Synaptic Cleft Width	61.63±2.21	71.34±1.59	**0.001**
Synaptic Cleft Area (Per µm of apposition length)	57.4±2.12	65.79±1.48	**0.002**
Secondary Cleft Number (Per µm of apposition length)	2.27±0.11	2.09±0.10	0.232
Secondary Cleft Termination Number (Per Cleft)	1.19±0.03	1.44±0.05	**0.000**
Synaptic Cleft Depth	385.44±16.74	483.65±22.12	**0.001**
Secondary Cleft Width	101.43±4.46	142.34±5.99	**0.000**
Secondary Cleft Area (Per secondary cleft number, nm^2)	52994.25±2718.98	114256.96±7715.42	**0.000**
Postsynaptic Perimeter Length (Per µm of apposition length)	3.45±0.17	4.14±0.19	**0.010**

Table 15. 97Q Between Subject Effects of Genotype and Age

Measure	p
Body Weight	**0.000**
Hang Test	**0.000**
Forepaw Grip Strength	**0.001**
Hindpaw Grip Strength	**0.000**
Horizontal Movement Distance	**0.002**
Vertical Movement Number	**0.002**

Table 16. 97Q Behavior Results

Body Weight

Age (Weeks)	WT	97Q	N	p
4	18.13±0.63	18.26±0.50	17	0.777
5	20.71±0.59	19.36±0.47	17	**0.006**
6	22.41±0.49	19.79±0.46	17	**0.000**
7	23.52±0.41	18.72±0.74	17	**0.000**
8	23.77±0.83	19.12±0.81	9	**0.003**
9	24.63±0.75	19.23±0.43	4	**0.009**
10	23.87±0.60	16.33±2.22	3	0.115

Hang Test

Age (Weeks)	WT	97Q	N	p
4	111.47±6.36	105.53±7.39	17	0.580
5	101.59±9.23	60.88±11.48	17	**0.023**
6	92.47±10.42	35.12±11.47	17	**0.002**
7	103.71±8.91	7.41±4.44	17	**0.000**
8	110.22±7.52	8.11±5.47	9	**0.000**
9	100.75±19.25	2.50±2.50	4	**0.013**
10	120.00±0.00	1.33±1.33	3	**0.000**

Table 16 (cont'd)

Forepaw Grip Strength

Age (Weeks)	WT	97Q	N	p
4	68.48±4.45	69.52±5.01	17	0.873
5	75.35±4.25	65.62±4.17	17	0.083
6	76.01±6.98	49.38±7.34	17	**0.002**
7	73.89±4.24	28.99±5.17	17	**0.000**
8	41.91±11.21	15.45±5.77	9	**0.014**
9	17.12±7.81	4.31±2.00	4	**0.048**
10	10.69±6.73	6.4±4.28	3	0.501

Hindpaw Grip Strength

Age (Weeks)	WT	97Q	N	p
4	68.08±4.07	62.93±3.9	17	0.139
5	74.42±3.69	60.28±3.71	17	**0.006**
6	71.08±5.83	47.19±3.33	17	**0.001**
7	69.67±3.34	30.61±4.42	17	**0.000**
8	48.38±11.58	18.05±5.53	9	**0.005**
9	16.32±7.62	5.28±2.56	4	0.060
10	7.75±4.84	7.93±4.89	3	0.971

Table 16 (cont'd)

Horizontal Movement Distance

Age (Weeks)	WT	97Q	N	p
4	1042.47±86.77	1076.35±77.61	17	0.756
5	895.35±67.54	927.88±66.17	17	0.700
6	815.41±93.17	642.65±72.34	17	0.084
7	856.67±64.26	573.67±79.10	15	**0.006**
8	901.67±364.22	821.00±212.47	3	0.844
9	1884.50±980.5	509.50±66.50	2	0.414
10	1031.50±633.5	198.00±110.00	2	0.357

Vertical Movement Number

Age (Weeks)	WT	97Q	N	p
4	34.24±2.90	31.06±3.55	17	0.482
5	31.00±3.09	30.41±2.66	17	0.846
6	32.65±3.89	19.29±3.09	17	**0.013**
7	35.33±3.30	14.00±3.80	15	**0.001**
8	35.00±4.04	21.67±9.61	3	0.208
9	51.50±7.50	3.00±3.00	2	0.059
10	27.00±16.00	0.50±0.50	2	0.337

Table 17. Possible Indices of Histopathology for NMJs in the 97Q Model based on Synaptophysin and AChR Co-Staining of Junctions

Measure (% of Junctions)	WT	TG	p
Denervation: None	98.00	100.00	ns
Denervation: Partial	2.00	0.00	ns
Denervation: Complete	0.00	0.00	ns
Fragmentation: None	96.00	72.00	0.085
Fragmentation: Partial	3.00	20.00	0.067
Fragmentation: Complete	0.00	8.00	0.242
Synaptophysin Intensity: Faint	14.00	23.00	0.178
Synaptophysin Intensity: Intermediate	51.00	59.00	0.399
Synaptophysin Intensity: Intense	34.00	18.00	0.557
Presence of Preterminal Synaptophysin	1.00	3.00	ns

Measure	WT	TG	p
Synaptophysin Area	122.411	137.933	0.172
Endplate Area	302.128	260.049	0.135
Synaptophysin to Endplate Area Ratio	0.410	0.522	**0.050**
Muscle Fiber Diameter	39.320	38.107	0.451

Table 18. Possible Indices of Histopathology for NMJs in the 97Q Model based on Neurofilament and AChR Co-Staining of Junctions

Measure	WT	TG	p
Preterminal Branch Number	1.456	1.613	**0.015**
Terminal Branch Number (per Junction)	4.363	4.175	0.281
Presence of Terminal Accumulations (% of Junctions)	14.375	58.125	**0.000**
Number of Terminal Accumulations (per Junction)	0.163	1.063	**0.000**
Presence of Axonal Accumulations (% of Junctions)	18.750	54.375	**0.003**
Number of Axonal Accumulations (per Junction)	0.225	0.831	**0.001**
Presence of Terminal Sprouts	3.125	14.375	**0.026**

Table 19. Possible Indices of Histopathology for NMJs in the 97Q Model based on S-100 and AChR Co-Staining of Junctions

Measure	WT	TG	p
Number of tSCs	2.338	2.463	0.080
Presence of tSC Sprouts (% of Junctions)	30.00	28.75	0.824

Table 20. 97Q Model Trafficking Results

Measure	WT	97Q	p
Net Velocity (μm/Second)	0.27±0.021	0.32±0.028	0.083
Instantaneous Velocity (μm/Second)	0.26±0.016	0.32±0.032	0.088
Flux (Endosomes/Minute)	4.61±0.55	4.71±0.31	0.875
Run Length (μm)	382.32±101.10	257.69±66.10	0.150
Total Endosome Number	32.39±3.03	34.04±3.18	0.692
Number of Velocity Changes	7.72±1.13	9.65±1.29	0.142
Total Endosomes with Velocity Changes	4.61±0.68	5.92±0.69	0.119
Endosomes with Velocity Changes (% Total Endosomes)	16.96±3.44	19.04±2.56	0.468
Number of Direction Reverses	1.30±0.73	1.09±0.63	0.854
Total Endosomes with Reverses	0.63±0.37	0.54±0.29	0.863
Endosomes with Reverses (% Total Endosomes)	2.31±1.52	1.56±0.79	0.702
Number of Stalls	5.39±1.20	6.22±0.98	0.515
Total Endosomes with Stalls	3.70±0.72	5.13±0.77	0.127
Endosomes with Stalls (% Total Endosomes)	14.41±3.44	17.47±3.21	0.350
Stall Length (Seconds)	42.54±5.99	39.68±7.45	0.801

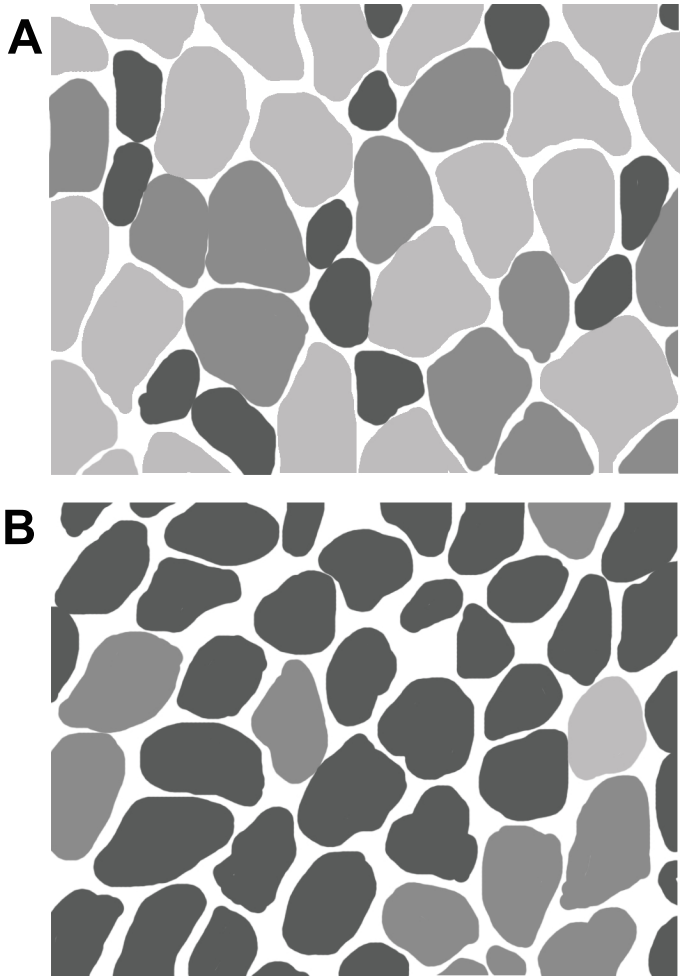

Figure 1. A representative comparison of healthy and diseased fiber type clustering. WT muscle has large diameter fibers with a mix of slow oxidative, fast fatigue resistant and fast glycolytic fibers (A, darker colors represent increased oxidative capacity). In comparison, diseased muscle fibers are hypertrophic, and show a shift towards increased oxidative metabolism (B). Fiber type groupings, particularly of slow oxidative fibers is evident and indicative of reinnervation.

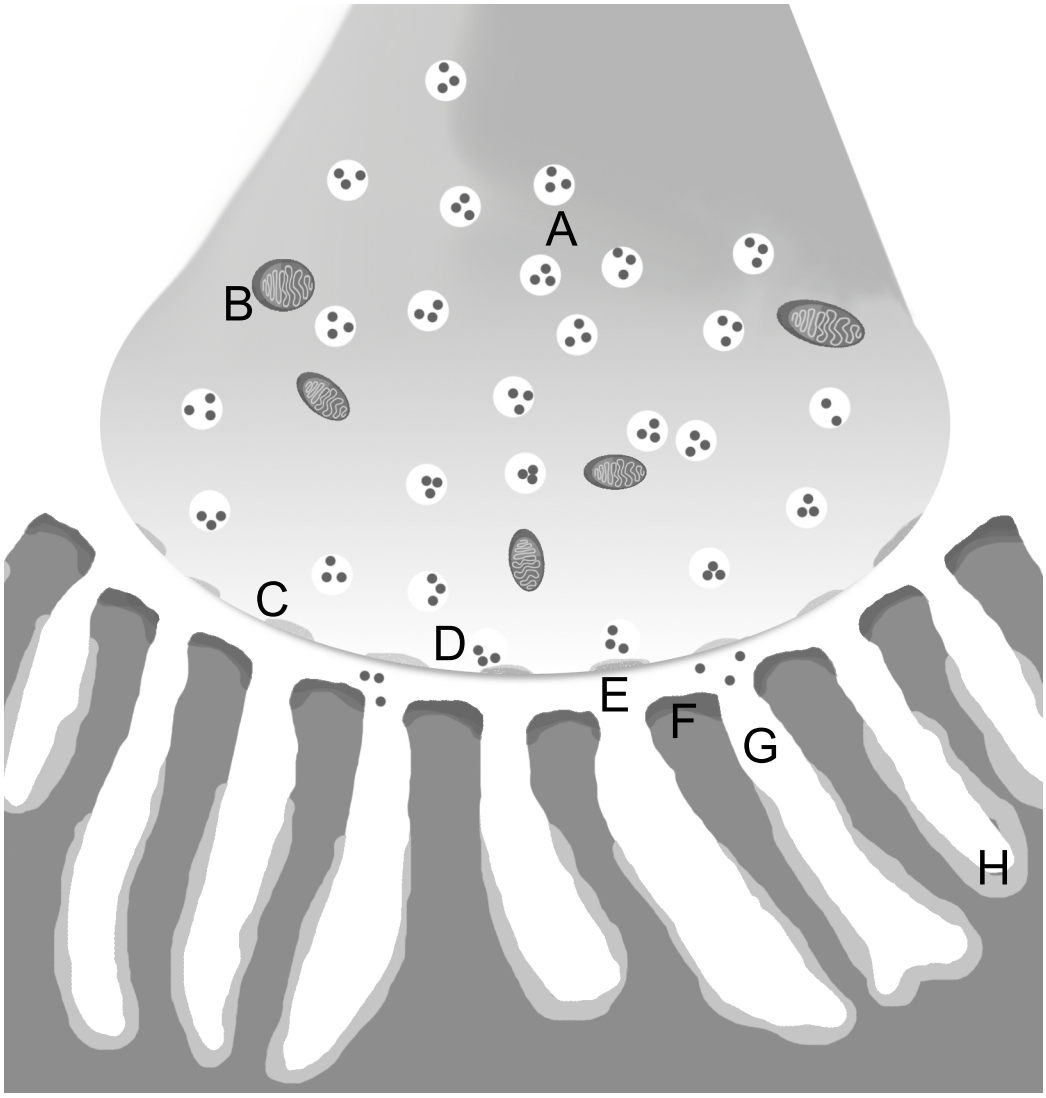

Figure 2. The neuromuscular junction is the intersection between the motoneuron and the postsynaptic muscle. Presynaptic terminals contain large pools of vesicles (A) prepared for mobilization to replace vesicles released after an action potential. Terminals also contain increased density of mitochondria (B). With the firing of an action potential, vesicles docked at a filamentous, electron dense active zone (C) fuse with the presynaptic membrane (D) and the neurotransmitter acetylcholine is released into the primary synaptic cleft (E). The acetylcholine traverses the synaptic cleft and binds to acetylcholine receptors located in densities along the crests of postsynaptic folds (F). With acetylcholine binding, sodium flows into the postsynaptic muscle and potassium flows out, potentially generating an action potential and contraction in the muscle. To increase the safety factor of transmission, additional concentrations of sodium channels (H) are located in the secondary postsynaptic clefts (G).

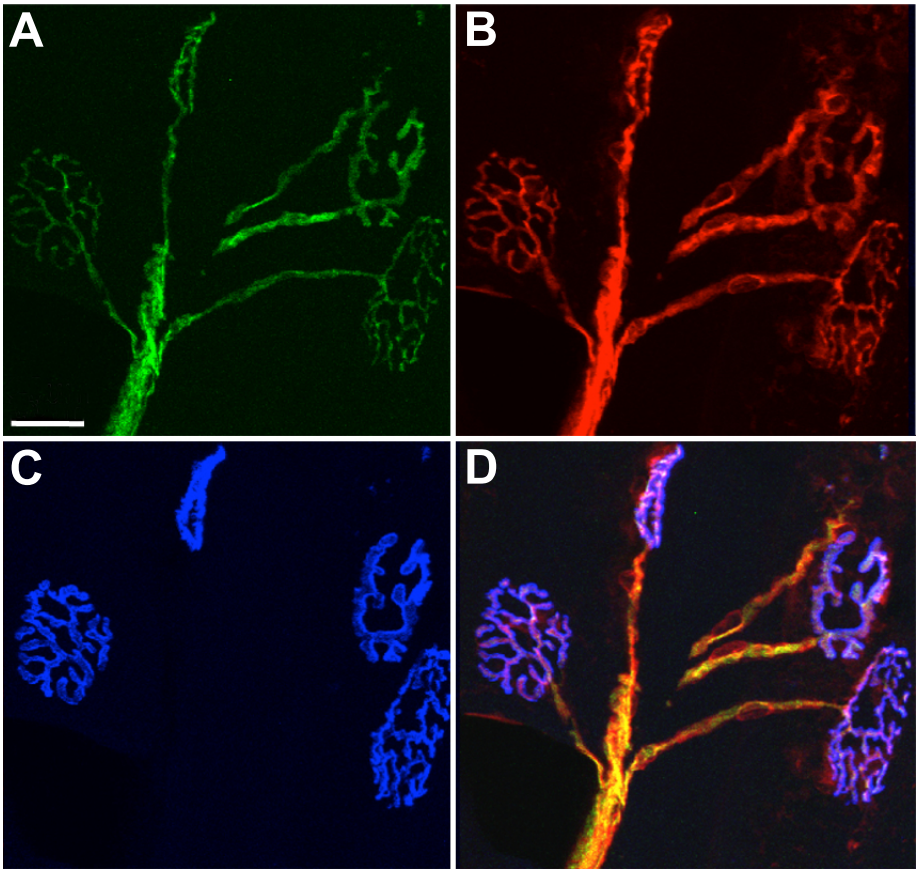

Figure 3. The tripartite junction. The neuromuscular junction is composed of three distinct cell types: motoneurons (A, shown with yellow fluorescent protein expression), terminal Schwann cells (B, shown with S100 labeling) and muscle fibers (C, acetylcholine receptors on the postsynaptic muscle are labeled with bungarotoxin in blue). In junctions from healthy animals, precise alignment of the three components is a consistent feature (D, overlay of the three components). This alignment breaks down in junctions from diseased animals. Scale bar represents 20 microns

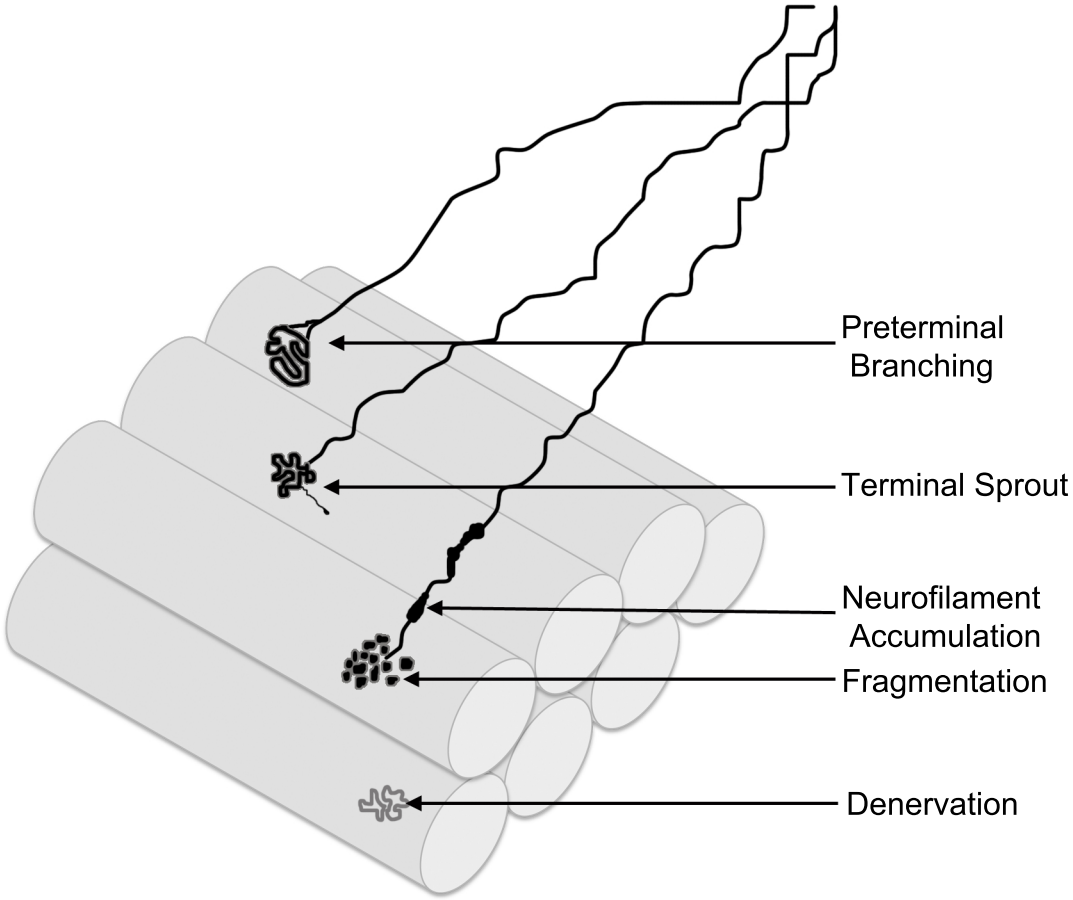

Figure 4. Indications of pathology at the neuromuscular junction. With disease, the precise alignment of the motoneuron, terminal Schwann cells and muscle begin to degrade. For example, particularly when muscle fibers reduce their signaling to motoneurons, the terminal begins to retract and denervation results, leaving behind the AChR-rich endplate. As a second form of pathology, the AChR in the endplate can have a punctate, fragmented appearance instead of the normal continuous pattern of receptors. In the preterminal axon, large, bulbous accumulations of neurofilament proteins form, potentially disrupting axonal transport. Often associated with denervation, motoneurons can be seen sending out sprouts from their terminals, presumed to be in an attempt to reform connections with at denervated endplates. Additionally, signals from the muscle can cause increases in the number of preterminal branches.

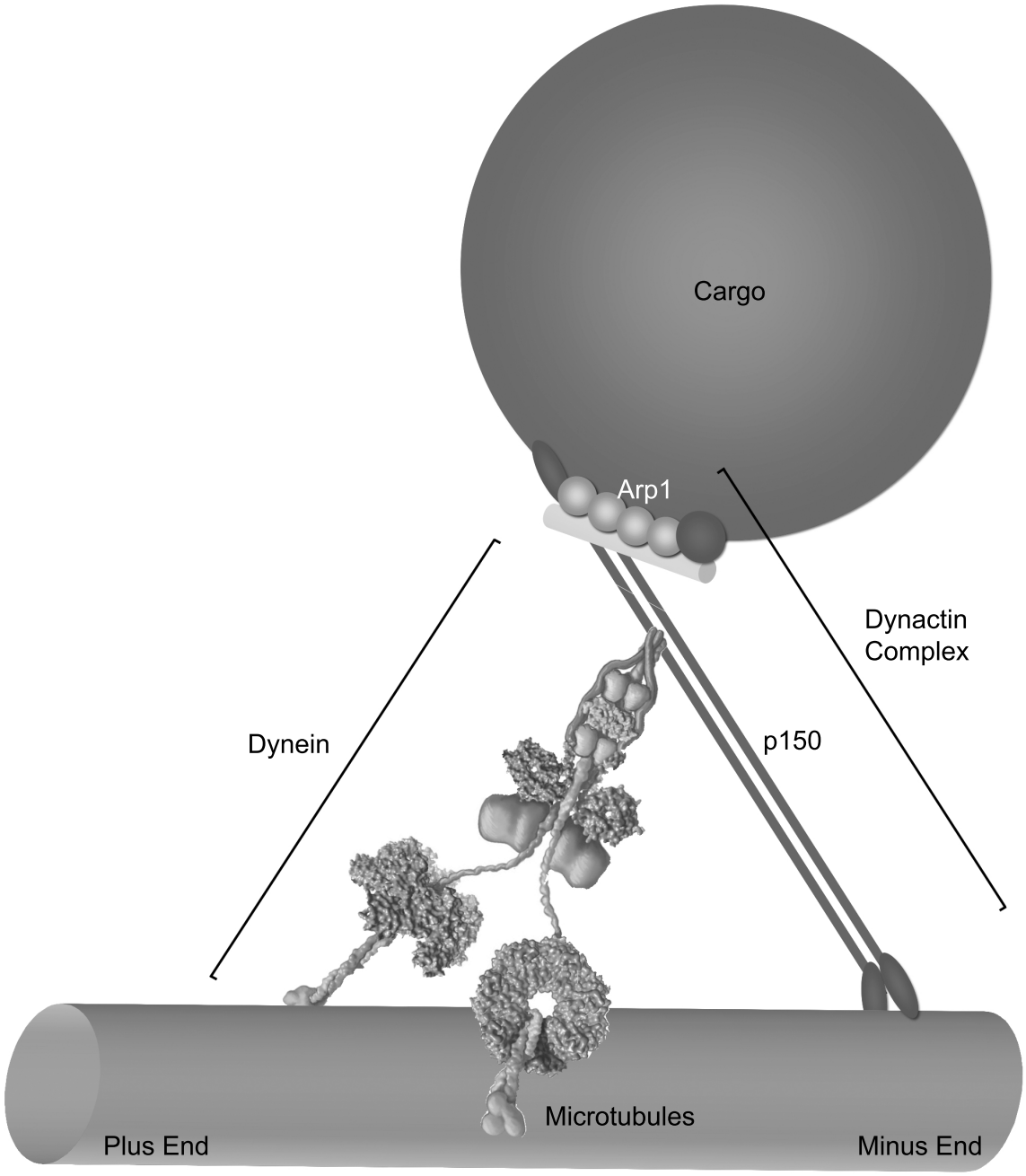

Figure 5. The dynein molecule interacts with the dynactin complex to produce minus end directed movement. The dynein molecule is composed of heavy and light chains and interacts with the microtubules and p150, a component of the dynactin complex. A second component of the dynactin complex, Arp1, interacts directly with the cargo.

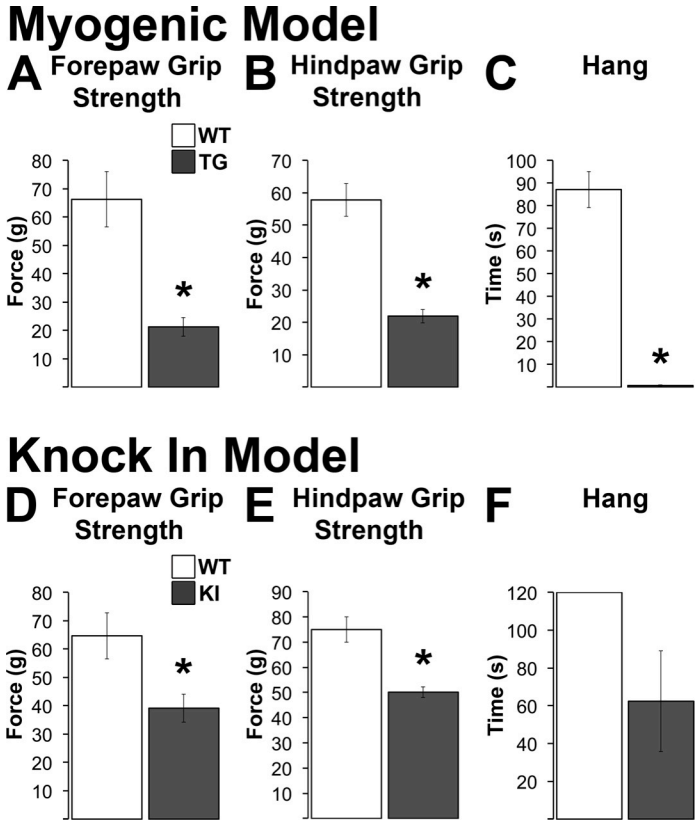

Figure 6. Male mice of two different SBMA models (myogenic transgenic (TG) and knock-in (KI)) show the expected motor impairments. Mean frontpaw and hindpaw grip strength were significantly decreased in myogenic TG males compared to wildtype (WT) control males (A, B). TG males also showed profound deficits in mean hang time (C). As expected, KI males were not as severely impaired as TG males, but nonetheless showed significant deficits in both fore- and hindpaw grip force (D, E). KI hang test measures were reduced, but were not significant due to the substantial variance in KI males (F). *$p < 0.05$ compared to WT controls. Error bars represent standard error of the mean, with n = 8 mice/group for TGs and 5 mice/group for KIs.

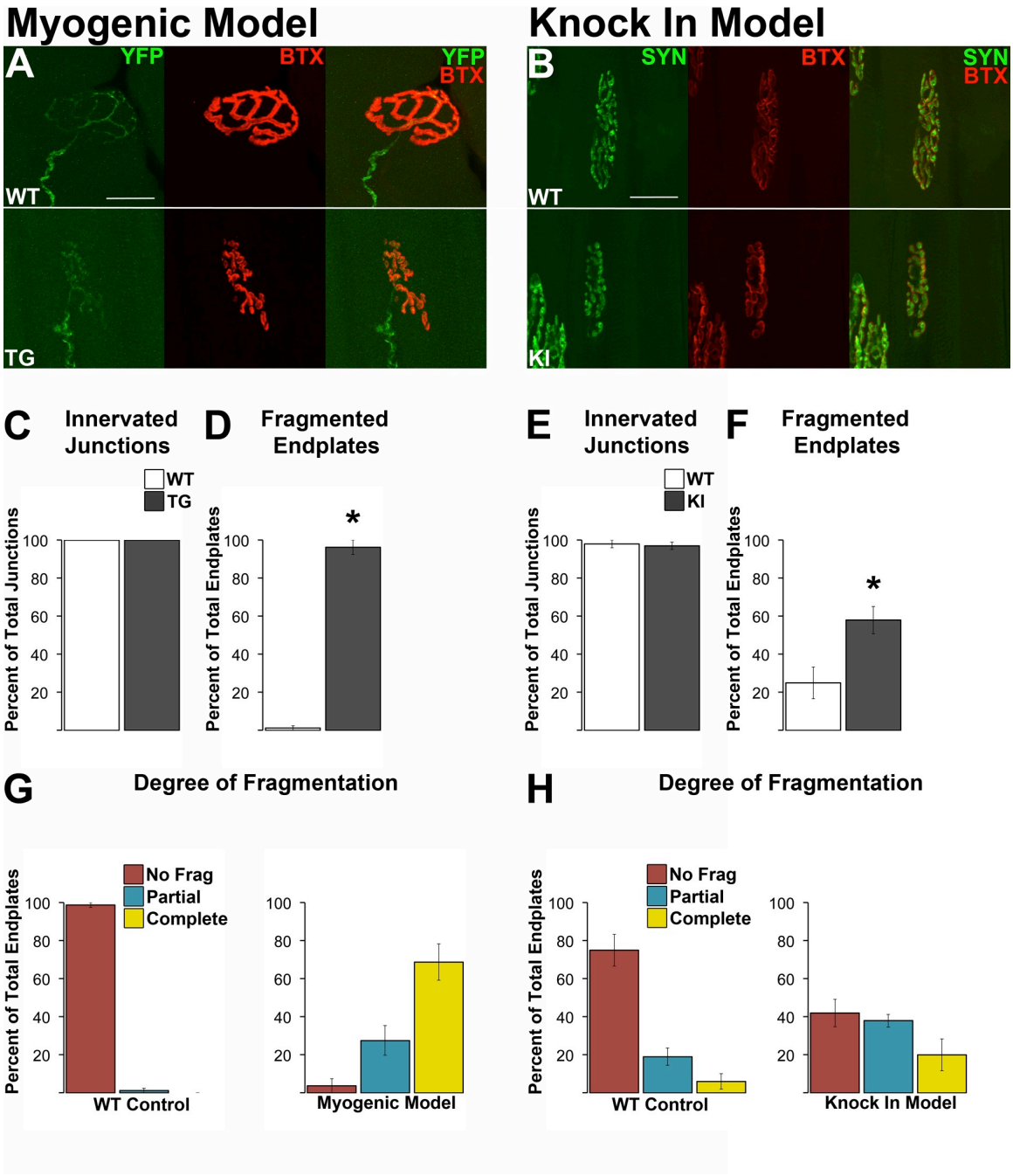

Figure 7. Neuromuscular junctions (NMJs) in both diseased TG and KI males show no evidence of morphological denervation but are consistently fragmented. Despite fragmentation, pre- and postsynaptic components of the NMJ showed precise alignment between the overlying YFP (A) or synaptophysin (B) labeled nerve terminal and the underlying α-bungarotoxin labeled (BTX) acetylcholine receptors (A, B). In short, there was no evidence of exposed endplates indicative of denervation (B, F). NMJs of wildtype (WT) muscle showed the typical, pretzel like morphology, while those in diseased muscle of both TG (A) and KI males (E) displayed a marked punctate appearance.

Figure 7 (cont'd)

Note that nearly every NMJ of myogenic TG males (C) was fragmented while only 58% of KI male junctions show fragmentation (G). Assessing the degree of fragmentation within each NMJ revealed that nearly all myogenic junctions are completely fragmented (D), while only about 20% of KI junctions show complete fragmentation. *$p < 0.05$ compared to WT controls. Error bars represent standard error of the mean, with $n = 4$ mice/group for TG and $N = 5$ mice/group for KI estimates of denervation and fragmentation, with twenty junctions examined per mouse. Scale bars represent 25 microns.

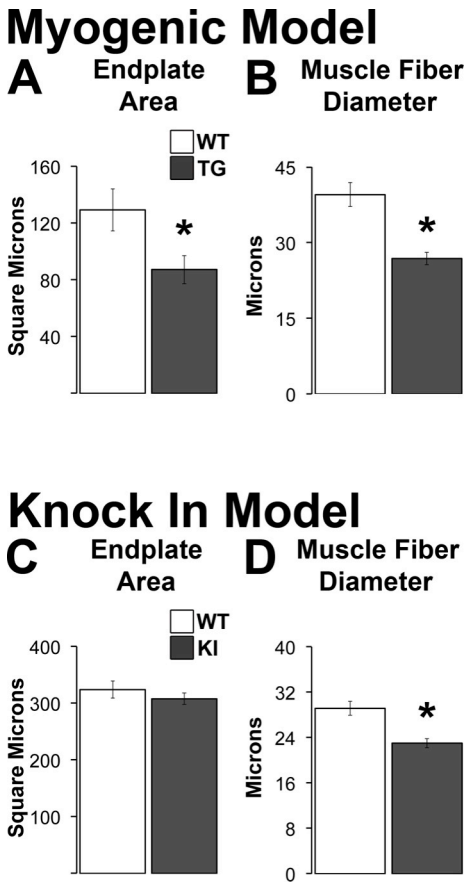

Figure 8. Endplates are reduced in size only in chronically affected myogenic TG males despite muscle fibers being smaller in both models. Both endplates and fiber size were significantly reduced in Tg males compared to WT males (A, B). In contrast, endplates in diseased KI muscle were normal in size (C) despite smaller muscle fibers (D). This dissociation between endplate and fiber size in diseased KI males raises the possibility that synaptic strength is spared if not enhanced compared to diseased males in the TG model. *$p < 0.05$ compared to WT controls. Error bars represent standard error of the mean. N = 6 - 7 mice/group for estimates of TG endplate area and n = 4 for TG fiber area estimates. N = 5 mice/group for estimates of KI endplate area and fiber area estimates, with twenty junctions sampled per muscle/animal.

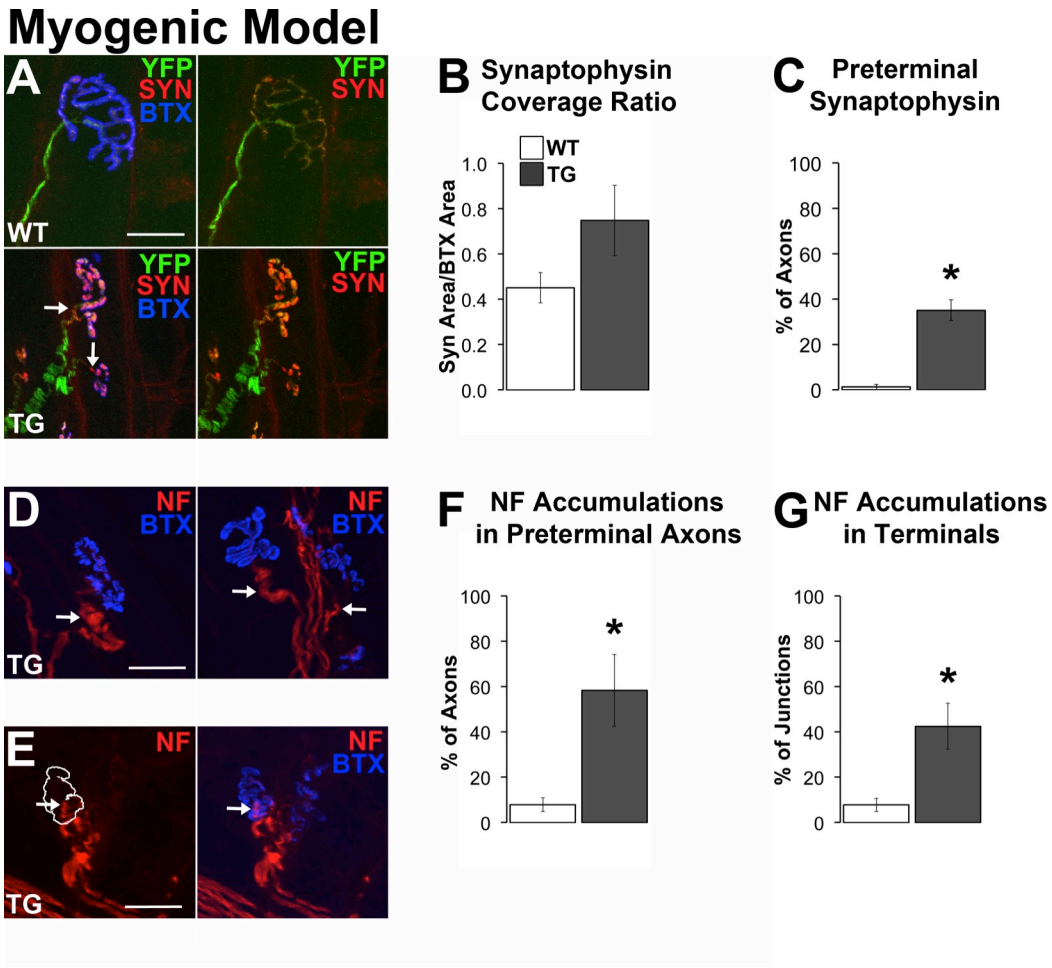

Figure 9. The distribution of synaptophysin (SYN) and neurofilament (NF) in preterminal axons and nerve terminals is affected by disease in TG male muscle. Synaptophysin staining was sparse in WT nerve terminals compared to an apparent greater density within the nerve terminals of TG males (A). As a result, a greater percentage of the endplate was covered by synaptophysin staining in TG nerve terminals compared to WT terminals (B). Moreover, synaptophysin staining extended into the preterminal axon (by about 5 μm, arrows in A) in nearly 40% of TG junctions (C) compared to little or no such staining in preterminal axons of WT junctions. Neurofilament accumulations, appearing as bulbous thickenings of NF staining in the preterminal axon (D, arrows) or nerve terminal (E, arrows) were also a prominent feature of junctions in diseased muscle from TG males. The white outline in E denotes where the postsynaptic BTX label is found in the second image as an indication of where the terminal is located. Forty – 60% of junctions contained NF accumulations in either presynaptic axons (F) and/or in the terminal itself (G). *$p < 0.05$ compared to WT controls. Error bars represent standard error of the mean, with 6 - 7 mice/group for synaptophysin estimates and 4 – 5 mice/group for neurofilament measures, with twenty junctions measured per mouse. Scale bars represent 25 microns.

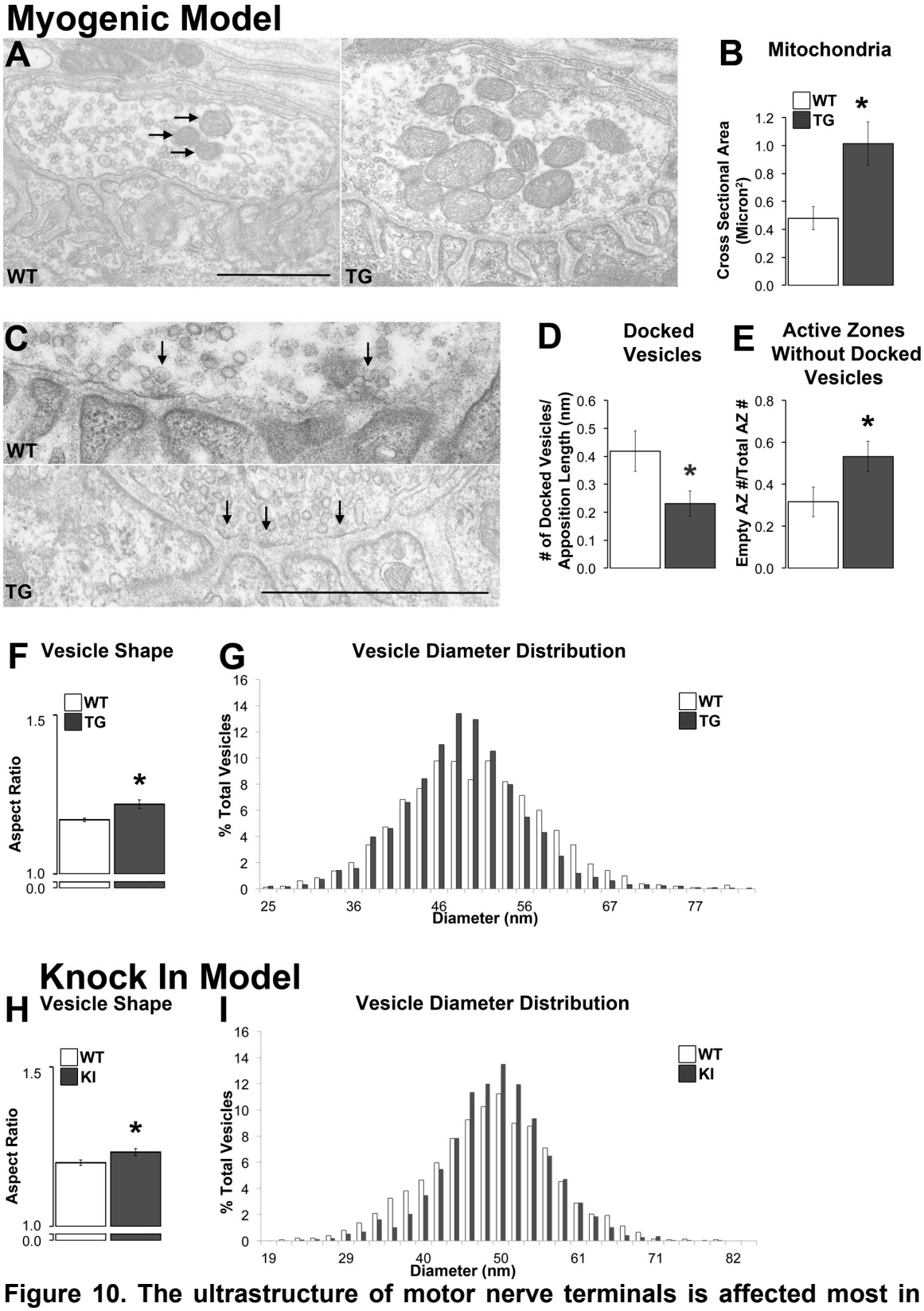

Figure 10. The ultrastructure of motor nerve terminals is affected most in myogenic TG males.

Figure 10 (cont'd)

The cross sectional area of mitochondria in TG nerve terminals was significantly larger than in WT terminals (A, B, arrows indicate mitochondria) despite no changes in their number. While the number of active zones, which were identified by as an electron dense area directly across from the mouth of a postsynaptic fold (C, denoted with arrows), per length of nerve terminal was unaffected by disease (Table 11), the number of docked vesicles (vesicles directly adjacent to the presynaptic membrane) per active zone was, with significantly fewer docked vesicles at active zones in TGs compared to WTs (D). Consistent with this finding, the number of active zones without docked vesicles was *increased* in TG terminals compared to WT terminals (E). Vesicles in TG nerve terminals were also less round than WT vesicles based on their aspect ratio (minimum diameter over maximum diameter; F). Although the distribution of average vesicle diameters appeared narrower and more centered around the mean in TG than WT terminals, WT and TG vesicle size did not differ significantly in size distribution (G). Nerve terminals in KI compared to WT males showed less effects of disease with no difference in number of active zones, docked vesicles, or active zones without docked vesicles (Table 12). However, vesicles in KI nerve terminals show an increase in their aspect ratio, like TG males, indicating that they are less round than those in WT males (H). Likewise, the distribution of vesicle diameters was narrower and more centered around the mean (I). *$p < 0.05$ compared to WT controls. Error bars represent standard error of the mean, with n = 30 junctions/group sampled from 3 animals/group, with 10 junctions sampled from each animal. Scale bars represent one micron.

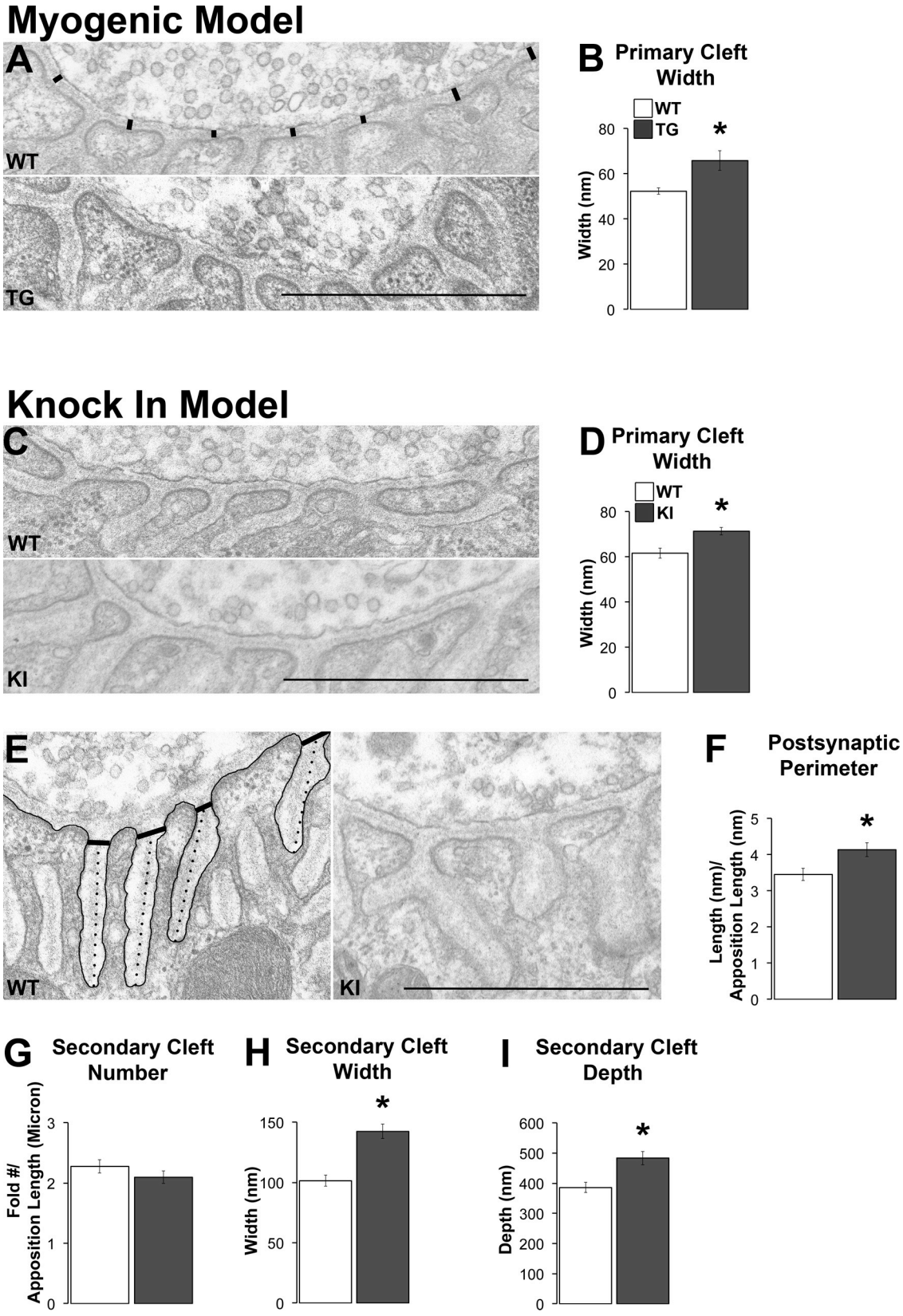

Figure 11. The ultrastructure of postsynaptic junctions is affected most in symptomatic KI males.

Figure 11 (cont'd)

Although the WT synaptic cleft showed tight apposition between the pre- and postsynaptic specializations, the synaptic cleft of TG junctions appeared much looser and is appreciably wider, based on measurements of the distances between the presynaptic membrane and the postsynaptic folds (A, black lines). In both disease models, the width of the primary cleft was increased (B, D). The postsynaptic folds of KI junctions also appeared simplified (E), a phenomenon not seen in TG junctions. The postsynaptic perimeter, indicated by the black tracing, was increased in KI junctions compared to WT junctions (F). While there was a decrease in secondary cleft number, this difference was not significant (G). The secondary cleft width, measured at a standard distance from the cleft opening (denoted by the thick black lines in E), was increased in KI junctions compared to WT junctions (H). The depth of the secondary cleft was also increased (I), measured as indicated by the dotted lines in E. *$p < 0.05$ compared to WT. Error bars represent standard error of the mean, with N = 30 junctions/group, with 3 animals/group, and 10 junctions sampled from each animal. Scale bars represent one micron.

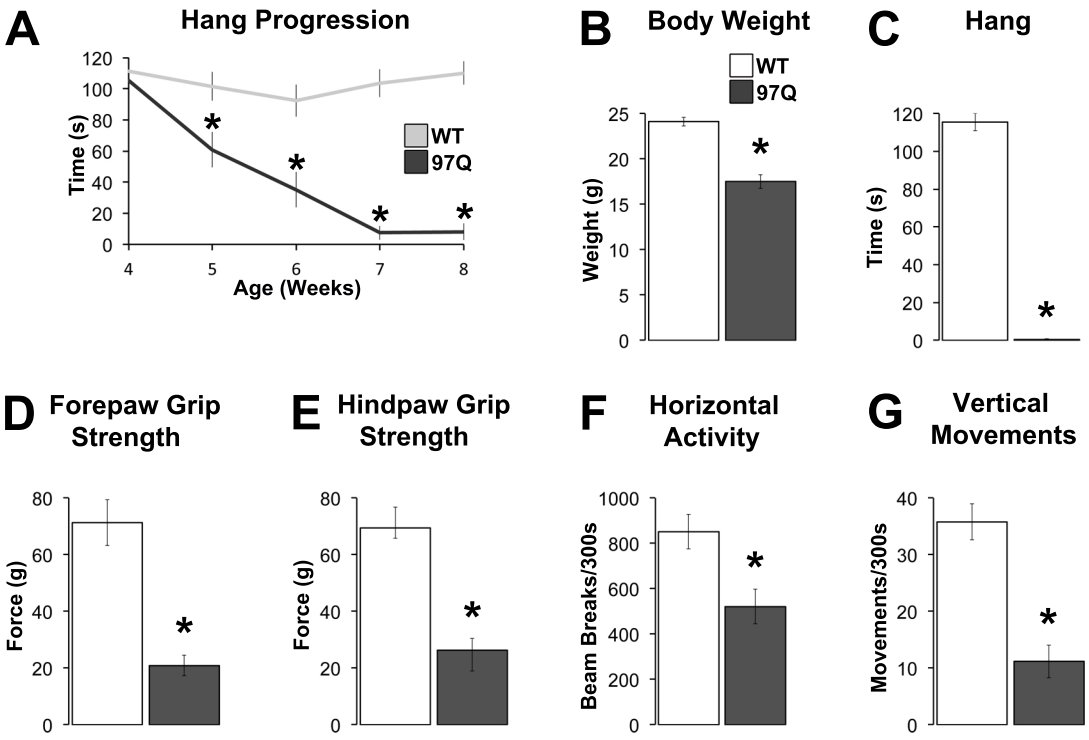

Figure 12. 97Q male mice show the expected motor impairments. Diseased 97Q males exhibit normal motor strength at four weeks but begin to show progressive motor deficits at five weeks as measured by the hang test (A). Body weight is decreased in affected 97Q males compared to their wildtype (WT) brothers (B). End-stage disease in 97Q males is marked by profound deficits in hang time (C), front- and hindpaw grip strengths (D, E), and decreased activity in an open field based on both horizontal (F) and vertical movements (G). Data in B - G is from the final day of testing for all animals used in either trafficking or junction morphology experiments. Once reaching the criteria for motor deficit, 97Q animals and their WT brothers were assigned to either trafficking or morphology experiments. *$p < 0.05$ for disease progression in A. *$p < 0.001$ compared to WT controls for endpoint measures in B - G. Error bars represent standard error of the mean, with n = 17 mice/group, with the exception of weeks 8 – 10 in the progression of hang test, as animals began to meet the criteria for motor deficit (Table 16).

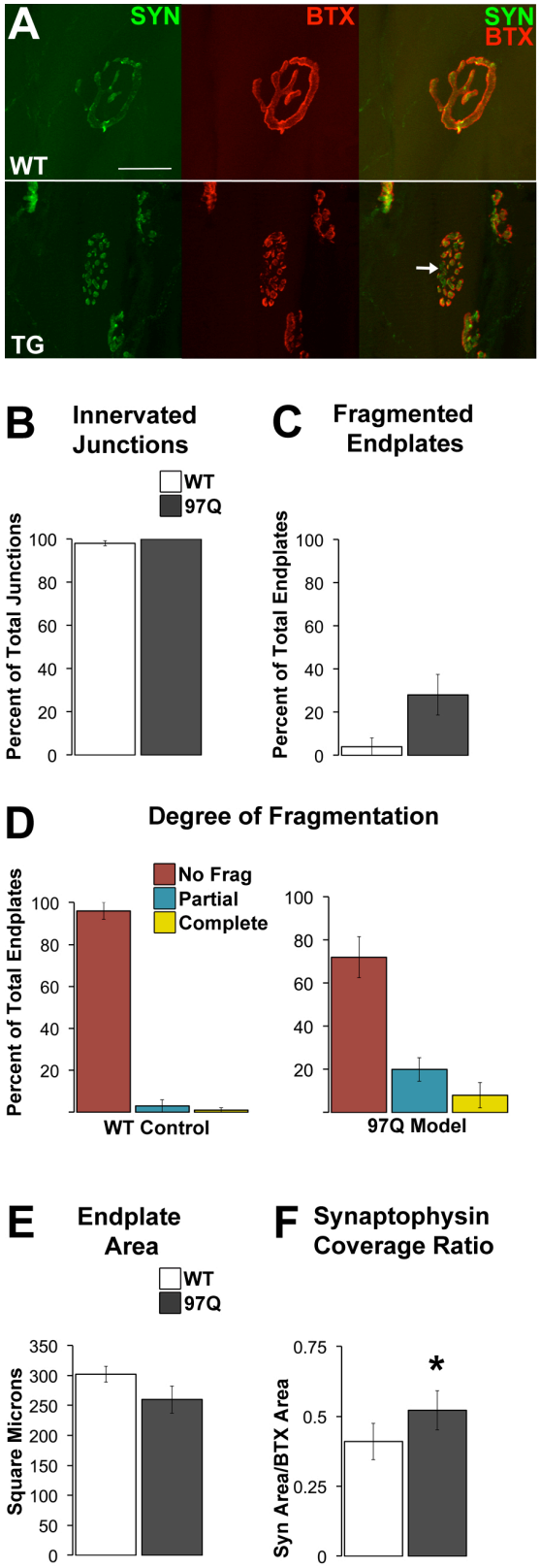

Figure 13. Neuromuscular junctions in 97Q males are not denervated but show fragmentation and enhanced synaptophysin immunoreactivity in nerve terminals.

Figure 13 (cont'd)

Fluorescent co-staining for synaptophysin in nerve terminals and postsynaptic acetylcholine receptors (AChR, using tagged α-bungarotoxin, BTX) revealed the same precise alignment of pre- and postsynaptic elements of the junction (A) in skeletal muscle from diseased males with no evidence of exposed endplates indicative of denervation (B). Despite junctions being fully innervated in diseased muscle, other indicators of pathology were seen, including junctional fragmentation. Nearly all NMJs in wildtype (WT) muscle showed the typical, pretzel like morphology, while some junctions in diseased muscle displayed a marked punctate appearance (A, white arrow). While there was clear qualitative evidence for the fragmented phenotype, only a minority of junctions showed this phenotype, which was not significantly more than WTs (C). The majority of 97Q junctions were partially fragmented (D). Endplate area was also slightly, but not significantly, decreased (E). However, the relative density of synaptophysin staining in nerve terminals of diseased junctions was increased, resulting in an apparent increase in the area of synaptophysin coverage relative to endplate size for diseased 97Q junctions compared to healthy WT junctions (F). *$p < 0.05$ compared to WT controls. Error bars represent standard error of the mean, with n = 5 mice/group. Scale bars represent 25 microns.

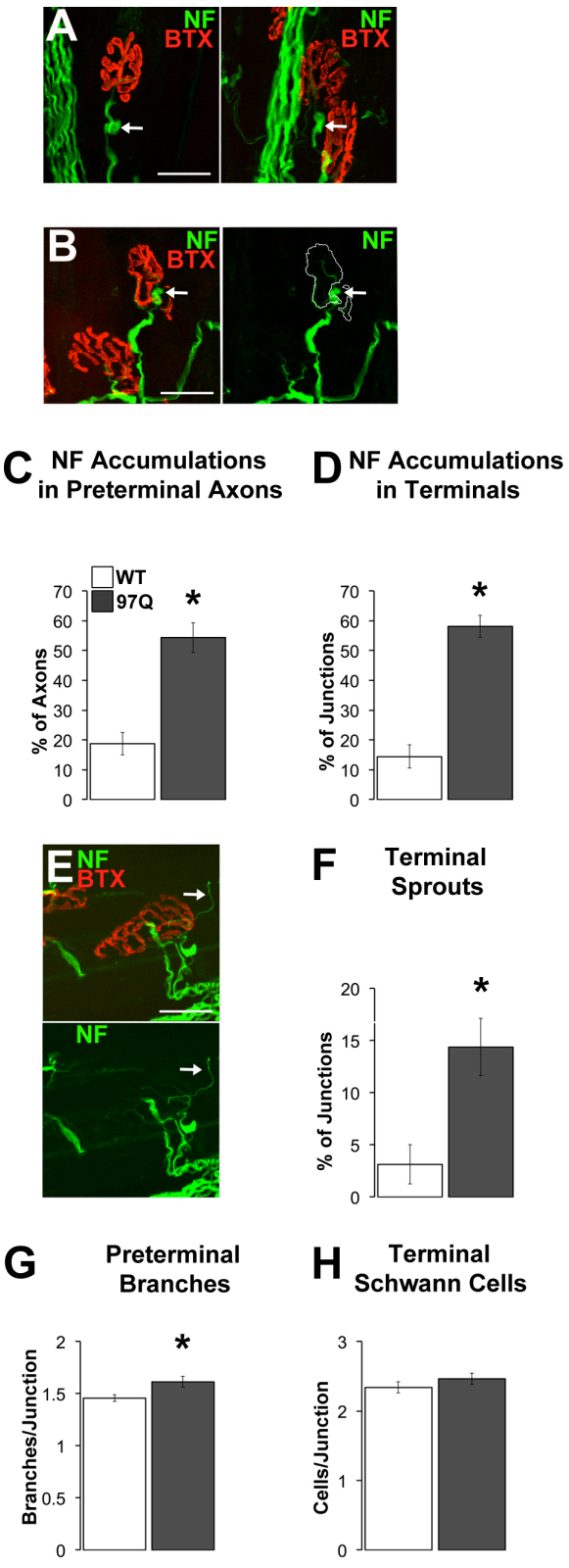

Figure 14. Disease is associated with prominent neurofilament accumulations (NF) and nerve terminal sprouting in the 97Q model.

Figure 14 (cont'd)

Neurofilament accumulations, appearing as bulbous thickenings of NF staining in the preterminal axons (A, arrows) and nerve terminals (B, arrow, endplate footprint outlined in white in right image) were prominent features of junctions in diseased muscle from affected 97Q males, with over half the junctions containing NF accumulations in either presynaptic axons (C) and/or in the terminal itself (D). In addition to these accumulations, significantly more junctions were associated with nerve terminal sprouts extending beyond the endplate (E, F). Junctions in diseased 97Q muscle were also characterized by having significantly more preterminal branches just proximal to the nerve terminal than junctions in WT muscle (G). In step with endplate size, which was unchanged by disease (Fig. 13E), the number of terminal Schwann cells was also not affected by disease in the 97Q model (H). *$p < 0.05$ compared to WT controls. Error bars represent standard error of the mean, with $n = 8$ mice/group for neurofilament, sprout and preterminal branching data and 4 mice/group for terminal Schwann cell data. Scale bars represent 25 microns.

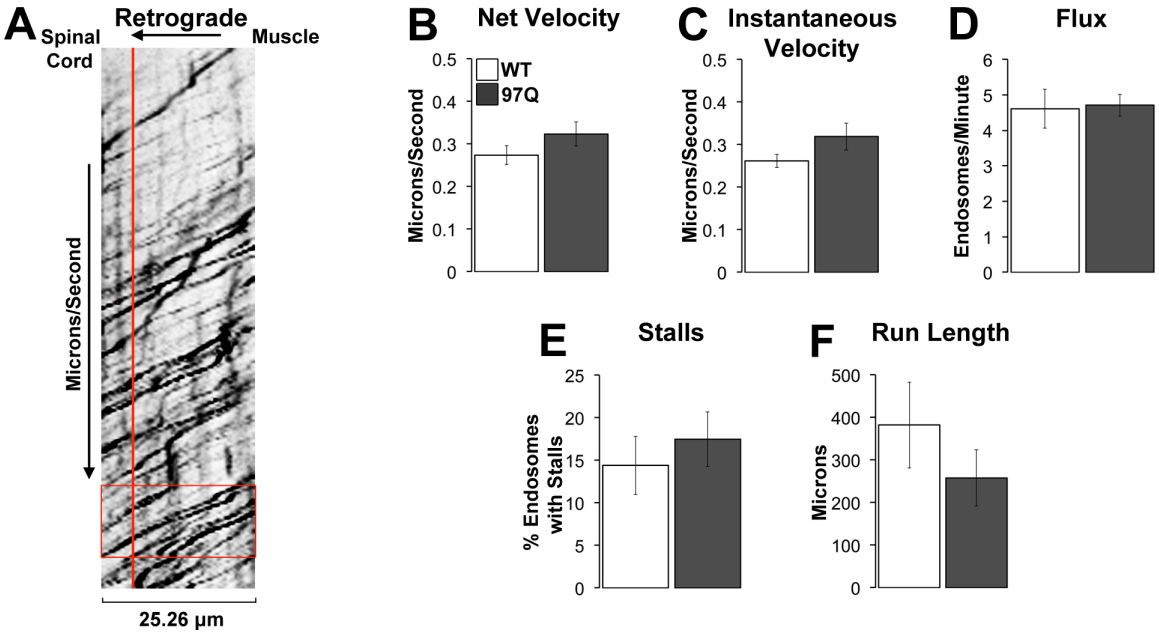

Figure 15. Live imaging of labeled endosomes reveals little to no deficits in endosomal transport in 97Q diseased males. Representative kymograph from live video imaging of transporting endosomes (called "endosomal traces," shown in black) labeled with cholera toxin-Alexa Fluor 488 (CT-AF488; A). Endosomal traces show the movement of single endosomes within a single axon over time and space. Endosomal flux is the number of endosomes that cross a point in the axon (indicated by the red vertical line) over time, whereas endosomal net velocity is the net distance traveled over a unit of time (indicated by the red rectangle for one endosomal trace). Unexpectedly, we find that disease affects neither net or instantaneous velocity (B, C) nor flux (D). More detailed analyses of kymographs revealed that endosomes tended to stall more and have shorter run lengths, but the effect of disease on both measures was not significant (E, F). Error bars represent standard error of the mean, with n = 9 mice/group.

REFERENCES

REFERENCES

Ackerley S, Grierson AJ, Banner S, Perkinton MS, Brownlees J, Byers HL, Ward M, Thornhill P, Hussain K, Waby JS, Anderton BH, Cooper JD, Dingwall C, Leigh PN, Shaw CE, Miller CC (2004) p38alpha stress-activated protein kinase phosphorylates neurofilaments and is associated with neurofilament pathology in amyotrophic lateral sclerosis. Mol Cell Neurosci 26:354-364.

Adachi H, Katsuno M, Minamiyama M, Sang C, Pagoulatos G, Angelidis C, Kusakabe M, Yoshiki A, Kobayashi Y, Doyu M, Sobue G (2003) Heat shock protein 70 chaperone overexpression ameliorates phenotypes of the spinal and bulbar muscular atrophy transgenic mouse model by reducing nuclear-localized mutant androgen receptor protein. J Neurosci 23:2203-2211.

Adachi H, Katsuno M, Minamiyama M, Waza M, Sang C, Nakagomi Y, Kobayashi Y, Tanaka F, Doyu M, Inukai A, Yoshida M, Hashizume Y, Sobue G (2005) Widespread nuclear and cytoplasmic accumulation of mutant androgen receptor in SBMA patients. Brain 128:659-670.

Anton ES, Weskamp G, Reichardt LF, Matthew WD (1994) Nerve growth factor and its low-affinity receptor promote Schwann cell migration. Proc Natl Acad Sci U S A 91:2795-2799.

Arbizu T, Santamaria J, Gomez JM, Quilez A, Serra JP (1983) A family with adult spinal and bulbar muscular atrophy, X-linked inheritance and associated testicular failure. J Neurol Sci 59:371-382.

Arrasate M, Mitra S, Schweitzer ES, Segal MR, Finkbeiner S (2004) Inclusion body formation reduces levels of mutant huntingtin and the risk of neuronal death. Nature 431:805-810.

Astrow SH, Son YJ, Thompson WJ (1994) Differential neural regulation of a neuromuscular junction-associated antigen in muscle fibers and Schwann cells. J Neurobiol 25:937-952.

Avila OL, Drachman DB, Pestronk A (1989) Neurotransmission regulates stability of acetylcholine receptors at the neuromuscular junction. J Neurosci 9:2902-2906.

Azzouz M, Ralph GS, Storkebaum E, Walmsley LE, Mitrophanous KA, Kingsman SM, Carmeliet P, Mazarakis ND (2004) VEGF delivery with retrogradely transported lentivector prolongs survival in a mouse ALS model. Nature 429:413-417.

Bailey CK, Andriola IF, Kampinga HH, Merry DE (2002) Molecular chaperones enhance the degradation of expanded polyglutamine repeat androgen receptor in a cellular model of spinal and bulbar muscular atrophy. Hum Mol Genet 11:515-523.

Balice-Gordon RJ, Smith DB, Goldman J, Cork LC, Shirley A, Cope TC, Pinter MJ (2000) Functional motor unit failure precedes neuromuscular degeneration in canine motor neuron disease. Ann Neurol 47:596-605.

Banks GB, Chamberlain JS, Froehner SC (2009) Truncated dystrophins can influence neuromuscular synapse structure. Mol Cell Neurosci 40:433-441.

Beauchemin AM, Gottlieb B, Beitel LK, Elhaji YA, Pinsky L, Trifiro MA (2001) Cytochrome c oxidase subunit Vb interacts with human androgen receptor: a potential mechanism for neurotoxicity in spinobulbar muscular atrophy. Brain research bulletin 56:285-297.

Birks RI (1974) The relationship of transmitter release and storage to fine structure in a sympathetic ganglion. J Neurocytol 3:133-160.

Birks RI, Macintosh FC (1957) Acetylcholine metabolism at nerve-endings. British medical bulletin 13:157-161.

Bloom FE, Aghajanian GK (1968) Fine structural and cytochemical analysis of the staining of synaptic junctions with phosphotungstic acid. Journal of ultrastructure research 22:361-375.

Bloom O, Evergren E, Tomilin N, Kjaerulff O, Low P, Brodin L, Pieribone VA, Greengard P, Shupliakov O (2003) Colocalization of synapsin and actin during synaptic vesicle recycling. J Cell Biol 161:737-747.

Boillee S, Yamanaka K, Lobsiger CS, Copeland NG, Jenkins NA, Kassiotis G, Kollias G, Cleveland DW (2006) Onset and progression in inherited ALS determined by motor neurons and microglia. Science 312:1389-1392.

Boon KL, Xiao S, McWhorter ML, Donn T, Wolf-Saxon E, Bohnsack MT, Moens CB, Beattie CE (2009) Zebrafish survival motor neuron mutants exhibit presynaptic neuromuscular junction defects. Hum Mol Genet 18:3615-3625.

Bosch-Marce M, Wee CD, Martinez TL, Lipkes CE, Choe DW, Kong L, Van Meerbeke JP, Musaro A, Sumner CJ (2011) Increased IGF-1 in muscle modulates the phenotype of severe SMA mice. Hum Mol Genet 20:1844-1853.

Breedlove SM, Arnold AP (1983) Hormonal control of a developing neuromuscular system. I. Complete Demasculinization of the male rat spinal nucleus of the bulbocavernosus using the anti-androgen flutamide. J Neurosci 3:417-423.

Brill LB, 2nd, Pfister KK (2000) Biochemical and molecular analysis of the mammalian cytoplasmic dynein intermediate chain. Methods (San Diego, Calif) 22:307-316.

Brown MC, Ironton R (1977) Motor neurone sprouting induced by prolonged tetrodotoxin block of nerve action potentials. Nature 265:459-461.

Browne SE, Beal MF (2006) Oxidative damage in Huntington's disease pathogenesis. Antioxidants & redox signaling 8:2061-2073.

Burkhardt JK, Echeverri CJ, Nilsson T, Vallee RB (1997) Overexpression of the dynamitin (p50) subunit of the dynactin complex disrupts dynein-dependent maintenance of membrane organelle distribution. J Cell Biol 139:469-484.

Butikofer L, Zurlinden A, Bolliger MF, Kunz B, Sonderegger P (2011) Destabilization of the neuromuscular junction by proteolytic cleavage of agrin results in precocious sarcopenia. FASEB J 25:4378-4393.

Caroni P, Becker M (1992) The downregulation of growth-associated proteins in motoneurons at the onset of synapse elimination is controlled by muscle activity and IGF1. J Neurosci 12:3849-3861.

Castonguay A, Robitaille R (2001) Differential regulation of transmitter release by presynaptic and glial Ca2+ internal stores at the neuromuscular synapse. J Neurosci 21:1911-1922.

Chahin N, Sorenson EJ (2009) Serum creatine kinase levels in spinobulbar muscular atrophy and amyotrophic lateral sclerosis. Muscle Nerve 40:126-129.

Chan YB, Miguel-Aliaga I, Franks C, Thomas N, Trulzsch B, Sattelle DB, Davies KE, van den Heuvel M (2003) Neuromuscular defects in a Drosophila survival motor neuron gene mutant. Hum Mol Genet 12:1367-1376.

Chang HC, Dimlich DN, Yokokura T, Mukherjee A, Kankel MW, Sen A, Sridhar V, Fulga TA, Hart AC, Van Vactor D, Artavanis-Tsakonas S (2008) Modeling spinal muscular atrophy in Drosophila. PLoS One 3:e3209.

Chevalier-Larsen ES, Merry DE (2012) Testosterone treatment fails to accelerate disease in a transgenic mouse model of spinal and bulbar muscular atrophy. Dis Model Mech 5:141-145.

Chevalier-Larsen ES, O'Brien CJ, Wang H, Jenkins SC, Holder L, Lieberman AP, Merry DE (2004) Castration restores function and neurofilament alterations of aged symptomatic males in a transgenic mouse model of spinal and bulbar muscular atrophy. J Neurosci 24:4778-4786.

Chevalier-Larsen ES, Wallace KE, Pennise CR, Holzbaur EL (2008) Lysosomal proliferation and distal degeneration in motor neurons expressing the G59S mutation in the p150Glued subunit of dynactin. Hum Mol Genet 17:1946-1955.

Chiu AY, Zhai P, Dal Canto MC, Peters TM, Kwon YW, Prattis SM, Gurney ME (1995) Age-dependent penetrance of disease in a transgenic mouse model of familial amyotrophic lateral sclerosis. Mol Cell Neurosci 6:349-362.

Chiu SY (1991) Functions and distribution of voltage-gated sodium and potassium channels in mammalian Schwann cells. Glia 4:541-558.

Choong CS, Kemppainen JA, Zhou ZX, Wilson EM (1996) Reduced androgen receptor gene expression with first exon CAG repeat expansion. Mol Endocrinol 10:1527-1535.

Cifuentes-Diaz C, Nicole S, Velasco ME, Borra-Cebrian C, Panozzo C, Frugier T, Millet G, Roblot N, Joshi V, Melki J (2002) Neurofilament accumulation at the motor endplate and lack of axonal sprouting in a spinal muscular atrophy mouse model. Hum Mol Genet 11:1439-1447.

Clement AM, Nguyen MD, Roberts EA, Garcia ML, Boillee S, Rule M, McMahon AP, Doucette W, Siwek D, Ferrante RJ, Brown RH, Jr., Julien JP, Goldstein LS, Cleveland DW (2003) Wild-type nonneuronal cells extend survival of SOD1 mutant motor neurons in ALS mice. Science 302:113-117.

Collard JF, Cote F, Julien JP (1995) Defective axonal transport in a transgenic mouse model of amyotrophic lateral sclerosis. Nature 375:61-64.

Conti-Fine BM, Milani M, Kaminski HJ (2006) Myasthenia gravis: past, present, and future. J Clin Invest 116:2843-2854.

Couteaux R, Pecot-Dechavassine M (1970) [Synaptic vesicles and pouches at the level of "active zones" of the neuromuscular junction]. Comptes rendus hebdomadaires des seances de l'Academie des sciences Serie D: Sciences naturelles 271:2346-2349.

Cummings CJ, Reinstein E, Sun Y, Antalffy B, Jiang Y, Ciechanover A, Orr HT, Beaudet AL, Zoghbi HY (1999) Mutation of the E6-AP ubiquitin ligase reduces nuclear inclusion frequency while accelerating polyglutamine-induced pathology in SCA1 mice. Neuron 24:879-892.

Deconinck AE, Rafael JA, Skinner JA, Brown SC, Potter AC, Metzinger L, Watt DJ, Dickson JG, Tinsley JM, Davies KE (1997) Utrophin-dystrophin-deficient mice as a model for Duchenne muscular dystrophy. Cell 90:717-727.

Deiraldi AP, Zieher LM, Derobertis E (1963) The 5-Hydroxytryptamine Content and Synthesis of Normal and Denervated Pineal Gland. Life sciences 9:691-696.

Dejager S, Bry-Gauillard H, Bruckert E, Eymard B, Salachas F, LeGuern E, Tardieu S, Chadarevian R, Giral P, Turpin G (2002) A comprehensive endocrine description of Kennedy's disease revealing androgen insensitivity linked to CAG repeat length. J Clin Endocrinol Metab 87:3893-3901.

Delcroix JD, Valletta J, Wu C, Howe CL, Lai CF, Cooper JD, Belichenko PV, Salehi A, Mobley WC (2004) Trafficking the NGF signal: implications for normal and degenerating neurons. Progress in brain research 146:3-23.

Di Carlo M, Giacomazza D, Picone P, Nuzzo D, San Biagio PL (2012) Are oxidative stress and mitochondrial dysfunction the key players in the neurodegenerative diseases? Free radical research 46:1327-1338.

Dobrowolny G, Giacinti C, Pelosi L, Nicoletti C, Winn N, Barberi L, Molinaro M, Rosenthal N, Musaro A (2005) Muscle expression of a local Igf-1 isoform protects motor neurons in an ALS mouse model. J Cell Biol 168:193-199.

Doussau F, Augustine GJ (2000) The actin cytoskeleton and neurotransmitter release: an overview. Biochimie 82:353-363.

Doyu M, Sobue G, Mukai E, Kachi T, Yasuda T, Mitsuma T, Takahashi A (1992) Severity of X-linked recessive bulbospinal neuronopathy correlates with size of the tandem CAG repeat in androgen receptor gene. Ann Neurol 32:707-710.

Duchen LW, Strich SJ (1968) The effects of botulinum toxin on the pattern of innervation of skeletal muscle in the mouse. Q J Exp Physiol Cogn Med Sci 53:84-89.

Eaton BA, Fetter RD, Davis GW (2002) Dynactin is necessary for synapse stabilization. Neuron 34:729-741.

Eccles JC (1957) The clinical significance of research work on the chemical transmitter substances of the nervous system. The Medical journal of Australia 44:745-753.

Elluru RG, Bloom GS, Brady ST (1995) Fast axonal transport of kinesin in the rat visual system: functionality of kinesin heavy chain isoforms. Mol Biol Cell 6:21-40.

Engel AG (1994) Congenital myasthenic syndromes. Neurologic clinics 12:401-437.

Engel AG, Santa T (1971) Histometric analysis of the ultrastructure of the neuromuscular junction in myasthenia gravis and in the myasthenic syndrome. Ann N Y Acad Sci 183:46-63.

English AW (2003) Cytokines, growth factors and sprouting at the neuromuscular junction. J Neurocytol 32:943-960.

Feany MB, Yee AG, Delvy ML, Buckley KM (1993) The synaptic vesicle proteins SV2, synaptotagmin and synaptophysin are sorted to separate cellular compartments in CHO fibroblasts. J Cell Biol 123:575-584.

Fischbeck KH, Ionasescu V, Ritter AW, Ionasescu R, Davies K, Ball S, Bosch P, Burns T, Hausmanowa-Petrusewicz I, Borkowska J, et al. (1986) Localization of the gene for X-linked spinal muscular atrophy. Neurology 36:1595-1598.

Fischbeck KH, Souders D, La Spada A (1991) A candidate gene for X-linked spinal muscular atrophy. Adv Neurol 56:209-213.

Fischer LR, Culver DG, Tennant P, Davis AA, Wang M, Castellano-Sanchez A, Khan J, Polak MA, Glass JD (2004) Amyotrophic lateral sclerosis is a distal axonopathy: evidence in mice and man. Exp Neurol 185:232-240.

Fitzsimonds RM, Poo MM (1998) Retrograde signaling in the development and modification of synapses. Physiol Rev 78:143-170.

Flucher BE, Daniels MP (1989) Distribution of Na+ channels and ankyrin in neuromuscular junctions is complementary to that of acetylcholine receptors and the 43 kd protein. Neuron 3:163-175.

Frey D, Schneider C, Xu L, Borg J, Spooren W, Caroni P (2000) Early and selective loss of neuromuscular synapse subtypes with low sprouting competence in motoneuron diseases. J Neurosci 20:2534-2542.

Friedman B, Scherer SS, Rudge JS, Helgren M, Morrisey D, McClain J, Wang DY, Wiegand SJ, Furth ME, Lindsay RM, et al. (1992) Regulation of ciliary neurotrophic factor expression in myelin-related Schwann cells in vivo. Neuron 9:295-305.

Funakoshi H, Belluardo N, Arenas E, Yamamoto Y, Casabona A, Persson H, Ibanez CF (1995) Muscle-derived neurotrophin-4 as an activity-dependent trophic signal for adult motor neurons. Science 268:1495-1499.

Georgiou J, Robitaille R, Trimble WS, Charlton MP (1994) Synaptic regulation of glial protein expression in vivo. Neuron 12:443-455.

Gordon T, Ly V, Hegedus J, Tyreman N (2009) Early detection of denervated muscle fibers in hindlimb muscles after sciatic nerve transection in wild type mice and in the G93A mouse model of amyotrophic lateral sclerosis. Neurol Res 31:28-42.

Grady RM, Teng H, Nichol MC, Cunningham JC, Wilkinson RS, Sanes JR (1997) Skeletal and cardiac myopathies in mice lacking utrophin and dystrophin: a model for Duchenne muscular dystrophy. Cell 90:729-738.

Grimby G, Einarsson G, Hedberg M, Aniansson A (1989) Muscle adaptive changes in post-polio subjects. Scandinavian journal of rehabilitation medicine 21:19-26.

Guzzini M, Raffa S, Geuna S, Nicolino S, Torrisi MR, Tos P, Battiston B, Grassi F, Ferretti A (2008) Denervation-related changes in acetylcholine receptor density and distribution in the rat flexor digitorum sublimis muscle. Italian journal of anatomy and embryology = Archivio italiano di anatomia ed embriologia 113:209-216.

Hafezparast M, Klocke R, Ruhrberg C, Marquardt A, Ahmad-Annuar A, Bowen S, Lalli G, Witherden AS, Hummerich H, Nicholson S, Morgan PJ, Oozageer R, Priestley JV, Averill S, King VR, Ball S, Peters J, Toda T, Yamamoto A, Hiraoka Y, Augustin M, Korthaus D, Wattler S, Wabnitz P, Dickneite C, Lampel S, Boehme F, Peraus G, Popp A, Rudelius M, Schlegel J, Fuchs H, Hrabe de Angelis M, Schiavo G, Shima DT, Russ AP, Stumm G, Martin

JE, Fisher EM (2003) Mutations in dynein link motor neuron degeneration to defects in retrograde transport. Science 300:808-812.

Harata N, Ryan TA, Smith SJ, Buchanan J, Tsien RW (2001) Visualizing recycling synaptic vesicles in hippocampal neurons by FM 1-43 photoconversion. Proc Natl Acad Sci U S A 98:12748-12753.

Harding AE, Thomas PK, Baraitser M, Bradbury PG, Morgan-Hughes JA, Ponsford JR (1982) X-linked recessive bulbospinal neuronopathy: a report of ten cases. J Neurol Neurosurg Psychiatry 45:1012-1019.

Hashizume A, Katsuno M, Banno H, Suzuki K, Suga N, Mano T, Atsuta N, Oe H, Watanabe H, Tanaka F, Sobue G (2012) Longitudinal changes of outcome measures in spinal and bulbar muscular atrophy. Brain 135:2838-2848.

Hegstrom CD, Jordan CL, Breedlove SM (2002) Photoperiod and androgens act independently to induce spinal nucleus of the bulbocavernosus neuromuscular plasticity in the Siberian hamster, Phodopus sungorus. Journal of neuroendocrinology 14:368-374.

Henderson CE, Phillips HS, Pollock RA, Davies AM, Lemeulle C, Armanini M, Simmons L, Moffet B, Vandlen RA, Simpson LC, et al. (1994) GDNF: a potent survival factor for motoneurons present in peripheral nerve and muscle. Science 266:1062-1064.

Henderson TA, Rhoades RW, Bennett-Clarke CA, Osborne PA, Johnson EM, Jacquin MF (1993) NGF augmentation rescues trigeminal ganglion and principalis neurons, but not brainstem or cortical whisker patterns, after infraorbital nerve injury at birth. J Comp Neurol 336:243-260.

Hervias I, Beal MF, Manfredi G (2006) Mitochondrial dysfunction and amyotrophic lateral sclerosis. Muscle Nerve 33:598-608.

Heumann R, Korsching S, Bandtlow C, Thoenen H (1987) Changes of nerve growth factor synthesis in nonneuronal cells in response to sciatic nerve transection. J Cell Biol 104:1623-1631.

Heuser JE, Reese TS (1973) Evidence for recycling of synaptic vesicle membrane during transmitter release at the frog neuromuscular junction. J Cell Biol 57:315-344.

Heuser JE, Reese TS, Dennis MJ, Jan Y, Jan L, Evans L (1979) Synaptic vesicle exocytosis captured by quick freezing and correlated with quantal transmitter release. J Cell Biol 81:275-300.

Hilfiker S, Pieribone VA, Czernik AJ, Kao HT, Augustine GJ, Greengard P (1999) Synapsins as regulators of neurotransmitter release. Philosophical transactions of the Royal Society of London Series B, Biological sciences 354:269-279.

Hoogerwaard EM, Schouten Y, van der Kooi AJ, Gorgels JP, de Visser M, Sanders GT (2001) Troponin T and troponin I in carriers of Duchenne and Becker muscular dystrophy with cardiac involvement. Clinical chemistry 47:962-963.

Hubbard JI, Llinas R, Quastel DMJ (1969) Electrophysiological analysis of synaptic transmission. London: Edward Arnold.

Igarashi S, Tanno Y, Onodera O, Yamazaki M, Sato S, Ishikawa A, Miyatani N, Nagashima M, Ishikawa Y, Sahashi K, et al. (1992) Strong correlation between the number of CAG repeats in androgen receptor genes and the clinical onset of features of spinal and bulbar muscular atrophy. Neurology 42:2300-2302.

Jang YC, Van Remmen H (2011) Age-associated alterations of the neuromuscular junction. Experimental gerontology 46:193-198.

Jiang YM, Yamamoto M, Kobayashi Y, Yoshihara T, Liang Y, Terao S, Takeuchi H, Ishigaki S, Katsuno M, Adachi H, Niwa J, Tanaka F, Doyu M, Yoshida M, Hashizume Y, Sobue G (2005) Gene expression profile of spinal motor neurons in sporadic amyotrophic lateral sclerosis. Ann Neurol 57:236-251.

Jirmanova I (1975) Ultrastructure of motor end-plates during pharmacologically-induced degeneration and subsequent regeneration of skeletal muscle. J Neurocytol 4:141-155.

Johansen JA, Troxell-Smith SM, Yu Z, Mo K, Monks DA, Lieberman AP, Breedlove SM, Jordan CL (2011) Prenatal Flutamide Enhances Survival in a Myogenic Mouse Model of Spinal Bulbar Muscular Atrophy. Neurodegener Dis.

Johansen JA, Yu Z, Mo K, Monks DA, Lieberman AP, Breedlove SM, Jordan CL (2009) Recovery of function in a myogenic mouse model of spinal bulbar muscular atrophy. Neurobiol Dis 34:113-120.

Jones SF, Kwanbunbumpen S (1970) Some effects of nerve stimulation andhemicholinium on quantal transmitter release at the mammalian neuromuscular junction. J Physiol 207:51-61.

Jordan CL, Letinsky MS, Arnold AP (1989a) The role of gonadal hormones in neuromuscular synapse elimination in rats. I. Androgen delays the loss of multiple innervation in the levator ani muscle. J Neurosci 9:229-238.

Jordan CL, Letinsky MS, Arnold AP (1989b) The role of gonadal hormones in neuromuscular synapse elimination in rats. II. Multiple innervation persists in the adult levator ani muscle after juvenile androgen treatment. J Neurosci 9:239-247.

Jordan CL, Lieberman AP (2008) Spinal and bulbar muscular atrophy: a motoneuron or muscle disease? Curr Opin Pharmacol 8:752-758.

Jordan CL, Pawson PA, Arnold AP, Grinnell AD (1992) Hormonal regulation of motor unit size and synaptic strength during synapse elimination in the rat levator ani muscle. J Neurosci 12:4447-4459.

Kamenskaya MA, Elmqvist D, Thesleff S (1975) Guanidine and neuromuscular transmission. II. Effect on transmitter release in response to repetitive nerve stimulation. Arch Neurol 32:510-518.

Kandel ER, Kupfermann I (1970) The functional organization of invertebrate ganglia. Annual review of physiology 32:193-258.

Kang H, Tian L, Thompson W (2003) Terminal Schwann cells guide the reinnervation of muscle after nerve injury. J Neurocytol 32:975-985.

Kariya S, Park GH, Maeno-Hikichi Y, Leykekhman O, Lutz C, Arkovitz MS, Landmesser LT, Monani UR (2008) Reduced SMN protein impairs maturation of the neuromuscular junctions in mouse models of spinal muscular atrophy. Hum Mol Genet 17:2552-2569.

Katsuno M, Adachi H, Doyu M, Minamiyama M, Sang C, Kobayashi Y, Inukai A, Sobue G (2003) Leuprorelin rescues polyglutamine-dependent phenotypes in a transgenic mouse model of spinal and bulbar muscular atrophy. Nat Med 9:768-773.

Katsuno M, Adachi H, Kume A, Li M, Nakagomi Y, Niwa H, Sang C, Kobayashi Y, Doyu M, Sobue G (2002) Testosterone reduction prevents phenotypic expression in a transgenic mouse model of spinal and bulbar muscular atrophy. Neuron 35:843-854.

Katsuno M, Adachi H, Minamiyama M, Waza M, Tokui K, Banno H, Suzuki K, Onoda Y, Tanaka F, Doyu M, Sobue G (2006a) Reversible disruption of dynactin 1-mediated retrograde axonal transport in polyglutamine-induced motor neuron degeneration. J Neurosci 26:12106-12117.

Katsuno M, Adachi H, Waza M, Banno H, Suzuki K, Tanaka F, Doyu M, Sobue G (2006b) Pathogenesis, animal models and therapeutics in spinal and bulbar muscular atrophy (SBMA). Exp Neurol 200:8-18.

Keating DJ (2008) Mitochondrial dysfunction, oxidative stress, regulation of exocytosis and their relevance to neurodegenerative diseases. J Neurochem 104:298-305.

Kemp M, Poort J, Baqri R, Breedlove S, Miller K, CL J (2009) Live imaging of endosomal trafficking deficits in sciatic nerves of a myogenic mouse model of SBMA. Society for Neuroscience 2009.

Kemp MQ, Poort JL, Baqri RM, Lieberman AP, Breedlove SM, Miller KE, Jordan CL (2011) Impaired motoneuronal retrograde transport in two models of SBMA implicates two sites of androgen action. Hum Mol Genet 20:4475-4490.

Kemppainen JA, Lane MV, Sar M, Wilson EM (1992) Androgen receptor phosphorylation, turnover, nuclear transport, and transcriptional activation. Specificity for steroids and antihormones. J Biol Chem 267:968-974.

Kennedy WR, Alter M, Sung JH (1968) Progressive proximal spinal and bulbar muscular atrophy of late onset. A sex-linked recessive trait. Neurology 18:671-680.

Kennel PF, Finiels F, Revah F, Mallet J (1996) Neuromuscular function impairment is not caused by motor neurone loss in FALS mice: an electromyographic study. Neuroreport 7:1427-1431.

Kinirons P, Rouleau GA (2008) Administration of testosterone results in reversible deterioration in Kennedy's disease. J Neurol Neurosurg Psychiatry 79:106-107.

Klement IA, Skinner PJ, Kaytor MD, Yi H, Hersch SM, Clark HB, Zoghbi HY, Orr HT (1998) Ataxin-1 nuclear localization and aggregation: role in polyglutamine-induced disease in SCA1 transgenic mice. Cell 95:41-53.

Kobayashi Y, Kume A, Li M, Doyu M, Hata M, Ohtsuka K, Sobue G (2000) Chaperones Hsp70 and Hsp40 suppress aggregate formation and apoptosis in cultured neuronal cells expressing truncated androgen receptor protein with expanded polyglutamine tract. J Biol Chem 275:8772-8778.

Koliatsos VE, Clatterbuck RE, Winslow JW, Cayouette MH, Price DL (1993) Evidence that brain-derived neurotrophic factor is a trophic factor for motor neurons in vivo. Neuron 10:359-367.

Kong L, Wang X, Choe DW, Polley M, Burnett BG, Bosch-Marce M, Griffin JW, Rich MM, Sumner CJ (2009) Impaired synaptic vesicle release and immaturity of neuromuscular junctions in spinal muscular atrophy mice. J Neurosci 29:842-851.

Korneliussen H (1972) Ultrastructure of normal and stimulated motor endplates with comments on the origin and fate of synaptic vesicles. Zeitschrift fur Zellforschung und mikroskopische Anatomie 130:28-57.

Kuno M, Turkanis SA, Weakly JN (1971) Correlation between nerve terminal size and transmitter release at the neuromuscular junction of the frog. J Physiol 213:545-556.

Kuromi H, Kidokoro Y (1998) Two distinct pools of synaptic vesicles in single presynaptic boutons in a temperature-sensitive Drosophila mutant, shibire. Neuron 20:917-925.

Kuromi H, Kidokoro Y (2003) Two synaptic vesicle pools, vesicle recruitment and replenishment of pools at the Drosophila neuromuscular junction. J Neurocytol 32:551-565.

Kwon YW, Gurney ME (1996) Brain-derived neurotrophic factor transiently stabilizes silent synapses on developing neuromuscular junctions. J Neurobiol 29:503-516.

La Spada AR, Wilson EM, Lubahn DB, Harding AE, Fischbeck KH (1991) Androgen receptor gene mutations in X-linked spinal and bulbar muscular atrophy. Nature 352:77-79.

Laird FM, Farah MH, Ackerley S, Hoke A, Maragakis N, Rothstein JD, Griffin J, Price DL, Martin LJ, Wong PC (2008) Motor neuron disease occurring in a mutant dynactin mouse model is characterized by defects in vesicular trafficking. J Neurosci 28:1997-2005.

LaMonte BH, Wallace KE, Holloway BA, Shelly SS, Ascano J, Tokito M, Van Winkle T, Howland DS, Holzbaur EL (2002) Disruption of dynein/dynactin inhibits axonal transport in motor neurons causing late-onset progressive degeneration. Neuron 34:715-727.

Lang B, Newsom-Davis J, Peers C, Prior C, Wray DW (1987) The effect of myasthenic syndrome antibody on presynaptic calcium channels in the mouse. J Physiol 390:257-270.

Langmeier M, Giogasova E, Zikova O, Mares J (1986) Changes in the size and shape of the synaptic vesicles in the sensorimotor cortex of the rat brain in the initial phases of kindling. Physiologia Bohemoslovaca 35:437-446.

Law PK, Saito A, Fleischer S (1983) Ultrastructural changes in muscle and motor end-plate of the dystrophic mouse. Exp Neurol 80:361-382.

Leopold PL, McDowall AW, Pfister KK, Bloom GS, Brady ST (1992) Association of kinesin with characterized membrane-bounded organelles. Cell motility and the cytoskeleton 23:19-33.

Leube RE, Leimer U, Grund C, Franke WW, Harth N, Wiedenmann B (1994) Sorting of synaptophysin into special vesicles in nonneuroendocrine epithelial cells. J Cell Biol 127:1589-1601.

Li M, Miwa S, Kobayashi Y, Merry DE, Yamamoto M, Tanaka F, Doyu M, Hashizume Y, Fischbeck KH, Sobue G (1998a) Nuclear inclusions of the androgen receptor protein in spinal and bulbar muscular atrophy. Ann Neurol 44:249-254.

Li M, Nakagomi Y, Kobayashi Y, Merry DE, Tanaka F, Doyu M, Mitsuma T, Hashizume Y, Fischbeck KH, Sobue G (1998b) Nonneural nuclear inclusions of androgen receptor protein in spinal and bulbar muscular atrophy. Am J Pathol 153:695-701.

Li M, Sobue G, Doyu M, Mukai E, Hashizume Y, Mitsuma T (1995) Primary sensory neurons in X-linked recessive bulbospinal neuropathy: histopathology and androgen receptor gene expression. Muscle Nerve 18:301-308.

Li W, Brakefield D, Pan Y, Hunter D, Myckatyn TM, Parsadanian A (2007) Muscle-derived but not centrally derived transgene GDNF is neuroprotective in G93A-SOD1 mouse model of ALS. Exp Neurol 203:457-471.

Lieberman AP, Fischbeck KH (2000) Triplet repeat expansion in neuromuscular disease. Muscle Nerve 23:843-850.

Lin MT, Beal MF (2006) Mitochondrial dysfunction and oxidative stress in neurodegenerative diseases. Nature 443:787-795.

Lino MM, Schneider C, Caroni P (2002) Accumulation of SOD1 mutants in postnatal motoneurons does not cause motoneuron pathology or motoneuron disease. J Neurosci 22:4825-4832.

Lobsiger CS, Boillee S, McAlonis-Downes M, Khan AM, Feltri ML, Yamanaka K, Cleveland DW (2009) Schwann cells expressing dismutase active mutant SOD1 unexpectedly slow disease progression in ALS mice. Proc Natl Acad Sci U S A 106:4465-4470.

Lohof AM, Ip NY, Poo MM (1993) Potentiation of developing neuromuscular synapses by the neurotrophins NT-3 and BDNF. Nature 363:350-353.

Love FM, Thompson WJ (1999) Glial cells promote muscle reinnervation by responding to activity-dependent postsynaptic signals. J Neurosci 19:10390-10396.

Lu B, Figurov A (1997) Role of neurotrophins in synapse development and plasticity. Rev Neurosci 8:1-12.

Lubischer JL, Bebinger DM (1999) Regulation of terminal Schwann cell number at the adult neuromuscular junction. J Neurosci 19:RC46.

Lyons PR, Slater CR (1991) Structure and function of the neuromuscular junction in young adult mdx mice. J Neurocytol 20:969-981.

McManamny P, Chy HS, Finkelstein DI, Craythorn RG, Crack PJ, Kola I, Cheema SS, Horne MK, Wreford NG, O'Bryan MK, De Kretser DM, Morrison JR (2002) A mouse model of spinal and bulbar muscular atrophy. Hum Mol Genet 11:2103-2111.

Merry DE, Kobayashi Y, Bailey CK, Taye AA, Fischbeck KH (1998) Cleavage, aggregation and toxicity of the expanded androgen receptor in spinal and bulbar muscular atrophy. Hum Mol Genet 7:693-701.

Merry DE, McCampbell A, Taye AA, Winston RL, Fischbeck KH (1996) Toward a mouse model for spinal and bulbar muscular atrophy: effect of neuronal expression of androgen receptor in transgenic mice. Am J Hum Genet A271.

Meyer M, Matsuoka I, Wetmore C, Olson L, Thoenen H (1992) Enhanced synthesis of brain-derived neurotrophic factor in the lesioned peripheral nerve: different mechanisms are responsible for the regulation of BDNF and NGF mRNA. J Cell Biol 119:45-54.

Mhatre AN, Trifiro MA, Kaufman M, Kazemi-Esfarjani P, Figlewicz D, Rouleau G, Pinsky L (1993) Reduced transcriptional regulatory competence of the androgen receptor in X-linked spinal and bulbar muscular atrophy. Nat Genet 5:184-188.

Miledi R, Slater CR (1970) On the degeneration of rat neuromuscular junctions after nerve section. J Physiol 207:507-528.

Miller KE, Sheetz MP (2006) Direct evidence for coherent low velocity axonal transport of mitochondria. J Cell Biol 173:373-381.

Miller TM, Kim SH, Yamanaka K, Hester M, Umapathi P, Arnson H, Rizo L, Mendell JR, Gage FH, Cleveland DW, Kaspar BK (2006) Gene transfer demonstrates that muscle is not a primary target for non-cell-autonomous toxicity in familial amyotrophic lateral sclerosis. Proc Natl Acad Sci U S A 103:19546-19551.

Mo K, Razak Z, Rao P, Yu Z, Adachi H, Katsuno M, Sobue G, Lieberman AP, Westwood JT, Monks DA (2010) Microarray analysis of gene expression by skeletal muscle of three mouse models of Kennedy disease/spinal bulbar muscular atrophy. PLoS One 5:e12922.

Monani UR, Pastore MT, Gavrilina TO, Jablonka S, Le TT, Andreassi C, DiCocco JM, Lorson C, Androphy EJ, Sendtner M, Podell M, Burghes AH (2003) A transgene carrying an A2G missense mutation in the SMN gene modulates phenotypic severity in mice with severe (type I) spinal muscular atrophy. J Cell Biol 160:41-52.

Monks DA, Johansen JA, Mo K, Rao P, Eagleson B, Yu Z, Lieberman AP, Breedlove SM, Jordan CL (2007) Overexpression of wild-type androgen receptor in muscle recapitulates polyglutamine disease. Proc Natl Acad Sci U S A 104:18259-18264.

Morfini G, Pigino G, Szebenyi G, You Y, Pollema S, Brady ST (2006) JNK mediates pathogenic effects of polyglutamine-expanded androgen receptor on fast axonal transport. Nat Neurosci 9:907-916.

Morfini GA, Burns M, Binder LI, Kanaan NM, LaPointe N, Bosco DA, Brown RH, Jr., Brown H, Tiwari A, Hayward L, Edgar J, Nave KA, Garberrn J, Atagi Y, Song Y, Pigino G, Brady ST (2009) Axonal transport defects in neurodegenerative diseases. J Neurosci 29:12776-12786.

Munch C, Rosenbohm A, Sperfeld AD, Uttner I, Reske S, Krause BJ, Sedlmeier R, Meyer T, Hanemann CO, Stumm G, Ludolph AC (2005) Heterozygous R1101K mutation of the DCTN1 gene in a family with ALS and FTD. Ann Neurol 58:777-780.

Murakami T, Nagano I, Hayashi T, Manabe Y, Shoji M, Setoguchi Y, Abe K (2001) Impaired retrograde axonal transport of adenovirus-mediated E.

coli LacZ gene in the mice carrying mutant SOD1 gene. Neurosci Lett 308:149-152.

Murray LM, Comley LH, Thomson D, Parkinson N, Talbot K, Gillingwater TH (2008) Selective vulnerability of motor neurons and dissociation of pre- and post-synaptic pathology at the neuromuscular junction in mouse models of spinal muscular atrophy. Hum Mol Genet 17:949-962.

Musa M, Fernando SM, Chatterjee D, Monks DA (2011) Subcellular effects of myocyte-specific androgen receptor overexpression in mice. J Endocrinol 210:93-104.

Musaro A, McCullagh K, Paul A, Houghton L, Dobrowolny G, Molinaro M, Barton ER, Sweeney HL, Rosenthal N (2001) Localized Igf-1 transgene expression sustains hypertrophy and regeneration in senescent skeletal muscle. Nat Genet 27:195-200.

Nagel A, Engel AG, Lang B, Newsom-Davis J, Fukuoka T (1988) Lambert-Eaton myasthenic syndrome IgG depletes presynaptic membrane active zone particles by antigenic modulation. Ann Neurol 24:552-558.

Nguyen QT, Parsadanian AS, Snider WD, Lichtman JW (1998) Hyperinnervation of neuromuscular junctions caused by GDNF overexpression in muscle. Science 279:1725-1729.

O'Malley JP, Waran MT, Balice-Gordon RJ (1999) In vivo observations of terminal Schwann cells at normal, denervated, and reinnervated mouse neuromuscular junctions. J Neurobiol 38:270-286.

Oki K, Wiseman RW, Breedlove SM, Jordan CL (2013) Androgen receptors in muscle fibers induce rapid loss of force but not mass: implications for spinal bulbar muscular atrophy. Muscle Nerve 47:823-834.

Orr CR, Montie HL, Liu Y, Bolzoni E, Jenkins SC, Wilson EM, Joseph JD, McDonnell DP, Merry DE (2010) An interdomain interaction of the androgen receptor is required for its aggregation and toxicity in spinal and bulbar muscular atrophy. J Biol Chem 285:35567-35577.

Orr HT, Zoghbi HY (2007) Trinucleotide repeat disorders. Annu Rev Neurosci 30:575-621.

Oude Ophuis RJ, Wijers M, Bennink MB, van de Loo FA, Fransen JA, Wieringa B, Wansink DG (2009) A tail-anchored myotonic dystrophy protein kinase isoform induces perinuclear clustering of mitochondria, autophagy, and apoptosis. PLoS One 4:e8024.

Palazzolo I, Stack C, Kong L, Musaro A, Adachi H, Katsuno M, Sobue G, Taylor JP, Sumner CJ, Fischbeck KH, Pennuto M (2009) Overexpression of IGF-1 in muscle attenuates disease in a mouse model of spinal and bulbar muscular atrophy. Neuron 63:316-328.

Panov AV, Gutekunst CA, Leavitt BR, Hayden MR, Burke JR, Strittmatter WJ, Greenamyre JT (2002) Early mitochondrial calcium defects in Huntington's disease are a direct effect of polyglutamines. Nat Neurosci 5:731-736.

Patton BL, Chiu AY, Sanes JR (1998) Synaptic laminin prevents glial entry into the synaptic cleft. Nature 393:698-701.

Perlson E, Jeong GB, Ross JL, Dixit R, Wallace KE, Kalb RG, Holzbaur EL (2009) A switch in retrograde signaling from survival to stress in rapid-onset neurodegeneration. J Neurosci 29:9903-9917.

Perrot R, Berges R, Bocquet A, Eyer J (2008) Review of the multiple aspects of neurofilament functions, and their possible contribution to neurodegeneration. Mol Neurobiol 38:27-65.

Phillips GR, Huang JK, Wang Y, Tanaka H, Shapiro L, Zhang W, Shan WS, Arndt K, Frank M, Gordon RE, Gawinowicz MA, Zhao Y, Colman DR (2001) The presynaptic particle web: ultrastructure, composition, dissolution, and reconstitution. Neuron 32:63-77.

Piccioni F, Pinton P, Simeoni S, Pozzi P, Fascio U, Vismara G, Martini L, Rizzuto R, Poletti A (2002) Androgen receptor with elongated polyglutamine tract forms aggregates that alter axonal trafficking and mitochondrial distribution in motor neuronal processes. FASEB J 16:1418-1420.

Pitts EV, Potluri S, Hess DM, Balice-Gordon RJ (2006) Neurotrophin and Trk-mediated signaling in the neuromuscular system. Int Anesthesiol Clin 44:21-76.

Pramatarova A, Laganiere J, Roussel J, Brisebois K, Rouleau GA (2001) Neuron-specific expression of mutant superoxide dismutase 1 in transgenic mice does not lead to motor impairment. J Neurosci 21:3369-3374.

Pratt SJ, Shah SB, Ward CW, Inacio MP, Stains JP, Lovering RM (2013) Effects of in vivo injury on the neuromuscular junction in healthy and dystrophic muscles. J Physiol 591:559-570.

Puigserver P (2005) Tissue-specific regulation of metabolic pathways through the transcriptional coactivator PGC1-alpha. International journal of obesity 29 Suppl 1:S5-9.

Puls I, Jonnakuty C, LaMonte BH, Holzbaur EL, Tokito M, Mann E, Floeter MK, Bidus K, Drayna D, Oh SJ, Brown RH, Jr., Ludlow CL, Fischbeck KH (2003) Mutant dynactin in motor neuron disease. Nat Genet 33:455-456.

Puls I, Oh SJ, Sumner CJ, Wallace KE, Floeter MK, Mann EA, Kennedy WR, Wendelschafer-Crabb G, Vortmeyer A, Powers R, Finnegan K, Holzbaur EL, Fischbeck KH, Ludlow CL (2005) Distal spinal and bulbar muscular atrophy caused by dynactin mutation. Ann Neurol 57:687-694.

Pun S, Santos AF, Saxena S, Xu L, Caroni P (2006) Selective vulnerability and pruning of phasic motoneuron axons in motoneuron disease alleviated by CNTF. Nat Neurosci 9:408-419.

Pysh JJ, Wiley RG (1974) Synaptic vesicle depletion and recovery in cat sympathetic ganglia electrically stimulated in vivo. Evidence for transmitter secretion by exocytosis. J Cell Biol 60:365-374.

Ranganathan S, Harmison GG, Meyertholen K, Pennuto M, Burnett BG, Fischbeck KH (2009) Mitochondrial abnormalities in spinal and bulbar muscular atrophy. Hum Mol Genet 18:27-42.

Rastad J, Jankowska E, Westman J (1977) Arborization of initial axon collaterals of spinocervical tract cells stained intracellularly with horseradish peroxidase. Brain Res 135:1-10.

Reddy LV, Koirala S, Sugiura Y, Herrera AA, Ko CP (2003) Glial cells maintain synaptic structure and function and promote development of the neuromuscular junction in vivo. Neuron 40:563-580.

Renger JJ, Egles C, Liu G (2001) A developmental switch in neurotransmitter flux enhances synaptic efficacy by affecting AMPA receptor activation. Neuron 29:469-484.

Rettig J, Neher E (2002) Emerging roles of presynaptic proteins in Ca++-triggered exocytosis. Science 298:781-785.

Reynolds ML, Woolf CJ (1992) Terminal Schwann cells elaborate extensive processes following denervation of the motor endplate. J Neurocytol 21:50-66.

Richards DA, Guatimosim C, Betz WJ (2000) Two endocytic recycling routes selectively fill two vesicle pools in frog motor nerve terminals. Neuron 27:551-559.

Richards DA, Guatimosim C, Rizzoli SO, Betz WJ (2003) Synaptic vesicle pools at the frog neuromuscular junction. Neuron 39:529-541.

Rinaldi C, Bott LC, Chen KL, Harmison GG, Katsuno M, Sobue G, Pennuto M, Fischbeck KH (2012) Insulinlike growth factor (IGF)-1 administration ameliorates disease manifestations in a mouse model of spinal and bulbar muscular atrophy. Molecular medicine 18:1261-1268.

Rizzoli SO, Betz WJ (2005) Synaptic vesicle pools. Nat Rev Neurosci 6:57-69.

Robitaille R (1995) Purinergic receptors and their activation by endogenous purines at perisynaptic glial cells of the frog neuromuscular junction. J Neurosci 15:7121-7131.

Robitaille R (1998) Modulation of synaptic efficacy and synaptic depression by glial cells at the frog neuromuscular junction. Neuron 21:847-855.

Robitaille R, Bourque MJ, Vandaele S (1996) Localization of L-type Ca2+ channels at perisynaptic glial cells of the frog neuromuscular junction. J Neurosci 16:148-158.

Robitaille R, Garcia ML, Kaczorowski GJ, Charlton MP (1993) Functional colocalization of calcium and calcium-gated potassium channels in control of transmitter release. Neuron 11:645-655.

Ross CA (1997) Intranuclear neuronal inclusions: a common pathogenic mechanism for glutamine-repeat neurodegenerative diseases? Neuron 19:1147-1150.

Ross CA (2002) Polyglutamine pathogenesis: emergence of unifying mechanisms for Huntington's disease and related disorders. Neuron 35:819-822.

Rusconi F, Mancinelli E, Colombo G, Cardani R, Da Riva L, Bongarzone I, Meola G, Zippel R (2010) Proteome profile in Myotonic Dystrophy type 2 myotubes reveals dysfunction in protein processing and mitochondrial pathways. Neurobiol Dis 38:273-280.

Salpeter MM, Loring RH (1985) Nicotinic acetylcholine receptors in vertebrate muscle: properties, distribution and neural control. Prog Neurobiol 25:297-325.

Sanes JR, Lichtman JW (1999) Development of the vertebrate neuromuscular junction. Annu Rev Neurosci 22:389-442.

Sasaki S, Maruyama S (1994) Synapse loss in anterior horn neurons in amyotrophic lateral sclerosis. Acta Neuropathol 88:222-227.

Saudou F, Finkbeiner S, Devys D, Greenberg ME (1998) Huntingtin acts in the nucleus to induce apoptosis but death does not correlate with the formation of intranuclear inclusions. Cell 95:55-66.

Savtchenko LP, Rusakov DA (2007) The optimal height of the synaptic cleft. Proc Natl Acad Sci U S A 104:1823-1828.

Schindelin J, Arganda-Carreras I, Frise E, Kaynig V, Longair M, Pietzsch T, Preibisch S, Rueden C, Saalfeld S, Schmid B, Tinevez JY, White DJ, Hartenstein V, Eliceiri K, Tomancak P, Cardona A (2012) Fiji: an open-source platform for biological-image analysis. Nature methods 9:676-682.

Schmidt BJ, Greenberg CR, Allingham-Hawkins DJ, Spriggs EL (2002) Expression of X-linked bulbospinal muscular atrophy (Kennedy disease) in two homozygous women. Neurology 59:770-772.

Sendtner M, Stockli KA, Thoenen H (1992) Synthesis and localization of ciliary neurotrophic factor in the sciatic nerve of the adult rat after lesion and during regeneration. J Cell Biol 118:139-148.

Sengelaub DR, Nordeen EJ, Nordeen KW, Arnold AP (1989) Hormonal control of neuron number in sexually dimorphic spinal nuclei of the rat: III. Differential effects of the androgen dihydrotestosterone. J Comp Neurol 280:637-644.

Seong IS, Ivanova E, Lee JM, Choo YS, Fossale E, Anderson M, Gusella JF, Laramie JM, Myers RH, Lesort M, MacDonald ME (2005) HD CAG repeat implicates a dominant property of huntingtin in mitochondrial energy metabolism. Hum Mol Genet 14:2871-2880.

Shiao T, Fond A, Deng B, Wehling-Henricks M, Adams ME, Froehner SC, Tidball JG (2004) Defects in neuromuscular junction structure in dystrophic muscle are corrected by expression of a NOS transgene in dystrophin-deficient muscles, but not in muscles lacking alpha- and beta1-syntrophins. Hum Mol Genet 13:1873-1884.

Sisodia SS (1998) Nuclear inclusions in glutamine repeat disorders: are they pernicious, coincidental, or beneficial? Cell 95:1-4.

Slater CR (2003) Structural determinants of the reliability of synaptic transmission at the vertebrate neuromuscular junction. J Neurocytol 32:505-522.

Slater CR, Fawcett PRW, Walls TJ, Lyons PR, Bailey SJ, Beeson D, Young C, Gardner-Medwin D (2006) Pre- and post-synaptic abnormalities associated with impaired neuromuscular transmission in a group of patients with ‘limb-girdle myasthenia’. Brain 129:2061-2076.

Sobue G, Hashizume Y, Mukai E, Hirayama M, Mitsuma T, Takahashi A (1989) X-linked recessive bulbospinal neuronopathy. A clinicopathological study. Brain 112 (Pt 1):209-232.

Son YJ, Thompson WJ (1995a) Nerve sprouting in muscle is induced and guided by processes extended by Schwann cells. Neuron 14:133-141.

Son YJ, Thompson WJ (1995b) Schwann cell processes guide regeneration of peripheral axons. Neuron 14:125-132.

Sopher BL, Thomas PS, Jr., LaFevre-Bernt MA, Holm IE, Wilke SA, Ware CB, Jin LW, Libby RT, Ellerby LM, La Spada AR (2004) Androgen receptor YAC transgenic mice recapitulate SBMA motor neuronopathy and implicate VEGF164 in the motor neuron degeneration. Neuron 41:687-699.

Soraru G, D'Ascenzo C, Polo A, Palmieri A, Baggio L, Vergani L, Gellera C, Moretto G, Pegoraro E, Angelini C (2008) Spinal and bulbar muscular atrophy: skeletal muscle pathology in male patients and heterozygous females. J Neurol Sci 264:100-105.

Spiegelman BM (2007) Transcriptional control of energy homeostasis through the PGC1 coactivators. Novartis Foundation symposium 286:3-6; discusssion 6-12, 162-163, 196-203.

Susalka SJ, Pfister KK (2000) Cytoplasmic dynein subunit heterogeneity: implications for axonal transport. J Neurocytol 29:819-829.

Suzuki K, Katsuno M, Banno H, Takeuchi Y, Atsuta N, Ito M, Watanabe H, Yamashita F, Hori N, Nakamura T, Hirayama M, Tanaka F, Sobue G (2008) CAG repeat size correlates to electrophysiological motor and sensory phenotypes in SBMA. Brain 131:229-239.

Takahashi A (2001) Hiroshi Kawahara (1858-1918). J Neurol 248:241-242.

Takeyama K, Ito S, Yamamoto A, Tanimoto H, Furutani T, Kanuka H, Miura M, Tabata T, Kato S (2002) Androgen-dependent neurodegeneration by polyglutamine-expanded human androgen receptor in Drosophila. Neuron 35:855-864.

Tam SL, Archibald V, Jassar B, Tyreman N, Gordon T (2001) Increased neuromuscular activity reduces sprouting in partially denervated muscles. J Neurosci 21:654-667.

Taylor JP, Tanaka F, Robitschek J, Sandoval CM, Taye A, Markovic-Plese S, Fischbeck KH (2003) Aggresomes protect cells by enhancing the degradation of toxic polyglutamine-containing protein. Hum Mol Genet 12:749-757.

Teuling E, van Dis V, Wulf PS, Haasdijk ED, Akhmanova A, Hoogenraad CC, Jaarsma D (2008) A novel mouse model with impaired dynein/dynactin function develops amyotrophic lateral sclerosis (ALS)-like features in motor neurons and improves lifespan in SOD1-ALS mice. Hum Mol Genet 17:2849-2862.

Thureson-Klein A, Klein RL, Chen Yen SH (1975) Morphological effects of osmolarity on purified noradrenergic vesicles. J Neurocytol 4:609-627.

Torres LF, Duchen LW (1987) The mutant mdx: inherited myopathy in the mouse. Morphological studies of nerves, muscles and end-plates. Brain 110 (Pt 2):269-299.

Trushina E, McMurray CT (2007) Oxidative stress and mitochondrial dysfunction in neurodegenerative diseases. Neuroscience 145:1233-1248.

Turko P (2013) An investigation into the transport and modulation of synaptophysin positive vesicles. University of Glasgow Thesis.

Uchida A, Alami NH, Brown A (2009) Tight functional coupling of kinesin-1A and dynein motors in the bidirectional transport of neurofilaments. Mol Biol Cell 20:4997-5006.

Valdivia O (1971) Methods of fixation and the morphology of synaptic vesicles. J Comp Neurol 142:257-273.

van Laar JH, Berrevoets CA, Trapman J, Zegers ND, Brinkmann AO (1991) Hormone-dependent androgen receptor phosphorylation is accompanied by receptor transformation in human lymph node carcinoma of the prostate cells. J Biol Chem 266:3734-3738.

Vautrin J, Mambrini J (1989) Synaptic current between neuromuscular junction folds. J Theor Biol 140:479-498.

Wagey RT, Krieger C (1998) Abnormalities of protein kinases in neurodegenerative diseases. Progress in drug research Fortschritte der Arzneimittelforschung Progres des recherches pharmaceutiques 51:133-183.

Wagner MC, Pfister KK, Bloom GS, Brady ST (1989) Copurification of kinesin polypeptides with microtubule-stimulated Mg-ATPase activity and kinetic analysis of enzymatic properties. Cell motility and the cytoskeleton 12:195-215.

Wairkar YP, Fradkin LG, Noordermeer JN, DiAntonio A (2008) Synaptic defects in a Drosophila model of congenital muscular dystrophy. J Neurosci 28:3781-3789.

Walberg F (1963) An Electron Microscopical Study of the Inferior Olive of the Cat, Normal and Experimental Findings. Acta neurologica Scandinavica Supplementum 39:SUPPL4:308-313.

Wang AM, Miyata Y, Klinedinst S, Peng HM, Chua JP, Komiyama T, Li X, Morishima Y, Merry DE, Pratt WB, Osawa Y, Collins CA, Gestwicki JE, Lieberman AP (2013) Activation of Hsp70 reduces neurotoxicity by promoting polyglutamine protein degradation. Nature chemical biology 9:112-118.

Wang J, Farr GW, Hall DH, Li F, Furtak K, Dreier L, Horwich AL (2009) An ALS-linked mutant SOD1 produces a locomotor defect associated with aggregation and synaptic dysfunction when expressed in neurons of Caenorhabditis elegans. PLoS Genet 5:e1000350.

Warita H, Itoyama Y, Abe K (1999) Selective impairment of fast anterograde axonal transport in the peripheral nerves of asymptomatic transgenic mice with a G93A mutant SOD1 gene. Brain Res 819:120-131.

Warner CL, Griffin JE, Wilson JD, Jacobs LD, Murray KR, Fischbeck KH, Dickoff D, Griggs RC (1992) X-linked spinomuscular atrophy: a kindred with associated abnormal androgen receptor binding. Neurology 42:2181-2184.

Williamson TL, Cleveland DW (1999) Slowing of axonal transport is a very early event in the toxicity of ALS-linked SOD1 mutants to motor neurons. Nat Neurosci 2:50-56.

Wong CI, Zhou ZX, Sar M, Wilson EM (1993) Steroid requirement for androgen receptor dimerization and DNA binding. Modulation by intramolecular interactions between the NH2-terminal and steroid-binding domains. J Biol Chem 268:19004-19012.

Wong M, Martin L (2009) Skeletal muscle-specific expression of human SOD1 causes motor neuron degeneration in transgenic mice. Society for Neuroscience 2009.

Wood SJ, Slater CR (2001) Safety factor at the neuromuscular junction. Prog Neurobiol 64:393-429.

Woolf CJ, Reynolds ML, Chong MS, Emson P, Irwin N, Benowitz LI (1992) Denervation of the motor endplate results in the rapid expression by terminal Schwann cells of the growth-associated protein GAP-43. J Neurosci 12:3999-4010.

Xiao H, Yu Z, Wu Y, Nan J, Merry DE, Sekiguchi JM, Ferguson DO, Lieberman AP, Dressler GR (2012) A polyglutamine expansion disease protein sequesters PTIP to attenuate DNA repair and increase genomic instability. Hum Mol Genet 21:4225-4236.

Yamada M, Tsuji S, Takahashi H (2002) Genotype-phenotype correlation in CAG-repeat diseases. Neuropathology : official journal of the Japanese Society of Neuropathology 22:317-322.

Yamanaka K, Boillee S, Roberts EA, Garcia ML, McAlonis-Downes M, Mikse OR, Cleveland DW, Goldstein LS (2008) Mutant SOD1 in cell types other than motor neurons and oligodendrocytes accelerates onset of disease in ALS mice. Proc Natl Acad Sci U S A 105:7594-7599.

Yoshikawa M, Vinsant S, Mansfield CM, Moreno RJ, Giffondorwa DJ, Pace L, Leles B, Messi LM, Caress J, Cartwright M, Delbono O, Oppenheim RW, Milligan CE (2009) Identification of changes in muscle, neuromuscular junctions and spinal cord at early pre-symptomatic stages in mutant SOD1 mouse model of ALS may provide novel insight for diagnosis and treatment development. Society for Neuroscience 2009.

Yu Z, Dadgar N, Albertelli M, Gruis K, Jordan C, Robins DM, Lieberman AP (2006) Androgen-dependent pathology demonstrates myopathic

contribution to the Kennedy disease phenotype in a mouse knock-in model. J Clin Invest 116:2663-2672.

Yu Z, Wang AM, Robins DM, Lieberman AP (2009) Altered RNA splicing contributes to skeletal muscle pathology in Kennedy disease knock-in mice. Dis Model Mech 2:500-507.

Zhai RG, Bellen HJ (2004) The architecture of the active zone in the presynaptic nerve terminal. Physiology (Bethesda) 19:262-270.